DEUTSCHES ELEKTRONEN-SYNCHROTRON

DESY 94-087
May 1994

Analysis of Spin Depolarizing Effects in Electron Storage Rings

M. Böge

Fachbereich Physik, Universität Hamburg

ISSN 0418-9833

NOTKESTRASSE 85 - 22603 HAMBURG

To be sure that your preprints are promptly included in the
HIGH ENERGY PHYSICS INDEX,
send them to (if possible by air mail):

DESY
Bibliothek
Notkestraße 85
22603 Hamburg
Germany

DESY-IfH
Bibliothek
Platanenallee 6
15738 Zeuthen
Germany

DESY 94-087
May 1994

ISSN 0418-9833

Analysis of Spin Depolarizing Effects in Electron Storage Rings

Dissertation
zur Erlangung des Doktorgrades
des Fachbereichs Physik
der Universität Hamburg

vorgelegt von
Michael Böge
aus Rendsburg

Hamburg
1994

Gutachter der Dissertation:	Prof. Dr. B. Wiik Prof. Dr. P. Schmüser
Gutachter der Disputation:	Prof. Dr. E. Lohrmann Prof. Dr. P. Schmüser
Datum der Disputation:	28.2.1994
Sprecher des Fachbereichs Physik und Vorsitzender des Promotionsausschusses:	Prof. Dr. E. Lohrmann

Übersicht

In der vorliegenden Arbeit werden spindepolarisierende Effekte in Elektronenspeicherringen untersucht. Im Detail wird hierbei das Verhalten des HERA Elektronenspeicherrings hinsichtlich Polarisation studiert. Bei hohen Strahlenergien begrenzen nichtlineare Effekte die Gleichgewichtspolarisation. Dies ist insbesondere bei HERA der Fall, da HERA mit sogenannten "Spinrotatoren" versehen wird, die longitudinale Elektronenpolarisation zunächst für das HERMES Experiment im Jahr 1994 und zu einem späteren Zeitpunkt für die Experimente H1 und ZEUS ermöglichen sollen. Es ist von großer Wichtigkeit den Einfluß dieser Effekte theoretisch durch eine Modellierung von HERA zu quantifizieren, um dann in der realen Maschine einen hohen Polarisationgrad erzielen zu können.

Die Modellierung wird im Rahmen dieser Arbeit durch das Monte-Carlo Teilchenverfolgungsprogramm SITROS vorgenommen, welches im Jahr 1982 von J. Kewisch zur Untersuchung der Polarisation in PETRA geschrieben wurde. Der erste Teil der Arbeit widmet sich der Beschreibung der in das Programm eingeflossenen theoretischen Grundlagen. Desweiteren werden die wegen Rechenzeitlimitierungen notwendigen Approximationen vorgestellt, die in den verwendeten Algorithmus eingegangen sind und deren möglicher Einfluß auf das Simulationsergebnis diskutiert. Dabei werden sowohl die auftretenden systematischen als auch die statistischen Fehler untersucht. Erweiterungen des Programms, die insbesondere den Vergleich der Ergebnisse von SITROS mit den Ergebnissen der "linearen" Theorie beinhalten, werden vorgestellt.

Nach der detaillierten Präsentation des Modells wird das Programm im zweiten Teil zunächst auf HERA ohne Rotator angewandt. Dabei werden Polarisationsmessungen, die bei HERA durchgeführt wurden, mit Simulationsergebnissen verglichen. Diese beinhalten dabei eine realistische Beschreibung der Maschinenkonditionen, die zum Zeitpunkt der Messungen vorlagen. Verschiedene Verfahren zur Optimierung der Polarisation werden in SITROS modelliert, analysiert und dann der korrespondierenden Messung gegenübergestellt. Dabei zeigt sich eine sehr gute Übereinstimmung der Vorhersagen des Modells und der experimentell gewonnenen Daten. Auf der Basis dieser Untersuchungen werden dann Vorhersagen für die zu erwartenden longitudinale Polarisation bei HERA mit einem Rotatorpaar für das HERMES Experiment gemacht. Abgeschlossen wird der zweite Teil durch die Analyse der Wirkung eines zeitabhängigen radialen Dipolfeldes auf die Polarisation. Die durch ein solches Feld erzeugte resonante Depolarisation des Elektronenstrahls kann zur Kalibration der Teilchenenergie verwendet werden. Zu erwartende Resonanzbreiten für verschiedene integrierte Dipolfeldstärken werden berechnet. Ein erster Vergleich mit den Messungen zeigt gute Übereinstimmung.

Im letzten Teil wird SITROS auf einen Modellring, der dem am KEK betriebenen Elektronenspeicherring TRISTAN ähnelt, und eine schwach gestörte HERA Optik angewandt, um einen Vergleich mit anderen Verfahren zur Berechnung der Gleichgewichtspolarisation vorzunehmen, die nichlineare Effekte berücksichtigen, jedoch gewissen Einschränkungen hinsichtlich ihrer Anwendbarkeit unterliegen. Es wird gezeigt, daß die SITROS Resultate mit denen der anderen Verfahren unter Berücksichtigung dieser Einschränkungen in guter Übereinstimmung sind.

Abstract

In this thesis spin depolarizing effects in electron storage rings are analyzed and the depolarizing effects in the HERA electron storage ring are studied in detail. At high beam energies the equilibrium polarization is limited by nonlinear effects. This will be particularly true in the case of HERA, when the socalled "spin rotators" are inserted which are designed to provide longitudinal electron polarization for the HERMES experiment in 1994 and later for the H1 and ZEUS experiment. It is very important to quantify the influence of these effects theoretically by a proper modelling of HERA, so that ways can be found to get a high degree of polarization in the real machine.

In this thesis HERA is modelled by the Monte-Carlo tracking program SITROS which was originally written by J. Kewisch in 1982 to study the polarization in PETRA. The first part of the thesis is devoted to a detailed description of the fundamental theoretical concepts on which the program is based. Then the approximations which are needed to overcome computing time limitations are explained and their influence on the simulation result is discussed. The systematic and statistical errors are studied in detail. Extensions of the program which allow a comparison of SITROS with the results given by "linear" theory are explained.

After the detailed presentation of the model, the second part of the thesis describes predictions for the polarization in a HERA machine without rotators and comparisons are made with several polarization measurements. The simulations contain a realistic description of the machine conditions pertaining during the measurements. Various schemes for the optimization of the polarization are modelled, analyzed and compared to the corresponding measurement. It is shown that the predictions of the model are in good agreement with the experimental data. On the basis of these studies predictions for the achievable degree of longitudinal polarization in HERA with one rotator pair for the HERMES experiment are made. At the end of this part of the thesis, SITROS is used to model the effect of an oscillating radial magnetic dipole field of the kind used to calibrate the beam energy via resonant depolarization. Resonance widths are calculated for various integrated dipole strengths. A first comparison with measurements indicates good agreement.

In the last part SITROS simulations are made for a model ring which is similar to the electron ring TRISTAN, operated at KEK, and for a weakly distorted HERA optic in order to perform comparisons with other approaches for the calculation of the equilibrium polarization in regimes where these are applicable. Taking into account the limitations of these treatments the results are in good agreement.

Contents

1 Introduction

The emission of synchrotron radiation by relativistic particles subject to transverse acceleration is a much studied and used phenomenon. For a charge in uniform, circular motion the detailed frequency spectrum and angular distributions were calculated in 1912 by Schott [1]. But it took more than 30 years until the synchrotron light was observed in the early synchrotrons.
Somewhat less well known is the fact that electrons and positrons gradually become spin polarized when they are travelling on a curved orbit in a storage ring. The mechanism is the emission of spin-flip synchrotron radiation, as first pointed out by Ternov, Loskutov and Korovina in 1961 [2]. Positrons are polarized parallel and electrons antiparallel to the main bending field which is perpendicular to both velocity and acceleration. Thus one denotes this natural polarization as "transverse" or "vertical" polarization.
Natural polarization was first detected at ACO and Novosibirsk [3]. It has been obtained at CESR, SPEAR, VEPP2M, VEPP4 [4] and at the DESY storage rings PETRA and DORIS where vertical polarizations of ~ 70 % and ~ 80 % at energies of 16 GeV and 5 GeV, respectively have been observed [5]. High vertical polarization has also been observed at LEP [6], TRISTAN [7] and HERA [8]. In the following a few applications of transverse polarization will be discussed.
Polarized beams provide the means for making precise absolute measurements of the beam energy in storage rings, using an artificially induced spin resonance [9]. Since the value of the gyromagnetic anomaly is known very accurately, the measurement of the spin precession frequency determines the beam energy (see section 5.3). This method has been extensively used at Novosibirsk, in particular for precise measurements of the masses of the Φ meson and of the K^+ and K^-, as well as for an accurate comparison of the gyromagnetic anomalies of the electron and the positron [10]. Transverse polarization in DORIS was used to perform a measurement of the Υ' mass to better than 1 MeV [11]. At LEP the beam energy was determined with a precision of 100 KeV around the Z-energy [12].
High energy physicists are much more interested in longitudinal polarization parallel or antiparallel to the particle momentum which has a wide field of applications. In 1957 it was shown by Wu et al. [13] that the β decay of the polarized nucleus of Co^{60} demonstrates a violation of the parity conservation law. The electrons are mainly emitted antiparallel to the polarization direction of the nucleus. They are longitudinally polarized parallel to the nuclear spin and antiparallel to the momentum of the electron. This illustrates the connection between parity violation in weak interaction and longitudinal polarization of electrons. Thus longitudinal electron polarization can be used to test properties of the weak interaction. An example is the experiment performed at SLAC by Prescott et al. [14] in 1978. It demonstrated that the cross section of the inelastic electron-nucleon scattering which is mainly a process of the electromagnetic interaction, depends slightly on the helicity of the incident longitudinally polarized electron. This confirms the existence of a small parity violating and thus weak interaction part in the scattering process.
Longitudinal electron polarization plays an important role in the determination of the spin structure functions of the proton and the neutron by deep inelastic scattering which can be compared with the predictions made by the fundamental theory QCD. In 1988 the data on deep inelastic scattering of polarized muons on polarized protons by the EMC collaboration at CERN [15] together with previous data from SLAC [16] implied that the total helicity carried by quarks and antiquarks in the proton is compatible with zero. These measurements are in contradiction to the naive parton model. Thus more data of the spin structure functions are necessary. The HERMES experiment at DESY will perform high-precision measurements on the structure functions of proton and neutron using internal gas targets of hydrogen, deuterium and ^{3}He and the longitudinally polarized electron beam of the HERA storage ring [17].
The experiments H1 and ZEUS at HERA have plans to collide longitudinally polarized electrons

and unpolarized protons to study one of the great mysteries of weak interaction namely the asymmetry between left- and right-handedness [18]. There are left-handed neutrinos and left-handed charged currents and no right-handed counterparts. It has long been speculated that left-right symmetry is restored at some very high energy. Longitudinally polarized electrons make HERA ideally suited to search for these missing right-handed currents.
For the experiments mentioned a high degree of longitudinal polarization has to be provided by HERA which is far from being trivial for a storage ring operating at an energy of about 30 GeV.
The electron ring of the electron-proton collider HERA [19] includes in its design the possibility to provide longitudinal electron polarization at the interaction points for high energy physics experiments. As a first step it has been demonstrated by measurement that high transverse polarization values of ~ 60 % are possible [8].
As already mentioned the natural polarization builds up in the transverse direction parallel to the main bending field. To deliver longitudinal polarization it is necessary to rotate the equilibrium polarization direction to the longitudinal direction in the straight section before the interaction point and back to the transverse afterwards. This is done by so called "spin rotators". In HERA the "Mini-Rotator" scheme of Buon and Steffen has been adopted [20]. A combination of horizontal and vertical bending magnets is used to rotate the equilibrium polarization direction by 90 degrees leaving the particle orbit undistorted outside the rotators. In 1994 one pair will be installed in the east straight section of HERA to deliver longitudinal polarization for the HERMES experiment.
The achievable polarization value depends strongly on the understanding and suppression of the main depolarizing effects in high energy storage rings which counteract the mentioned natural polarization build up. As one goes to higher energies, progressively more care is required to avoid the influence of depolarizing effects, mainly by proper choices of machine parameters and careful correction of errors. It is the main aim of this thesis to get a phenomenological understanding of polarization in HERA based on a Monte-Carlo treatment and to make estimates for the maximum achievable polarization after suitable applications of corrections.
The work presented was started in 1990 and is based on the Monte-Carlo program SITROS written by J. Kewisch in 1982 [21]. In 1988 T. Limberg [22] made some first predictions for HERA using this tracking code. He studied one of the main limitations of Monte-Carlo programs in general, namely the underestimated influence of the tails of the tracked particle distributions and developed a diffusion model to quantify the influence of the tails on the polarization.
Motivated by this and other limitations of SITROS and the urgent need to have an analytical tool to calculate the polarization at high energies, D.P. Barber in collaboration with S. Mane and H. Grote brought the program SMILE written by S. Mane [23] to a state in which it could be used for HERA. It was found that due to the presence of large depolarizing effects it was not possible to make credible predictions for HERA mainly due to convergence problems of the perturbation theory used in SMILE.
This led to the idea to study the capability of the Monte-Carlo program SITROS in greater detail, to try to overcome the shortcomings of the Monte-Carlo treatment at least partially and to get a better understanding of the systematic and statistical errors of the simulation results. In this case it is possible to benefit from the following main advantages of SITROS:

1. The handling of all kinds of magnet distortions
2. The thick lens representation of the magnets
3. The inclusion of chromatic terms and sextupole corrections
4. The simple classical spin diffusion model

5. The possibility to apply time varying magnetic fields (RF-depolarization)
6. The simulation of beam-beam interaction

It will be shown that all approximations made in SITROS are physically sensible and, taking care of the limitations of the Monte-Carlo treatment, the simulation results are fully consistent with experimental results (see section 5) and analytical approaches in regimes where these are applicable (see section 6).

2 Fundamental concepts

For initially unpolarized electrons or positrons of charge e, mass m_e, energy $E = \gamma m_e c^2$ in uniform motion in a circle of radius ρ in a uniform magnetic field, there is a gradual build up of polarization according to:

$$P_{\tau_{ST}}(t) = P_{ST}\left(1 - \exp\left(-\frac{t}{\tau_{ST}}\right)\right), \tag{2.1}$$

where the asymptotic polarization is:

$$P_{ST} = \frac{8}{5\sqrt{3}} = 0.9238$$

and the characteristic build up time is given by:

$$\tau_{ST} = \left(\frac{5\sqrt{3}r_e\hbar}{8m_e}\right)^{-1} \quad \left[\frac{\gamma^5}{|\rho|^3}\right]^{-1}$$

(Sokolov and Ternov, 1963 [24]), where r_e denotes the classical electron radius. The polarization is perpendicular to both velocity and acceleration and thus lies in the direction of the bending field. Positrons are polarized parallel, electrons antiparallel to the magnetic field. The work of Sokolov and Ternov was based on exact solutions of the Dirac equation in a uniform magnetic field.
In terms of classical normalized centre of mass spin vectors $\vec{S}_i$ of individual particles the ensemble polarization vector $\vec{P}$ for N particles is given by:

$$\vec{P} = \frac{1}{N}\sum_{i=1}^{N}\vec{S}_i. \tag{2.2}$$

The amount of spin-flip radiation is extremely small compared to the ordinary synchrotron radiation. The ratio is given by:

$$\frac{\Pi_{spin-flip}}{\Pi_{ordinary}} = 3\left(\frac{\hbar\gamma^2}{m_e c\rho}\right)^2\left(1 \pm \frac{35\sqrt{3}}{64}\right),$$

where the sign in the brackets depends on the initial spin state of the particle. For the HERA electron ring ($\gamma \sim 5 \times 10^4$ for $E \sim 27$ GeV and an effective bending radius $\rho \sim 750$ m) the ratio is of the order 1×10^{-10}. The smallness of this ratio reflects the largeness of the build up time τ_{ST} (~ 42 min at 27 GeV and ~ 11 min at 35 GeV in HERA). Thus polarization changes slowly compared to other phenomena occurring in storage rings.
So far it has been assumed that the magnetic field is everywhere vertical and uniform. In real rings however not only vertical fields but also horizontal and even longitudinal magnetic and electric fields are present. In addition, the electrons oscillate around the central orbit. Thus a thorough analysis is necessary starting with the dynamics of a classical spin vector in arbitrary magnetic and electric fields. The motion of the centre of mass spin vector $\vec{S}$ of a nonradiating electron is described by the Thomas-Bargmann-Michel-Telegdi (T-BMT) equation [25][26] in the laboratory frame:

$$\frac{d\vec{S}}{ds} = \vec{\Omega}_l \times \vec{S} \quad ,$$

where $\vec{\Omega}_l(\vec{B}, \vec{E}, \gamma)$ is a function of the fields and the energy:

$$\vec{\Omega}_l = -\frac{e}{m_e}\left(\left[a + \frac{1}{\gamma}\right]\vec{B} - \frac{a\gamma}{1+\gamma}(\vec{\beta}\vec{B})\vec{\beta} - \left(a + \frac{1}{1+\gamma}\right)\left[\vec{\beta} \times \vec{E}\right]\right). \tag{2.3}$$

For an ultrarelativistic electron ($1/\gamma \ll 1$) moving in a magnetic field this can be rewritten in the form:

$$\frac{d\vec{S}}{ds} = \frac{e}{cm_e\gamma}\left((1+a)\vec{B}_{\parallel} + (1+a\gamma)\vec{B}_{\perp}\right) \times \vec{S}, \tag{2.4}$$

where $\vec{B}_{\parallel}$, $\vec{B}_{\perp}$ are the magnetic fields parallel and perpendicular to the trajectory, s is the longitudinal coordinate and a denotes the gyromagnetic anomaly $(g-2)/2$, which is $a = 1.159652 \times 10^{-3}$ in the case of electrons and 1.792846 in the case of protons. One sees that the frequency of precession around $\vec{B}_{\perp}$ in eq. (2.4) is almost independent of energy ($1/\gamma \ll 1$) but that the rate of precession around $\vec{B}_{\parallel}$ varies inversely with the energy. For vanishing $\vec{B}_{\parallel}$ and $\vec{B}_{\perp} || \vec{e}_z$ in a "flat" ring and after transformation to a frame which is circulating with the particle (i.e. to machine coordinates, see fig. (4)), $\vec{\Omega}_l$ transforms to:

$$\vec{\Omega} = \frac{e\vec{B}_{\perp}}{cm_e\gamma} \quad a\gamma, \tag{2.5}$$

where the first part is the relativistic cyclotron frequency ω_c and $a\gamma$ is called the spin tune ν. This means that the spin vector precesses ν times around the bending field for one turn of the particle around the ring.
For real rings the analysis of Sokolov and Ternov, which is based on the assumption that the applied magnetic field is uniform, must be generalized. This yields the Baier-Katkov-Strakhovenko (BKS) equation [27] for the rate of change of the ensemble polarization vector:

$$\frac{d\vec{P}}{dt} = \vec{\Omega}_s \times \vec{P} - \frac{1}{\tau_{ST}}\left[\vec{P} - \frac{2}{9}(\vec{P}\vec{v})\vec{v} + P_{ST}\vec{b}\right]. \tag{2.6}$$

This equation contains a "large" part describing a T-BMT like precession and a "small" part describing the build up of polarization in a direction parallel to the normalized vector $\vec{b} = \vec{v} \times \dot{\vec{v}}/|\vec{v} \times \dot{\vec{v}}|$ which is perpendicular to the velocity vector $\vec{v}$ normalized to unit length and the acceleration vector $\dot{\vec{v}}$.
The concept of spin tune must also be generalized. This is achieved straightforwardly by integrating the T-BMT equation around the periodic closed orbit (see section 3.1 for the definition) of the ring and extracting the periodic spin vector which is defined as the periodic solution of eq. (2.4) on the closed orbit. This is denoted by $\vec{n}_0$ and obeys $\vec{n}_0(s+L) = \vec{n}_0(s)$, where L denotes the circumference of the ring. The spin tune ν is now the number of spin precessions around $\vec{n}_0$ for one turn around the machine (see section 3.4 and appendix A). For non integer ν a periodic solution of eq. (2.4) is unique. In a perfectly flat ring $\vec{n}_0$ is parallel to the main bending field ($\vec{n}_0 || \vec{e}_z$) as expected.
To obtain the value of the asymptotic polarization and its direction one assumes that the electrons are all on the closed orbit and one ignores the energy changes caused by the synchrotron radiation. The BKS equation is then integrated along the closed orbit and it is found that even when starting with an arbitrary polarization vector the polarization value approaches [28]:

$$P_{\infty} = P_{ST}\frac{\oint \frac{ds}{|\rho(s)|^3}(\vec{b}\vec{n}_0)}{\oint \frac{ds}{|\rho(s)|^3}\left[1 - \frac{2}{9}(\vec{n}_0\vec{v})^2\right]}, \tag{2.7}$$

where $\vec{b}$ is the direction of the bending field. The corresponding build up time τ_p is determined to be:

$$\frac{1}{\tau_p} = \frac{5\sqrt{3}r_e\hbar\gamma^5}{8m_e L}\oint \frac{ds}{|\rho(s)|^3}\left[1 - \frac{2}{9}(\vec{n}_0\vec{v})^2\right]. \tag{2.8}$$

The asymptotic direction of the polarization is $\vec{n}_0(s)$, the only T-BMT solution in the system stable over the time needed for the polarization to build up. It is clear from eq. (2.7) that

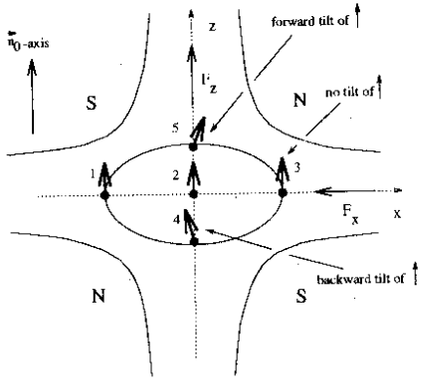

Figure 1: *An illustration of the additional tilts which five sample spin vectors get inside a quadrupole at a location where the $\vec{n}_0$-axis is parallel to the z-axis. The spin vectors of the "on axis" particle 2 and the particles 1 and 3 on horizontal betatron trajectories get no additional tilts with respect to the $\vec{n}_0$-axis. The spin vectors of the particles 4 and 5 on vertical betatron trajectories are rotated backward/forward with respect to the x-axis due to the horizontal magnetic field components of the quadrupole and thus become tilted. The rotation angles depend on the position of the particles inside the quadrupole. If $\vec{n}_0$ is not vertical even pure horizontal betatron oscillations lead to additional spin vector tilts*

the polarization is maximized by arranging that $\vec{n}_0$ is parallel to $\vec{B}$ in as much of the ring as possible. In real rings with $\vec{B}_\perp \cdot \vec{e}_x \neq 0$ $\vec{n}_0$ is almost never everywhere parallel to the main bending field but $\vec{n}_0$ still defines the direction of the polarization vector.
So far only the natural polarization build up process for electrons constrained to remain on the closed orbit has been considered. But for the description in an electron storage ring an important ingredient is missing. The emitted synchrotron radiation and the acceleration by the longitudinal electric fields of the cavities change the particle energy and this leads to damping and to an excitation of the electron motion (see section 3) due to the stochasticity of the photon emission process. The equilibrium emittances in an electron storage ring are the result of the balance of these two processes. The magnetic moment of an electron experiences the same electric and magnetic fields as the particle on its betatron trajectory. Thus in quadrupoles, for example, the individual spins $\vec{S}_i$ see fields which depend on the position of the electron in the ensemble (fig. (1)). Due to the stochastic nature of the betatron motion the orbit dynamics leads to a diffusion of the spins away from $\vec{n}_0$ for an ensemble of spins which are initially all parallel to the equilibrium direction $\vec{n}_0$. As a result the average projection of the $\vec{S}_i$ on $\vec{n}_0$ is reduced leading to a smaller polarization value. One also expects and finds that the spin diffusion is strongest when the spin tune and the orbital tunes are related by the resonance condition:

$$\nu = k + m_x Q_x + m_z Q_z + m_s Q_s, \tag{2.9}$$

where $k, m_{x,z,s}$ are integers and $Q_{x,z,s}$ are the orbital tunes. In stored proton beams where there is no synchrotron radiation an ensemble initially polarized along $\vec{n}_0$ remains polarized providing that the beam is not accelerated through resonances. In the latter case it depends on the speed of the resonance crossing whether the ensemble remains polarized or not [29]. In the presence

of spin diffusion a depolarization term has to be included in eq. (2.6):

$$\frac{d\vec{P}}{dt} = \vec{\Omega}_s \times \vec{P} - \frac{1}{\tau_{ST}}\left[\vec{P} - \frac{2}{9}(\vec{P}\vec{v})\vec{v} + P_{ST}\vec{b}\right] - \frac{1}{\tau_{ST}}|\vec{d}|^2\vec{P}.$$

Eq. (2.7) must then be modified and becomes:

$$P_{eff} = P_{ST}\frac{\oint \frac{ds}{|\rho(s)|^3}(\vec{b}\vec{n}_0)}{\oint \frac{ds}{|\rho(s)|^3}\left[1 - \frac{2}{9}(\vec{n}_0\vec{v})^2 + \frac{11}{18}|\vec{d}|^2\right]}, \tag{2.10}$$

where $|\vec{d}|^2$ describes the diffusion process with respect to $\vec{n}_0$. Eq. (2.10) can be approximately rewritten in the form:

$$P_{eff} = P_\infty \frac{1}{1 + (\tau_p/\tau_d)} \tag{2.11}$$

with τ_p defined in eq. (2.8) and τ_d given by:

$$\frac{1}{\tau_d} = \frac{55 r_e \hbar \gamma^5}{48\sqrt{3} m_e L}\oint \frac{ds}{|\rho(s)|^3}|\vec{d}|^2. \tag{2.12}$$

In analogy to eq. (2.1) the polarization build up process is described again by an exponential:

$$\begin{aligned} P_{\tau_{eff}}(t) &= P_{eff}\left(1 - \exp\left(-\frac{t}{\tau_{eff}}\right)\right) \\ \tau_{eff} &= \frac{\tau_p \tau_d}{\tau_p + \tau_d}. \end{aligned} \tag{2.13}$$

If the characteristic time τ_d for this depolarization process is of the same order or even smaller than the build up time τ_p there is a significant decrease of the asymptotic equilibrium polarization (see eq. (2.11)). It is therefore obvious that the 92.4% level of polarization is in general not reachable and that a method of calculating τ_d is needed so that predictions can be made at the design stage of a storage ring or methods found for minimizing $1/\tau_d$ during the operating period.
Fig. (2) collects time scales of various processes in electron storage rings and spans more than fourteen orders of magnitude. An important aspect is the clustering of synchro-betatron oscillation, orbit-harmonic and spin-precession periods, a feature which has a strong influence on the spectrum of depolarizing resonances (see eq. (2.9)) and their excitation. The polarization time constants τ_p and τ_d are far away from these typical quantities governing the particle motion in electron storage rings. This fact justifies the application of averaging methods which are extensively used by various formalisms. An example is the appearance of one turn averages in eq. (2.6). The separations between the synchro-betatron time scales, the interval between quanta emitted by a single electron and the duration of the quantum emission permit the latter to be considered as a random process with no correlation between successive photons.
Fig. (3) illustrates the analogy between the radiation damping process for the orbital motion and the natural polarization build up due to the Sokolov-Ternov effect for the spin motion. The excitation of the particle motion due to quantum emissions corresponds to the diffusion process for the spin motion. Damping and excitation lead to the equilibrium emittances. The polarization build up and the counteracting depolarization process lead to the equilibrium polarization.
The first attempt known to the author to calculate depolarization was made by Baier and Orlov [30]. The first computer code able to make detailed realistic calculations was SLIM written by Chao [31]. SLIM takes a standard optic file and computes depolarization effects

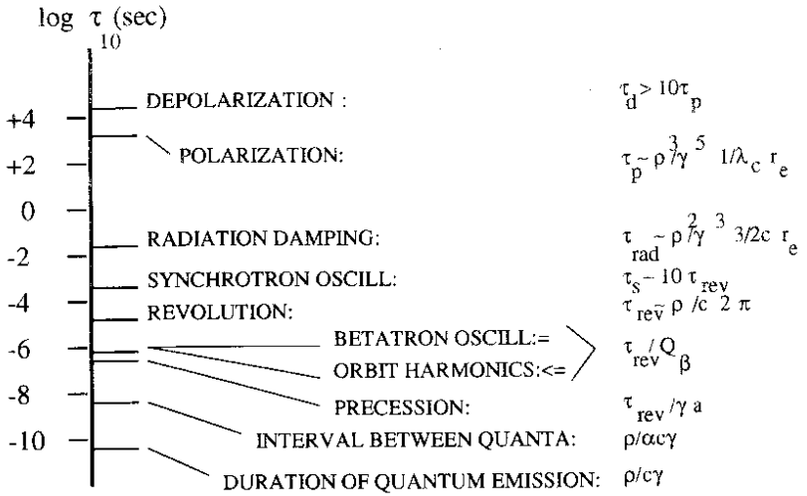

Figure 2: *Characteristic time scales in a typical 25 GeV electron storage ring: ρ=bending radius, λ_c=Compton wavelength, r_e=classical electron radius, Q_β=betatron tune, α=fine-structure constant, a=gyromagnetic anomaly [28]*

analytically using spin-orbit transfer matrix techniques on the basis of the simple diffusion model. As expected it is found that the spin diffusion effects are strongest (τ_p/τ_d large) at energy points (defined by $\nu = a\gamma$) where the resonance condition eq. (2.9) is fulfilled. Since the SLIM formalism treats the orbit and spin motion in linear approximation assuming that all spins are almost parallel to $\vec{n}_0$, hence ignoring the noncommutativity of three dimensional rotations, SLIM only finds the so called first order resonances ($|m_x| + |m_z| + |m_s| = 1$) [32]. A detailed description is given in appendix A.

A more comprehensive semi-classical quantum mechanical treatment which takes into account various effects in a unified way has been given by Derbenev and Kondratenko in 1973 [33] and Mane in 1987 [23]. They derived the following expression for the equilibrium polarization P_{eff}:

$$P_{eff} = P_{ST} \frac{\left\langle \oint \frac{ds}{|\rho(s)|^3} \vec{b} \left[\vec{n} - \gamma \frac{\partial \vec{n}}{\partial \gamma} \right] \right\rangle}{\left\langle \oint \frac{ds}{|\rho(s)|^3} \left[1 - \frac{2}{9}(\vec{n}\vec{v})^2 + \frac{11}{18} \left| \gamma \frac{\partial \vec{n}}{\partial \gamma} \right|^2 \right] \right\rangle}. \qquad (2.14)$$

The angle brackets $<>$ denote the average over the distribution of the phase space coordinates. In eq. (2.14) the vector $\vec{n}$ is a solution to the T-BMT equation and a single valued function of the particle position in phase space (see section 3) and the longitudinal position s. $\vec{n}$ acts as a phase space dependent spin quantization axis, the only direction in which polarization can be observed. It is thus a natural generalization of $\vec{n}_0$ defined previously and away from spin-orbit resonances it is indeed almost parallel to $\vec{n}_0$. $\gamma \partial \vec{n}/\partial \gamma$ describes the variation of $\vec{n}$ with respect to the fractional energy deviation $\Delta E/E$ of the particle. Eq. (2.14) contains the whole resonance structure given by eq. (2.9).

Eq. (2.14) bears an obvious similarity to eq. (2.10) and one sees that the diffusion vector $\vec{d}$ is replaced by $\gamma \partial \vec{n}/\partial \gamma$ which includes the quantum mechanics of the effect of the orbit motion on the spin and which is now the quantity determining the limiting polarization value. In this formalism the polarization is small near the spin-orbit resonances (see eq. (2.9)) confirming the

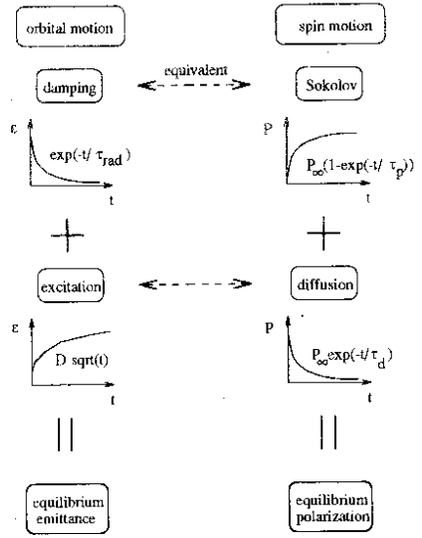

Figure 3: *Analogy between processes governing the orbital and spin motion in an electron storage ring*

previous expectation. In this picture it is due to the fact that near a resonance $\vec{n}$ is a strong function of the phase space coordinates so that the term $|\gamma \partial \vec{n}/\partial \gamma|^2$ in the denominator becomes large. The contribution of $\gamma \partial \vec{n}/\partial \gamma$ in the numerator is normally negligible because the diffusion takes place in the plane perpendicular to the direction of the bending field $\vec{b}$. $|\gamma \partial \vec{n}/\partial \gamma|^2$ can increase strongly with beam energy.

In practice the analytical evaluation of $\vec{n}$ and $\gamma \partial \vec{n}/\partial \gamma$ needed in the Derbenev-Kondratenko formula for realistic storage rings has turned out to be nontrivial. A perturbation expansion in the phase space coordinates can be used to calculate $\vec{n}$ and $\gamma \partial \vec{n}/\partial \gamma$ and this has been implemented in the program SMILE written by S. Mane [23]. By going to higher and higher order more and more resonances are included.

A new method to calculate $\vec{n}$ was introduced in 1992 by K. Yokoya and implemented in the computer code SODOM [34], where $\vec{n}$ is evaluated by numerical tracking over one turn of the spin-orbit motion for nonradiating particles without using a perturbation expansion. The main problem remains in the calculation of $\gamma \partial \vec{n}/\partial \gamma$. Up to now SODOM uses first-order differences for points in phase space in an infinitesimal neighbourhood of $\vec{n}$. Thus the result for $\gamma \partial \vec{n}/\partial \gamma$ depends on the chosen set of samples. In addition the method involves Fourier expansions which have to be truncated in a suitable way. Eq. (2.14) is then used to estimate P_{eff}. Nevertheless the results of SODOM are encouraging. SODOM results have been compared with results of the Monte-Carlo program SITROS (see section 6.1).

SMILE and SODOM can only handle linear orbit motion. Eidelman and Yakimenko [35] have written the computer code SPINLIE using a Lie algebra approach. At the moment SPINLIE can handle the effects of sextupoles but cannot calculate $\vec{n}$ above second order. In all three formalisms, to reproduce the resonance structure in sufficient detail, $\vec{n}$ must be evaluated to high order in the orbital coordinates and this requires very large amounts of computing time and storage space.

In spite of the availability of analytical methods it is interesting to see if the more naive

picture of combined spin-flip and diffusion can be simulated and thereby produce a realistic description of the polarization phenomenology of a storage ring. This is the method adopted in the Monte-Carlo program SITROS ((SI)multaneous (TR)acking of (O)rbit and (S)pin motion) written by J. Kewisch at DESY in 1982 [21]. The SITROS program tracks an ensemble of electrons carrying classical spin vectors with built in orbital damping and stochastic excitation and "measures" the depolarization time τ_d by "observing" the spin diffusion. The stochastic excitations are chosen by a random number generator. The depolarization time τ_d together with the build up time τ_p from eq. (2.8) and P_∞ from eq. (2.7) leads to an estimate of the equilibrium polarization. The Monte-Carlo treatment of SITROS is the topic of this thesis and in particular this work will focus on the simulation of polarization in HERA. SITROS is up to now the only program which is able to handle all aspects of the real HERA machine. SITROS is used extensively to understand the polarization phenomenology of HERA. Several comparisons between predicted and measured polarization have been performed (section 5)[36],[8].

3 Description of the SITROS program

This section is devoted to a detailed description of the SITROS algorithm and to the presentation of tests designed to show how well SITROS represents the spin-orbit dynamics in electron storage rings.

3.1 Description of the 6×6 matrix formalism for the orbit motion

The motion of a charged particle with energy E in the presence of electric and magnetic fields $\vec{E}, \vec{B}$ is determined by the Abraham-Lorentz equation [37]:

$$\frac{d}{dt}\left(\frac{E}{c^2}\dot{\vec{r}}\right) = e\vec{E} + \frac{e}{c}\left(\dot{\vec{r}} \times \vec{B}\right) + \vec{R}_{rad},$$

where $\vec{R}_{rad}$ represents the radiation reaction force originating in the fact that a charged accelerated particle emits synchrotron radiation. In SITROS $\vec{R}_{rad}$ is represented as a sum of two terms [38][39]:

$$\vec{R}_{rad} = \vec{R}^D + \delta\vec{R}, \tag{3.1}$$

a continuous part $\vec{R}^D$ describing the average (smooth) emission [38]:

$$\vec{R}^D = -\frac{2}{3}\frac{e^2}{c^5}\dot{\vec{r}}\gamma^4\left(\ddot{\vec{r}}^2 + \frac{\gamma^2}{c^2}\left(\dot{\vec{r}}\ddot{\vec{r}}\right)^2\right)$$

which leads to damping effects and a stochastic part $\delta\vec{R}$ describing the quantum fluctuations of the radiation field. $\delta\vec{R}$ leads to an excitation of the system. In the following the assumption is made that both contributions can be treated separately. In the first step only the damping term $\vec{R}^D$ is included. In order to establish a formalism in which the dynamical variables are small so that approximations can be made, one describes the motion in coordinates following the design orbit [40][41]. The change of the independent variable time t to the pathlength s,

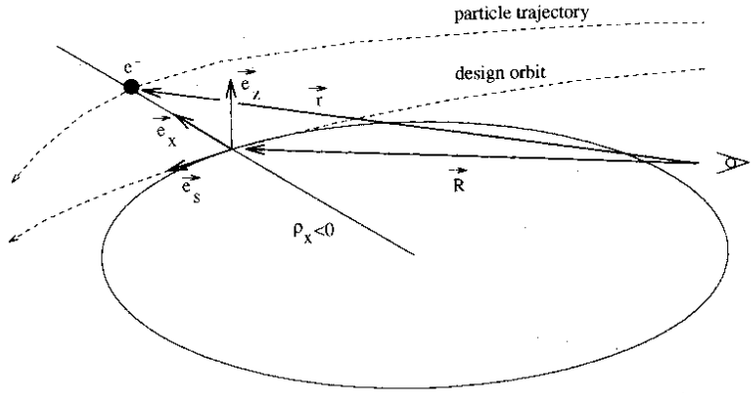

Figure 4: *Description of a particle trajectory with respect to the coordinate system moving along the design orbit*

describing the position of a particle along the design orbit (see fig. (4)) yields:

$$\frac{e}{E_0}\vec{E} + \frac{1}{\bar{\ell}'}\frac{e}{E_0}\vec{r}' \times \vec{B} - \frac{2}{3}\frac{e^2}{m_e}\gamma_0(1+\delta)^4\frac{\vec{r}'}{\bar{\ell}'^5}\left(\vec{r}'^2 - \bar{\ell}'^2\right) = \frac{1}{\bar{\ell}'}\left[\delta'\vec{r}' + (1+\delta)\left(\vec{r}'' - \frac{\bar{\ell}''}{\bar{\ell}'}\vec{r}'\right)\right] \tag{3.2}$$

with

$$\frac{d}{dt} = \frac{ds}{d\bar{\ell}}\frac{d\bar{\ell}}{dt} \quad \frac{d}{ds} = \frac{v}{\bar{\ell}'}\frac{d}{ds},$$

$\bar{\ell}$ = length of the particle trajectory, $d\bar{\ell}/dt \simeq c$, because the particles are ultrarelativistic, and $E = E_0(1+\delta), \delta = \Delta E/E_0$. The vector $\vec{r}$ and its derivative with respect to s can be represented by:

$$\begin{aligned}\vec{r} &= \vec{R} + x\vec{e}_x + z\vec{e}_z \\ \vec{r}\,' &= \frac{d\vec{R}}{ds} + \frac{dx}{ds}\vec{e}_x + x\frac{d\vec{e}_x}{ds} + \frac{dz}{ds}\vec{e}_z + z\frac{d\vec{e}_z}{ds},\end{aligned}$$

where $\vec{e}_x, \vec{e}_z, \vec{e}_s$ are unit vectors. The derivatives of $\vec{e}_x, \vec{e}_z, \vec{e}_s$ are given via the Frenet formulae in terms of the curvatures $h_x(s), h_z(s)$ of the design orbit:

$$\frac{d\vec{R}}{ds} = \vec{e}_s, \quad \frac{d\vec{e}_x}{ds} = -h_x\vec{e}_s, \quad \frac{d\vec{e}_z}{ds} = -h_z\vec{e}_s, \quad \frac{d\vec{e}_s}{ds} = h_x\vec{e}_x + h_z\vec{e}_z,$$

where $h_x(s), h_z(s)$ are defined by the design fields $B_x^{des} = E_0 h_z/e$, $B_z^{des} = -E_0 h_x/e$. In the new curved coordinate system one gets the expressions for $\vec{r}\,'$ and $\vec{r}\,''$:

$$\begin{aligned}\vec{r}\,' &= x'\vec{e}_x + z'\vec{e}_z + (1 - xh_x - zh_z)\vec{e}_s \\ \vec{r}\,'' &= (x'' + h_x - xh_x^2 - zh_xh_z)\vec{e}_x + (z'' + h_z - xh_xh_z - zh_z^2)\vec{e}_z \\ &\quad +(-2x'h_x - 2z'h_z)\vec{e}_s.\end{aligned}$$

ℓ' is given by:

$$\bar{\ell}'^2 = \vec{r}\,'^2 = 1 - 2xh_x - 2zh_z + x'^2 + z'^2 + 2xzh_xh_z + x^2h_x^2 + z^2h_z^2.$$

The electric and magnetic fields are defined with respect to the design orbit. The magnetic fields are expanded in the small coordinates x and z:

$$\begin{aligned}\frac{e}{E_0}B_x(x,z,s) &= -h_x(s) - j_x(s) + k(s)x + \bar{k}(s)z + O(2) \\ \frac{e}{E_0}B_z(x,z,s) &= h_z(s) + j_z(s) + k(s)z - \bar{k}(s)x + O(2) \\ \frac{e}{E_0}B_s(x,z,s) &= h_s(s)\end{aligned}$$

with the following abbreviations:

$$\left.\begin{array}{rll} h_x + j_x &= \frac{e}{E_0}B_z(x,z=0) & \text{horizontal dipole} \\ -h_z - j_z &= \frac{e}{E_0}B_x(x,z=0) & \text{vertical dipole} \\ h_s &= \frac{e}{E_0}B_s(x,z=0) & \text{solenoidal} \\ k &= \frac{e}{E_0}\frac{dB_z}{dz} = \frac{e}{E_0}\frac{dB_x}{dx} & \text{skew quadrupole} \\ k &= \frac{e}{E_0}\frac{dB_x}{dz} = -\frac{e}{E_0}\frac{dB_z}{dx} & \text{quadrupole} \end{array}\right\} \text{strength at } E_0. \qquad (3.3)$$

Here j_x and j_z represent additional dipole fields in the horizontal and vertical plane due to misaligned quadrupoles etc. and corrector magnets. $O(2)$ includes the sextupole terms, which are neglected in the following derivation but will be discussed later.
The electric fields, which are mainly found inside the cavities to accelerate the particles longitudinally, are given by:

$$\begin{aligned}\epsilon_x &= \frac{e}{E_0}E_x \\ \epsilon_z &= \frac{e}{E_0}E_z \qquad (3.4) \\ \epsilon_s &= \frac{e}{E_0}V_0\sin\left(\phi_0 + \frac{2\pi}{\lambda}\ell\right) = \frac{e}{E_0}V_0\left(\sin\phi_0 + \frac{2\pi}{\lambda}\ell\cos\phi_0\right) + O(2) \quad = \quad \epsilon_{s0} + \ell\epsilon_{sl} + O(2).\end{aligned}$$

ϕ_0 describes the nominal phase of the cavities, ℓ the longitudinal deviation of the particle from a particle at ϕ_0 given by $\ell = \int_0^s \bar{\ell}'ds - s$, λ is the wavelength of the RF system, the quantity L/λ is the harmonic number, where L is the circumference of the ring. As a first step one can neglect the sextupoles, the higher order multipoles, the nonlinearities of the RF field and the energy dependence of the terms in eq. (3.3) related to chromatic effects. The resulting particle motion is "linear" in the sense that the forces which the particle experiences are linear in the phase space coordinates. In this approximation for piecewise constant magnetic fields $d\vec{B}/ds = 0$ the system of the differential equations takes the form:

$$\begin{aligned}x'' &= G_x x + \bar{G}_x z + \epsilon_{s0}x' + h_s z' - h_x\delta + \epsilon_x + j_x \\ z'' &= G_z x + \bar{G}_z x + \epsilon_{s0}z' + h_s x' - h_z\delta + \epsilon_z + j_z \\ \delta' &= \epsilon_{s0} + \epsilon_s - \epsilon_{s0}(h_x x + h_z z) + \epsilon_x x' + \epsilon_z z' \qquad (3.5) \\ &\quad +C_\gamma b^2 + F_x x + F_z z + F_{x'}x' + F_{z'}z' + 2C_\gamma b^2\delta \\ \ell' &= -h_x x - h_z z\end{aligned}$$

with

$$\begin{aligned}C_\gamma &= -\frac{2}{3}\frac{e^2}{m_e}\gamma_0^3 \\ G_x &= -k - h_x^2 - 2j_x h_x + \epsilon_{s0}h_x \\ G_z &= -k - h_z^2 - 2j_z h_z + \epsilon_{s0}h_z \\ \bar{G}_x &= -\bar{k} - h_x h_z - 2j_x h_z + \epsilon_{s0}h_z \\ \bar{G}_z &= -\bar{k} - h_x h_z - 2j_z h_x + \epsilon_{s0}h_x \\ F_x &= C_\gamma\left(-2kb_x - 2\bar{k}b_z - 2h_x^2 b_x - 2h_x h_z b_z + h_x b^2\right) \\ F_z &= C_\gamma\left(-2kb_z - 2\bar{k}b_x - 2h_z^2 b_z - 2h_x h_z b_x + h_z b^2\right) \\ F_{x'} &= 2C_\gamma\left(b_x\epsilon_{s0} + b_z h_s\right) \\ F_{z'} &= 2C_\gamma\left(b_z\epsilon_{s0} - b_x h_s\right) \\ h^2 &= h_x^2 + h_z^2 \\ b_x &= h_x + j_x + \epsilon_x \\ b_z &= h_z + j_z + \epsilon_z \\ b^2 &= b_x^2 + b_z^2.\end{aligned}$$

This system of differential equations of second order in x,z and first order in ℓ,δ can be rewritten as a system of first order:

$$\vec{X}\,' = \hat{A}\vec{X} + \vec{C}$$

with $\vec{X}^T = (x, x', z, z', \ell, \delta)$,

$$\hat{A} = \begin{pmatrix} 0 & 1 & h_s & 0 & 0 & 0 \\ G_x & \epsilon_{s0} & \bar{G}_x & h_s & 0 & h_x \\ -h_s & 0 & 0 & 1 & 0 & 0 \\ \bar{G}_z & -h_s & G_z & \epsilon_{s0} & 0 & h_z \\ h_x & 0 & -h_z & 0 & 0 & 0 \\ F_x - \epsilon_{s0}h_x & F_{x'} + \epsilon_{s0} & F_z - \epsilon_{s0}h_z & F_{z'} + \epsilon_{s0} & \epsilon_{sl} & 2C_\gamma b^2 \end{pmatrix}$$

and

$$\vec{C}^T = (0, \epsilon_x + j_x, 0, \epsilon_z + j_z, 0, C_\gamma b^2 + \epsilon_{s0}). \qquad (3.6)$$

All terms containing the factor C_γ and ϵ_{s0} are dissipative terms. The F_x and F_z terms include contributions from combined function magnets. The radiation in quadrupoles is neglected.

One gets the corresponding equations for ultrarelativistic protons by setting C_γ and ϵ_{s0} to zero. In the case of electrons the cavity phases and voltages are set so that the radiative energy loss (described by the "damping term" $C_\gamma b^2$) is replenished by the cavities (described by the "acceleration term" ϵ_{s0}) in eq. (3.6). The synchrotron radiation just affects the energy deviation δ. The change of x',z' due to the photon emission with an angle of order $1/\gamma$ with respect to the particle direction is neglected. For a more rigorous treatment see [39]. The transformation of the vector $\vec{X}$ through an element can be written in the following form:

$$\vec{X}(s_1) = \hat{M}(s_1, s_0)\vec{X}(s_0) + \vec{H}(s_1, s_0) \tag{3.7}$$

with the matrices:

$$\begin{aligned} \hat{M}(s_1, s_0) &= \exp\left(\hat{A}(s_1 - s_0)\right) \equiv \sum_{n=0}^{\infty} \frac{1}{n!}\hat{A}^n(s_1 - s_0)^n \\ \vec{H}(s_1, s_0) &= \left(\sum_{n=1}^{\infty} \frac{1}{n!}\hat{A}^{n-1}(s_1 - s_0)^n\right)\vec{C} \\ &= \left(\hat{M}(s_1, s_0) - \hat{1}\right)\hat{A}^{-1}\vec{C} \end{aligned} \tag{3.8}$$

if $\det \hat{A} \neq 0$. Derivations of $\hat{M}$ for various magnet types can be found in [42]. By adding a 7th component (=1) to $\vec{X}$ one is able to combine $\hat{M}$ and $\vec{H}$ into an enlarged $\hat{M}_{7\times7}$ matrix:

$$\begin{pmatrix} \vec{X}(s_1) \\ 1 \end{pmatrix} = \hat{M}_{7\times7}(s_1, s_0)\begin{pmatrix} \vec{X}(s_0) \\ 1 \end{pmatrix} \tag{3.9}$$

with

$$\hat{M}_{7\times7}(s_1, s_0) = \begin{pmatrix} \hat{M}(s_1, s_0) & \vec{H}(s_1, s_0) \\ 0 & 1 \end{pmatrix}.$$

Introducing the periodicity condition $\vec{X}(s_1) = \vec{X}(s_0 + L) = \vec{X}(s_0)$ for a ring with circumference L one can calculate the "initial vector" of the periodic solution $\vec{X}_0(s_0)$:

$$\begin{aligned} \begin{pmatrix} \vec{X}_0(s_0) \\ 1 \end{pmatrix} &= \hat{M}_{7\times7}(s_0 + L, s_0)\begin{pmatrix} \vec{X}_0(s_0) \\ 1 \end{pmatrix} \\ \vec{X}_0(s_0) &= \left(\hat{1} - \hat{M}(s_0 + L, s_0)\right)^{-1}\vec{H}(s_0 + L, s_0) \end{aligned}$$

with $\hat{M}(s_0 + L, s_0) \neq \hat{1}$.
If the condition $\hat{M}(s_0 + L, s_0) = \hat{1}$ is fulfilled (corresponding to integer orbital "tunes") no bounded motion is possible. Using eq. (3.9) it is possible to calculate $\vec{X}_0(s)$ at each position s. $\vec{X}_0(s)$ describes the closed orbit. In practice the closed orbit determination in SITROS must include the sextupoles. The problem is then nonlinear and the periodic solution has to be found by iteration. This orbit corresponds to the trajectory of the central particle in the beam and the position $\vec{X} - \vec{X}_0$ describing synchro-betatron oscillations with respect to $\vec{X}_0$ obeys the homogeneous equation:

$$\vec{X}\,' = \hat{A}\vec{X} \tag{3.10}$$

with the solution

$$\vec{X}(s) = \hat{M}(s, s_0)\vec{X}(s_0).$$

Having removed the closed orbit from the discussion one is now in a position to look more closely at the stability of the motion and the damping behaviour. Examination of the coefficient matrix

$\hat{A}$ in eq. (3.10) shows that it can be written as the sum of two parts, $\hat{A}_0$ and $\delta\hat{A}$ [42]:

$$\begin{aligned} \hat{A}_0 &= \begin{pmatrix} 0 & 1 & h_s & 0 & 0 & 0 \\ -k - (h_x^2 + 2j_x h_x) & 0 & -\bar{k} - (h_x h_z + 2j_x h_z) & h_s & 0 & h_x \\ -h_s & 0 & 0 & 1 & 0 & 0 \\ -\bar{k} - (h_x h_z + 2j_z h_x) & -h_s & -k - (h_z^2 + 2j_z h_z) & 0 & 0 & h_z \\ h_x & 0 & -h_z & 0 & 0 & 0 \\ 0 & 0 & 0 & 0 & \epsilon_{sl} & 0 \end{pmatrix} \\ \delta\hat{A} &= \begin{pmatrix} 0 & 0 & 0 & 0 & 0 & 0 \\ \epsilon_{s0}h_x & \epsilon_{s0} & \epsilon_{s0}h_z & 0 & 0 & 0 \\ 0 & 0 & 0 & 0 & 0 & 0 \\ \epsilon_{s0}h_x & 0 & \epsilon_{s0}h_z & \epsilon_{s0} & 0 & 0 \\ 0 & 0 & 0 & 0 & 0 & 0 \\ F_x - \epsilon_{s0}h_x & F_{x'} + \epsilon_{s0} & F_z - \epsilon_{s0}h_z & F_{z'} + \epsilon_{s0} & 0 & 2C_\gamma b^2 \end{pmatrix} \end{aligned} \tag{3.11}$$

$\hat{A}_0$ can be derived from a Hamiltonian and describes purely oscillatory motion with conservation of the phase space volume [42]. $\delta\hat{A}$ contains dissipative terms which can cause the phase space volume to contract (or expand). In these coordinates the dissipation comes about because longitudinal acceleration (the terms in ϵ_{s0}) causes x' and z' to shrink and because the radiation rate depends on the energy of the particle [39]. In pure dipole fields the radiation leads to a damping of the δ coordinate (the $2C_\gamma b^2$ term in eq. (3.11)). In combined function magnets where bending and gradient fields are present the radiation can cause antidamping of the horizontal motion (F_x and F_z terms in eq. (3.11))[43].
The first step in designing a storage ring optic is to establish a situation where the motion described by the one turn transfer matrix $\hat{M}_0$, corresponding to the coefficient matrix $\hat{A}_0$, is stable.
One can always express the particle position in phase space, characterized by $\vec{X}$, as a linear combination of the six undamped eigenvectors $\vec{E}_k$ ($k = 1, 2, 3, 4, 5, 6$) of $\hat{M}_0$:

$$\vec{X} = \sum a_k \vec{E}_k,$$

where the $\vec{E}_k$ obey the relation

$$\hat{M}_0(s + L, s)\vec{E}_k = \lambda_k \vec{E}_k.$$

Stability is achieved by ensuring that the eigenvalues $|\lambda_k|$=1 [42]. In this case the λ_k come in complex conjugate pairs and can be written as $\exp(\pm i2\pi Q_k)$, where the Q_k are the fractional parts of the oscillation frequencies ("tunes") of the linear system in units of the revolution time T. The full frequencies for HERA are $Q_x \sim 47.1$, $Q_z \sim 47.2$, $Q_s \sim 0.07$.
In the corresponding eigenvalue problem for the full one turn matrix $\hat{M}(s + L, s)$ derived from the full coefficient matrix $\hat{A}$, i.e. including dissipation, it is found that the tunes already calculated are shifted slightly and acquire an imaginary part:

$$\hat{M}(s + L, s)\tilde{\vec{E}}_k = \tilde{\lambda}_k \tilde{\vec{E}}_k$$

with

$$\tilde{\lambda}_{k/k+1} = \exp(-\alpha_k \pm i2\pi Q_k) \quad , k = 1, 3, 5.$$

Then if at position s_0 one now writes the orbit coordinate in terms of the damped eigenvectors $\tilde{\vec{E}}_k$:

$$\vec{X}(s_0) = \sum \tilde{a}_k \tilde{\vec{E}}_k \tag{3.12}$$

with $\vec{E}_k(t_0) \approx \vec{E}_k$. Transporting $\vec{X}$ using $\hat{M}$ one sees that in the absence of a source of orbit excitation the coordinates would either grow or shrink exponentially depending on the sign of the α_k. Clearly all three α_k have to be positive so that the motion is intrinsically stable. The damping times of the system τ_k are given by T/α_k. The α_k can be calculated directly analytically [39] in terms of the eigenvectors $\vec{E}_k$ and $\delta\hat{A}$. For HERA the time constants are approximately τ_x =15 msec, τ_z =17 msec and τ_s =7 msec at 26.666 GeV. The damping effect can also be discussed in the framework of the Fokker-Planck equation for the phase space distribution [39].

3.2 The stochastic part of the synchrotron radiation process

The stochasticity of the radiation process leads to an excitation of the orbital and spin motion. $\delta\vec{R} = \vec{R}_{rad} - \vec{R}^D$ (eq. (3.1)) is a stochastic quantity with the properties:

$$\begin{aligned} < \delta\vec{R} > &= 0 \\ < \delta\vec{R}(s)\delta\vec{R}(s') > &= \frac{55 r_e \hbar \gamma^5}{24\sqrt{3} m_e c} \quad \frac{1}{|\rho|^3} \quad \delta(s-s'), \end{aligned}$$

where ρ describes the curvature of the trajectory [38]. The beam dimensions are the result of the equilibrium of the excitation ($\delta\vec{R}$) and the damping ($\vec{R}^D$). Using the undamped $\vec{E}_k$ instead of the damped eigenvectors $\vec{\tilde{E}}_k$ the amplitudes $\check{a}_k$ in eq. (3.12) become time dependent. Although a rigorous treatment of the combined excitation and damping is best carried out using stochastic differential equations or the Fokker-Planck equation [39], the equilibrium beam size can be derived heuristically as follows [44]:
The rate of change of the second moment of the centred amplitude distribution for a given particle ensemble $< |\check{a}_k|^2 >$ due to damping for a mode k is given by:

$$\frac{d}{dt} < |\check{a}_k|^2 >= -2\frac{\alpha_k}{T} < |\check{a}_k|^2 > . \tag{3.13}$$

The rate of change of the amplitude spread due to excitation is:

$$\frac{d}{dt} < |\check{a}_k|^2 >= \frac{1}{T} \quad \frac{55 r_e \hbar \gamma^5}{24\sqrt{3} m_e c} \quad \oint |E_{5k}|^2 \frac{1}{|\rho|^3} ds \quad = \frac{C_k}{T}, \tag{3.14}$$

where E_{5k} is the fifth component of the kth undamped eigenvector, normalized as in [44]. The equilibrium is reached for:

$$2 < |\check{a}_k|^2 >= \frac{C_k}{\alpha_k} \quad = \epsilon_k,$$

where ϵ_k is called the "mean particle emittance" of the beam for the mode k [45], describing the mean value of the single particle emittances of an ensemble (see eq. (3.30)). Using more complete treatments and assuming that the equations of motion are linear it is found that the particle distributions in phase space are Gaussian [39]. For a typical HERA optic with imperfections and corrections the mean particle emittances are $\epsilon_x \sim 8 \times 10^{-8}$ rad m, $\epsilon_z \sim 8 \times 10^{-10}$ rad m and $\epsilon_s \sim 1.6 \times 10^{-5}$ rad m at 26.666 GeV. The ratio ϵ_z/ϵ_x describes the "emittance coupling" between the x and z motion. In this case the ratio is calculated to be 1% (see also section 3.5.6).
Using the relation $\vec{X}(s_0) = \sum \check{a}_k \vec{E}_k$ and

$$< |\check{a}_k|^2 >=< |\check{a}_{k+1}|^2 > \quad , k = 1,3,5$$

the "particle distribution parameters" $< x_i x_j > (i,j = 1,2,3,4,5,6)$ at a certain position s_0 in the ring are given by [44]:

$$< x_i x_j > (s_0) = 2 \sum_{k=1,3,5} < |\check{a}_k|^2 > Re\left[E_{ik} E^*_{jk}\right] . \tag{3.15}$$

The parameters $< x_k^2 >$ denote the second moments of the Gaussian distribution functions $w(x_k)$ for the x, x', z, z', ℓ and δ motion:

$$w(x_k) = \frac{1}{\sqrt{2\pi < x_k^2 >}} \exp\left(-\frac{x_k^2}{2 < x_k^2 >}\right).$$

The quantity $\sigma_y = \sqrt{2 < y^2 >}$ $(y = x, z, s)$ (in the following the index s is identified with the index ℓ) is called the "equilibrium beam size" describing the mean value of the single particle amplitudes of an ensemble (see eq. (3.29)) under the condition that the nondiagonal elements of the matrix $< x_i x_j >$ are small. The tilt angle θ of the x-z beam profile relative to the horizontal axis can be found from:

$$\tan(2\theta) = \frac{2 < xz >}{< x^2 > - < z^2 >}. \tag{3.16}$$

θ describes the "betatron coupling" between the x and z motion introduced by systematic skew quadrupole components in the ring (see section 3.3) [46].

3.3 The representation of the nonlinear motion

So far only the linearized orbit motion has been considered. In this case the motion is completely determined by the 6×6 transfer matrices of the ring elements.
However the natural chromaticities describing the momentum dependence of the focusing in HERA are ~ -60. This would cause a strong transverse single bunch instability ("head-tail effect") [47]. Furthermore, for a fractional energy spread of $\sigma_\delta = 1 \times 10^{-3}$ at 26.666 GeV this would cause a rms tune range of 0.06 which would lead to the crossing of unstable low order orbit resonances and hence particle loss. Thus this chromatic dependence of the $\hat{A}_0$ cannot be ignored and in practice the tunes must be made δ independent by introducing sextupoles into the lattice at places where the horizontal dispersion is large. Nonlinearities above second order can be neglected at this stage of the description of the particle motion. This is justified by the strong damping of the synchrotron oscillations. The damping time corresponds to $\tau_s \sim 300$ turns in HERA which together with the stochastic excitation by quantum emission in effect means that the particles have a very short "memory".
In the presence of chromatic effects and sextupole corrections the above methods for solving linear differential equations are no longer applicable. One way to solve the problem is to track a particle through the structure using a transfer matrix formalism for the nonlinear elements and then to include nonlinearities by means of kicks. To determine particle distributions a certain number of particles representing the real particle distribution is tracked in Monte-Carlo programs. This is the approach used in SITROS.
As mentioned in eq. (3.5) the δ dependence of the fields was neglected (the terms in eq. (3.3) are evaluated at E_0). Thus in the "next order" of approximation, eq. (3.5) has to be modified to include these chromatic effects. Replacing the energy E_0 in eq. (3.3) by the energy of a particle with an energy deviation δ, the system of differential equations takes the form:

$$x'' \quad = \quad G_x x + G_x z + \frac{\epsilon_{s0}}{1+\delta} x' + \frac{h_s}{1+\delta} z' - \frac{h_x}{1+\delta}\delta + \frac{\epsilon_x + j_x}{1+\delta}$$

$$
\begin{aligned}
z'' &= G_z x + \bar{G}_z x + \frac{\epsilon_{s0}}{1+\delta} z' + \frac{h_s}{1+\delta} x' - \frac{h_z}{1+\delta}\delta + \frac{\epsilon_z + j_z}{1+\delta} \qquad (3.17)\\
\delta' &= \epsilon_{s0} + \epsilon_s - \epsilon_{s0}(h_x x + h_z z) + \epsilon_x x' + \epsilon_z z' \\
&\quad +(1+\delta)^2[C_\gamma b^2 + F_x x + F_z z + F_{x'} x' + F_{z'} z'] \\
\ell' &= -h_x x - h_z z
\end{aligned}
$$

with

$$
\begin{aligned}
C_\gamma &= -\frac{2}{3}\frac{e^2}{m_e}\gamma_0^3 \\
G_x &= -\frac{k}{1+\delta} - h_x^2 - \frac{2j_x h_x}{1+\delta} + \frac{\epsilon_{s0} h_x}{1+\delta} \\
G_z &= -\frac{k}{1+\delta} - h_z^2 - \frac{2j_z h_z}{1+\delta} + \frac{\epsilon_{s0} h_z}{1+\delta} \\
\bar{G}_x &= -\frac{\bar{k}}{1+\delta} - h_x h_z - \frac{2j_z h_x}{1+\delta} + \frac{\epsilon_{s0} h_z}{1+\delta} \\
\bar{G}_z &= -\frac{\bar{k}}{1+\delta} - h_x h_z - \frac{2j_z h_x}{1+\delta} + \frac{\epsilon_{s0} h_x}{1+\delta} \\
F_x &= C_\gamma\left(-2kb_x - 2\bar{k}b_z - 2h_x^2 b_x - 2h_x h_z b_z + h_x b^2\right) \\
F_z &= C_\gamma\left(-2kb_z - 2\bar{k}b_x - 2h_z^2 b_z - 2h_x h_z b_x + h_z b^2\right) \\
F_{x'} &= 2C_\gamma\left(b_x\epsilon_{s0} + b_z h_s\right) \\
F_{z'} &= 2C_\gamma\left(b_z\epsilon_{s0} - b_x h_s\right) \\
h^2 &= h_x^2 + h_z^2 \\
b_x &= h_x + j_x + \epsilon_x \\
b_z &= h_z + j_z + \epsilon_z \\
b^2 &= b_x^2 + b_z^2.
\end{aligned}
$$

In principle the "weak focusing" terms h_x^2, h_z^2 also have a $1+\delta$ dependence as shown in [48]. The chromatic contributions of these terms are negligible and only of interest if one wants to preserve symplecticity and thereby the phase space volume in the nondissipative case ($C_\gamma = \epsilon_{s0} = 0$). The term $1+\delta$ (in HERA at 26.666 GeV the energy spread is $\sigma_\delta = 1\times 10^{-3}$) can be treated as a constant inside a ring element. The transformation for an element is then given by a matrix which depends on the energy deviation of the individual particle.
In the derivation of eq. (3.5) the sextupole fields:

$$
B_z^{sex} = \frac{1}{2} g'\left(x^2 - z^2\right) \quad , \quad B_x^{sex} = g' x z,
$$

were not taken into account. These fields are treated in a thin lens approximation neglecting the change of x and z within a sextupole magnet. The resulting kick is applied to the particles between the transfer matrices for linear elements which are given by the solution of eq. (3.17). If there is a closed orbit deviation in a sextupole the transformation effectively acquires quadrupole, dipole and also skew quadrupole components which leads to a betatron coupling of the x and z motion and in the case of systematically distributed skew components to a twist of the equilibrium beam ellipse (eq. (3.16), see also section 5.1.1)[44].

3.4 The representation of the spin motion

The centre of mass spin motion for a single particle with the unit spin vector $\vec{S}$ is governed by the Thomas-BMT (T-BMT) equation [25][26]:

$$
\frac{d\vec{S}}{ds} = \vec{\Omega}_l \times \vec{S} \quad ,
$$

where $\vec{\Omega}_l(\vec{B}, \vec{E}, \gamma)$ given by eq. (2.3) is a function of the fields and the energy. $\vec{\Omega}_l$ can be rewritten in terms of the coordinates in the moving frame:

$$
\vec{\Omega}_l = \frac{e}{E_0}\left(a\gamma\left[l'\vec{B} - \frac{\gamma}{1+\gamma}\frac{1}{l'}(\vec{r}\,'\vec{B})\vec{r}\,' - \vec{r}\,' \times \vec{E}\right] + l'\vec{B} - \left(a\gamma + \frac{\gamma}{1+\gamma}\right)\left[\vec{r}\,' \times \vec{E}\right]\right).
$$

The derivative of $\vec{S} = S_x\vec{e}_x + S_z\vec{e}_z + S_s\vec{e}_s$ with respect to s is given by:

$$
(\vec{S})' = S_x'\vec{e}_x + S_z'\vec{e}_z + S_s'\vec{e}_s + h_x S_s\vec{e}_x + h_z S_s\vec{e}_z - (h_x S_x + h_z S_z)\vec{e}_s.
$$

The equations of spin motion with respect to the coordinate frame of the design orbit are obtained by substituting the vector $\vec{S}\,' = S_x'\vec{e}_x + S_z'\vec{e}_z + S_s'\vec{e}_s$ and the vector $\vec{\Omega} = \vec{\Omega}_l + \vec{\Omega}_r$ with $\vec{\Omega}_r = -h_z\vec{e}_x + h_x\vec{e}_z$, where $\vec{\Omega}_r$ describes the contribution to $\vec{\Omega}$ due to the rotation of the coordinate system. The T-BMT equation can then be written in the form:

$$
\vec{S}\,' = \vec{\Omega} \times \vec{S}, \qquad (3.18)
$$

where $\vec{\Omega}$ describes the precession with respect to the rotating design coordinate frame. After linearization in the orbital coordinates and by treating the δ dependence in the same way as in eq. (3.17) the following relations for the components of the vector $\vec{\Omega}$ hold:

$$
\begin{aligned}
\Omega_x &= \left(a\gamma_0 + \frac{1}{1+\delta}\right)\left(h_z + j_z + \epsilon_z + \left(k - h_z^2 - j_z h_z - \epsilon_z h_z\right) z\right. \\
&\quad \left. + \left(-\bar{k} - h_x h_z - j_z h_x - \epsilon_z h_x\right) x - \epsilon_{s0} z'\right) - a\gamma_0 h_s x' - h_z \\
\Omega_z &= \left(a\gamma_0 + \frac{1}{1+\delta}\right)\left(h_x + j_x + \epsilon_x + \left(-k + h_x^2 + j_x h_x + \epsilon_x h_x\right) x\right. \\
&\quad \left. + \left(\bar{k} - h_x h_z - j_x h_z - \epsilon_x h_x\right) z - \epsilon_{s0} x'\right) - a\gamma_0 h_s z' - h_x \\
\Omega_s &= (1+a)\frac{h_s - h_s h_x x - h_s h_z z}{\delta + 1} - \left(a\gamma_0 + \frac{1}{1+\delta}\right)\left(\epsilon_z x' - \epsilon_x z'\right). \qquad (3.19)
\end{aligned}
$$

The differential equation (3.18) can be written in matrix form:

$$
\vec{S}\,' = \hat{\Omega}\vec{S}
$$

$$
\hat{\Omega} = \begin{pmatrix} 0 & -\Omega_z & \Omega_x \\ \Omega_z & 0 & -\Omega_s \\ -\Omega_x & \Omega_s & 0 \end{pmatrix}.
$$

For constant $\vec{\Omega}$ the spin transfer matrix for an element of length Δs is given by:

$$
\hat{D} = \begin{pmatrix} \omega_x^2(1-\mathbf{C}) + \mathbf{C} & \omega_x\omega_z(1-\mathbf{C}) - \omega_s\mathbf{S} & \omega_x\omega_s(1-\mathbf{C}) + \omega_z\mathbf{S} \\ \omega_x\omega_z(1-\mathbf{C}) + \omega_s\mathbf{S} & \omega_z^2(1-\mathbf{C}) + \mathbf{C} & \omega_z\omega_s(1-\mathbf{C}) - \omega_x\mathbf{S} \\ \omega_x\omega_s(1-\mathbf{C}) - \omega_z\mathbf{S} & \omega_z\omega_s(1-\mathbf{C}) + \omega_x\mathbf{S} & \omega_s^2(1-\mathbf{C}) + \mathbf{C} \end{pmatrix} \qquad (3.20)
$$

with $\omega_{x,z,s} = \tilde{\Omega}_{x,z,s}/|\vec{\tilde{\Omega}}|$, $\mathbf{S} = \sin|\vec{\tilde{\Omega}}|$, $\mathbf{C} = \cos|\vec{\tilde{\Omega}}|$ and $\vec{\tilde{\Omega}} = \int\vec{\Omega}ds = \vec{\Omega}\cdot\Delta s$ denotes the effective rotation vector of the element of length Δs.

In analogy to the definition of the closed orbit for the orbital particle motion it is possible to find a periodic solution of eq. (3.18) on the particle closed orbit given by:

$$\vec{n}_0(s_1) = \left(\prod_i \hat{D}_i\right) \vec{n}_0(s_0) \tag{3.21}$$

with the periodicity condition $\vec{n}_0(s_1) = \vec{n}_0(s_0 + L) = \vec{n}_0(s_0)$ and the $\hat{D}_i$ describe the spin motion along $\vec{X}_0$. The solution $\vec{n}_0(s)$ defines the equilibrium polarization axis mentioned in section 2 (see also appendix A). The one turn rotation angle around $\vec{n}_0$ is obtained from the trace of the product of all matrices $\hat{D}_i$:

$$|\vec{\Omega}_{ring}| \quad = \quad 2\pi\nu' \quad = \quad \arccos\left(\frac{Tr\left(\prod_i \hat{D}_i\right) - 1}{2}\right),$$

where ν' is the fractional part of the "spin tune" ν already defined in eq. (2.5). In a flat ring ν is proportional to the energy ($\nu = a\gamma_0$). A HERA beam energy of 26.666 GeV corresponds to a spin tune $a\gamma_0 = 60.5$.

3.5 The Monte-Carlo program SITROS

In the last section the basic concepts which are needed to discuss the spin-orbit tracking algorithm of SITROS were summarized. As explained in section 2 the aim is to track electrons under the influence of linear and nonlinear fields, damping and stochastic excitation and to study the resulting spin diffusion. It is desirable to track a "large" number of particles for a sufficiently "long" time so to model the real storage ring as closely as possible. Since the integration of the T-BMT equation is very computing time consuming methods have to be found to increase the tracking speed. There are three basic components:

1. the use of carefully chosen approximations for the integration of the T-BMT equation,
2. the reduction of the number of effective elements in the ring by lumping groups of elements into sections,
3. emitting a small number of "high" energy photons ($\sim$ 300 KeV) between the sections instead of simulating the emission of a large number of "low" energy photons ($\sim$ 60 KeV).

3.5.1 A few notes on approximations of the nonlinearities in the spin motion

The rotation vector $\vec{\Omega}$ depends on the phase space coordinates of the incoming particle (eq. (3.19)) and is not piecewise constant in the orbital coordinates. Even for linear orbit motion the spin motion is nonlinear (see the sine **S** and cosine **C** terms in eq. (3.20). In SITROS the following approximations are made:

1. Dipoles have strong constant fields which lead to large phase advances of the spin vector. Only a small dependence on the phase space coordinates is introduced by the weak focusing of the magnets. Thus in good approximation one can average the phase space coordinates over the element length and calculate $\vec{\Omega}$ by using eq. (3.19). The dipole fields generated by the correction magnets and a nonzero closed orbit with respect to the centre of quadrupoles and sextupoles are also treated in this way. These fields mainly contribute to the closed orbit part $\vec{\Omega}^{co}$ of the rotation vector $\vec{\Omega}$ (see eq. (3.23)).

2. In elements with magnetic fields of higher order than dipoles (especially quadrupoles and sextupoles) the dependence of $\vec{\Omega}$ on the phase space coordinates is very strong. But the phase advance is very small. Under this condition the rotations of the spin vector around the coordinate axes commute and can be integrated independently. In the absence of longitudinal fields the relation $\int \vec{\Omega} ds = (a\gamma + 1)(-\Delta z', \Delta x', 0)$ holds. This relation is a solution of the T-BMT equation, remains valid up to arbitrarily high order in the orbital coordinates and does not rely on the approximations leading to eq. (3.19). The problem is thus reduced to the determination of the orbital motion. These fields mainly contribute to the the transformation matrix $\hat{\tilde{M}}^{spin}_{sec}$ which will be defined in eq. (3.23) while introducing the dependence of $\vec{\Omega}$ on the coordinates.

3.5.2 Transformation of the phase space coordinates

A central point in the description of the algorithm is the concept of "sectioning". The basic idea is to divide the ring structure into sections and to reduce the number of elements (typically a few 1×10^3) to a relatively small number of "section elements" (< 100), which represent the transformation through the collected elements in a section up to second order. The advantage of this method is a gain in computing speed of nearly two orders of magnitude reducing the needed computing time for a SITROS run to an acceptable level (see appendix B). The disadvantages and limitations of the sectioning method will be discussed in detail.
The ring is divided into N_S sections (currently 16 or 32). Each section is described by a transformation which contains the nonlinearities up to second order. The particle trajectory is described by a $6 + 21$ dimensional vector $\vec{\tilde{X}}$ constructed from the 6 dimensional vector $\vec{X}$ and 21 quadratic combinations of the phase space coordinates with respect to the closed orbit:

$$\vec{\tilde{X}}^T = (x, x', z, z', \ell, \delta, x^2, xx', xz, ..., \ell^2, \ell\delta, \delta^2)$$

The transformation of $\vec{X}$ is given by a 6×27 matrix $\hat{\tilde{M}}^{orbit}_{sec}$:

$$\vec{X}^{\sim} = \hat{M}^{orbit}_{sec} \vec{X}. \tag{3.22}$$

In order to determine the linear (columns 1-6) and the nonlinear (columns 7-27) parts of $\hat{\tilde{M}}^{orbit}_{sec}$ for a section, a simple ray tracing method is used in which the closed orbit particle and 72 particles with specially chosen starting points are tracked with respect to the closed orbit and their output coordinates are noted.
Twelve starting vectors $\vec{X}$ are needed to determine the linear and the quadratic coefficients for $x, x^2, \ldots, \delta, \delta^2$ of the matrix $\hat{M}^{orbit}_{sec}$:

$$\begin{array}{rccccccc} i = & 1 \to 2 & & 3 \to 4 & & 9 \to 10 & & 11 \to 12 \\ \vec{X}_i = & \begin{bmatrix} \pm\sigma_x \\ 0 \\ 0 \\ 0 \\ 0 \\ 0 \end{bmatrix} & , & \begin{bmatrix} 0 \\ \pm\sigma_{x'} \\ 0 \\ 0 \\ 0 \\ 0 \end{bmatrix} & \cdots\cdots & \begin{bmatrix} 0 \\ 0 \\ 0 \\ 0 \\ \pm\sigma_s \\ 0 \end{bmatrix} & , & \begin{bmatrix} 0 \\ 0 \\ 0 \\ 0 \\ 0 \\ \pm\sigma_\delta \end{bmatrix} \end{array}$$

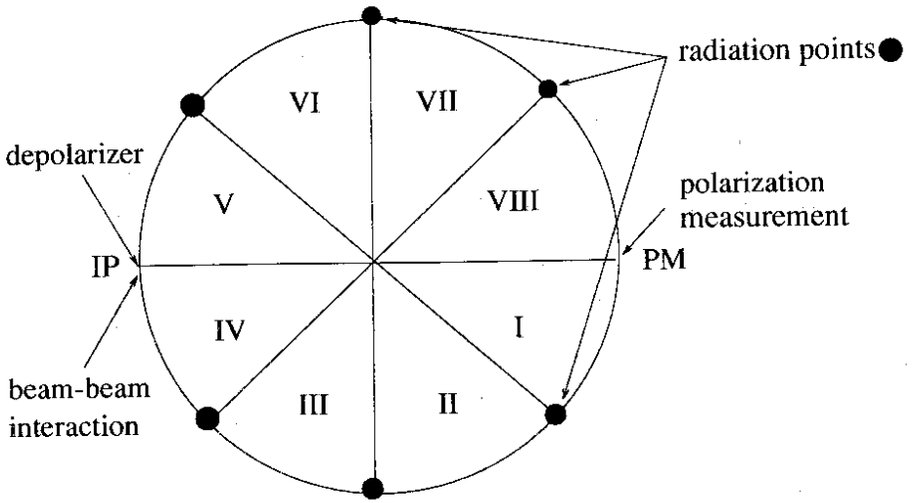

Figure 5: *Example for a partition of the HERA ring. At "PM" the tracking data are analyzed. At the interaction point "IP" a time dependent depolarizing field can be added (see section 5.3) and the beam-beam interaction can be simulated. At the "radiation points" photons with randomly chosen energy are emitted to simulate the stochastic excitation (see section 3.5.5)*

and sixty ($4\binom{6}{2}$) starting vectors:

$$\begin{array}{rccccc} i = & 1 \to 4 & & 5 \to 8 & & 53 \to 56 \quad 57 \to 60 \\ \vec{X}_i = & \begin{bmatrix} \pm\sigma_x \\ \pm\sigma_{x'} \\ 0 \\ 0 \\ 0 \\ 0 \end{bmatrix}, & \cdots & \begin{bmatrix} \pm\sigma_x \\ 0 \\ \pm\sigma_z \\ 0 \\ 0 \\ 0 \end{bmatrix} & \cdots\cdots & \begin{bmatrix} 0 \\ 0 \\ 0 \\ \pm\sigma_{z'} \\ 0 \\ \pm\sigma_\delta \end{bmatrix}, \begin{bmatrix} 0 \\ 0 \\ 0 \\ 0 \\ \pm\sigma_s \\ \pm\sigma_\delta \end{bmatrix} \end{array}$$

which are used to determine the mixed coefficients. The $\sigma_k^2/2 = < x_k^2 >$ are the second moments of the Gaussian distributions of the x, x', z, z', ℓ and δ coordinate of the linear theory (see eq. (3.15)) and they therefore represent a typical particle position in the beam at the beginning of a section.
All coefficients are calculated by taking the appropriate differential quotients of the starting vectors $\vec{X}$ and the corresponding transformed vectors $\vec{X}^{\sim}$. The coefficients of the linear part can be checked against the coefficients of the transfer matrices derived from the linear calculation. The same method is used for the determination of the coefficients of the transformation matrix $\hat{M}_{sec}^{spin}$ for the spin motion. An example for a ring with $N_S = 8$ sections $N_R = N_S - 2$ radiation points is given in fig. (5).

3.5.3 Transformation of the spin vector

In SITROS the spin vector $\vec{S}$ of a particle is described by a 3 component vector $\vec{S} = (S_x, S_z, S_s)$. This vector is transformed by the matrix $\hat{D}$ (eq. (3.20)) which depends on $\vec{\Omega}$ which itself is a nonlinear function of the phase space coordinates. Limiting the influence of the particle

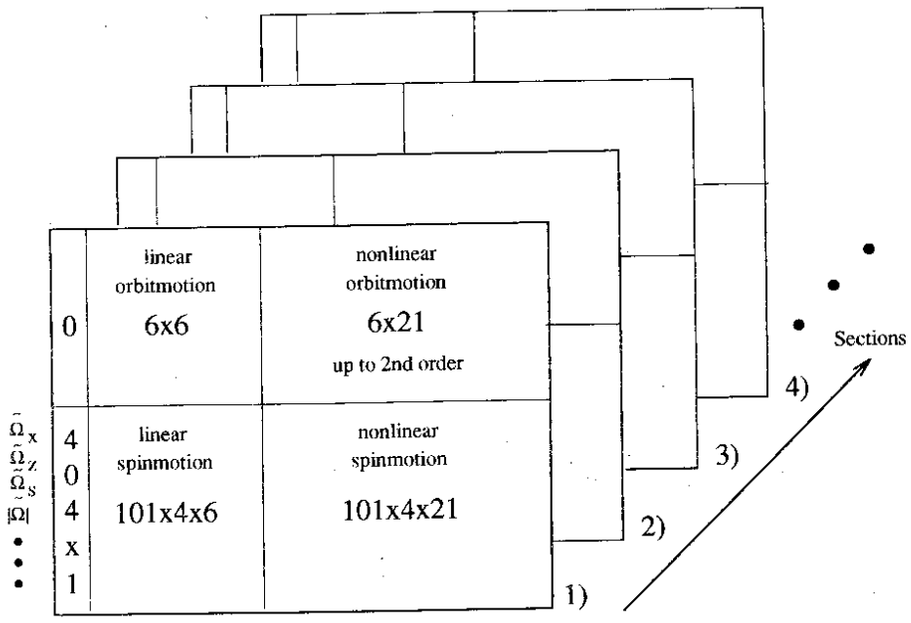

Figure 6: *Structure of the matrices representing the sections for the orbital and spin tracking. The orbital tracking is performed with respect to the closed orbit and the rotation vector $\vec{\Omega}_{sec}$ is determined with respect to the design orbit*

trajectory to second order terms one can describe the rotation $\vec{\Omega}_{sec}$ for a section by a 4×27 matrix $\hat{M}_{sec}^{spin}$:

$$\begin{pmatrix} \tilde{\Omega}_x \\ \tilde{\Omega}_z \\ \tilde{\Omega}_s \\ |\vec{\Omega}| \end{pmatrix}_{sec} = \begin{pmatrix} \tilde{\Omega}_x^{co} \\ \tilde{\Omega}_z^{co} \\ \tilde{\Omega}_s^{co} \\ |\vec{\Omega}^{co}| \end{pmatrix}_{sec} + \hat{M}_{sec}^{spin} \vec{X}, \tag{3.23}$$

where $\vec{\Omega}_{sec}^{co}$ represents the rotation vector of the particle on the closed orbit.
For a detailed analysis of the resonance structure given by the conditions of eq. (2.9) it is necessary to calculate the equilibrium polarization for a certain energy range covering several resonances. Normally the range between two integer values of spin tune which are ~ 440 MeV apart is appropriate (see section 4).
In SITROS spin vectors are tracked simultaneously at different beam energies by including these vectors in an enlarged transformation matrix. For the spin tracking at these energies SITROS uses the particle orbits for the middle point in the chosen energy interval because the change in the orbital motion of the particles is negligible for an energy range of 440 MeV (the variation of the radiated power is of the order of a few percent and the tune change is a second order effect). Using eq. (3.22) for the central energy and eq. (3.23) for 101 energies one can construct a matrix consisting of $(6 + 4 \cdot 101) \times (1 + 27)$ elements (see fig. (6)).

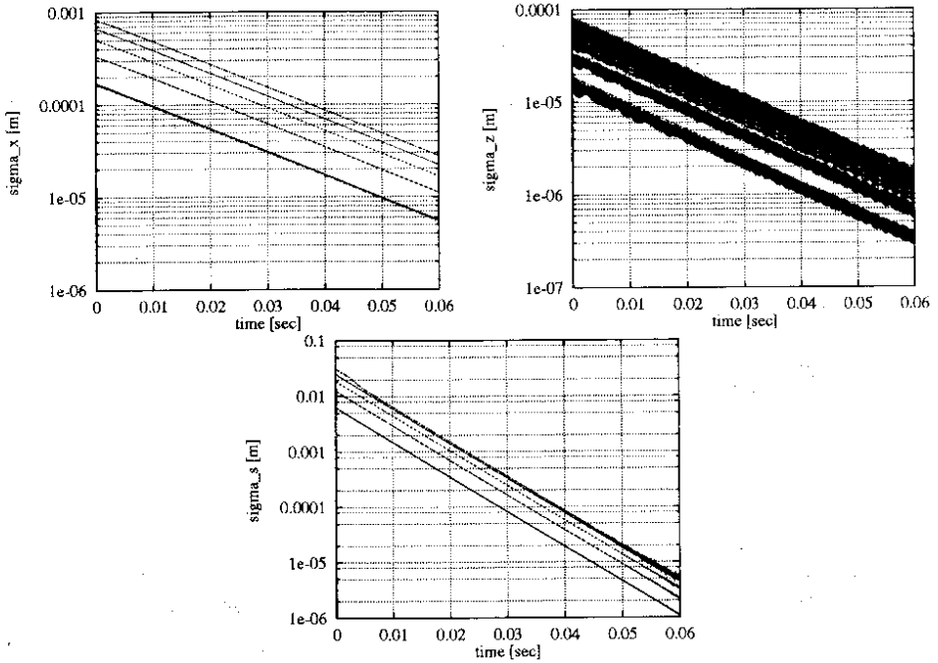

Figure 7: *Determination of the damping times τ_y $(y = x, z, s)$ for five starting Gaussian particle distributions with $1, 2, 3, 4, 5\sigma_y^{lin}$, where the σ_y^{lin} are given by linear theory. The beam excitation by quantum emission is switched off in the simulation. The ratio of σ_z and σ_x corresponds to 2% emittance coupling*

3.5.4 Problems induced by approximations

Even if no damping is included, the quadratic matrices $\hat{\tilde{M}}_{sec}^{orbit}$ are nonsymplectic. This can lead to an artificial growth of the phase space volume covered by the particles. To be sure that this effect is insignificant one has to check the damping times for the modes k which should be close to the values of τ_k expected from the linear theory. In fig. (7) the results of a simulation without beam excitation by quantum emission for a HERA optic at 26.666 GeV and an RF voltage of 150 MV with 2% emittance coupling between the x and z mode are shown. The curves correspond to starting Gaussian distributions of 500 particles with different mean beam sizes $(1\sigma_y^{lin} \rightarrow 5\sigma_y^{lin}, y = x, z, s)$, which are given by linear theory. The method to determine the beam sizes in the simulation is described in section 3.5.6. The damping times calculated from the simulation are $\tau_x = 17.5$ msec, $\tau_z = 15.1$ msec and $\tau_s = 7.0$ msec. These values are identical to the damping times given by linear theory within the expected precision. In addition the slope of the "straight" lines in logarithmic scaling does not change with increasing variance of the starting distribution, although one expects that the nonsymplecticity gets more important for particles with large amplitudes. One can conclude that for the phase space region covered in the simulation the nonsymplecticity of the matrices does not lead to an artificial excitation or damping.

For the determination of the matrices $\hat{M}_{sec}^{spin}$ another problem occurs. The calculation of $\vec{\tilde{\Omega}}_{sec}$

for a section is done by using the spinor formalism. For a single element of length Δs with the rotation vector $\vec{\tilde{\Omega}} = \phi_{\tilde{\Omega}} \vec{e}_{\tilde{\Omega}}$, where $\vec{e}_{\tilde{\Omega}}$ is a unit vector and $\phi_{\tilde{\Omega}}$ denotes the rotation angle, the spinor transformation is given by [28]:

$$\begin{aligned} \hat{M}^{spinor} &= \exp\left(-\frac{1}{2} i (\vec{\hat{\sigma}} \cdot \vec{e}_{\tilde{\Omega}}) \phi_{\tilde{\Omega}}\right) \\ &= \hat{I} \cos\left(\frac{\phi_{\tilde{\Omega}}}{2}\right) - i (\vec{\hat{\sigma}} \cdot \vec{e}_{\tilde{\Omega}}) \sin\left(\frac{\phi_{\tilde{\Omega}}}{2}\right), \end{aligned} \tag{3.24}$$

where the $\vec{\hat{\sigma}} = (\hat{\sigma}_x, \hat{\sigma}_z, \hat{\sigma}_s)$ are the 2×2 Pauli spin matrices and $\hat{I}$ is the unit matrix. The transformation of a string of elements is obtained by multiplying the corresponding 2×2 matrices. The angle and the direction of the resulting rotation vector are calculated to be:

$$\begin{aligned} \cos\left(\frac{\phi_{\tilde{\Omega}_{sec}}}{2}\right) &= \frac{1}{2} Tr\left(\hat{M}_{sec}^{spinor}\right) \\ \vec{e}_{\tilde{\Omega}_{sec}} &= \left[\frac{i}{2} \sin\left(\frac{\phi_{\tilde{\Omega}_{sec}}}{2}\right)\right] Tr\left(\vec{\hat{\sigma}} \hat{M}_{sec}^{spinor}\right). \end{aligned}$$

In SITROS the transformation in eq. (3.24) can be represented by 4×4 matrices with real coefficients:

$$\begin{pmatrix} \xi_1 \\ \xi_2 \\ \xi_3 \\ \xi_4 \end{pmatrix} = \begin{pmatrix} \mathbf{C} & -\mathbf{S}_x & -\mathbf{S}_z & -\mathbf{S}_s \\ \mathbf{S}_x & \mathbf{C} & -\mathbf{S}_s & \mathbf{S}_z \\ \mathbf{S}_z & \mathbf{S}_s & \mathbf{C} & -\mathbf{S}_x \\ \mathbf{S}_s & -\mathbf{S}_z & \mathbf{S}_x & \mathbf{C} \end{pmatrix} \begin{pmatrix} \xi_1 \\ \xi_2 \\ \xi_3 \\ \xi_4 \end{pmatrix} \tag{3.25}$$

with

$$\mathbf{C} = \cos\left(\frac{\phi_{\tilde{\Omega}}}{2}\right) \quad , \quad \begin{pmatrix} \mathbf{S}_x \\ \mathbf{S}_z \\ \mathbf{S}_s \end{pmatrix} = \sin\left(\frac{\phi_{\tilde{\Omega}}}{2}\right) \vec{e}_{\tilde{\Omega}}. \tag{3.26}$$

The starting vector $\vec{\xi}^T = (1, 0, 0, 0)$ is transformed through the string of elements using the matrices given by eq. (3.25). This starting condition enables $\vec{\tilde{\Omega}}_{sec}$ to be extracted directly from the transformed vector using eq. (3.26). The matrix $\hat{\tilde{M}}_{sec}^{spin}$ is then calculated with the ray tracing method just described.

How good is the approximation by the matrix $\hat{\tilde{M}}_{sec}^{spin}$?
This depends strongly on the fractional part ν'_{sec} of the integral spin tune of a given section. If the condition $|\vec{\tilde{\Omega}}_{sec}|/2\pi = n$, n =integer, corresponding to $\nu'_{sec} = 0$ is fulfilled, the $S_{x,z,s}$ terms in eq. (3.25) vanish for the resulting transformation through a section. This leads to a situation where nonlinear terms higher than second order in the initial phase space coordinates become important. (In the following discussion the index sec will be omitted.) Fig. (8) shows the difference between $\tilde{\Omega}_y$ and the closed orbit contribution $\tilde{\Omega}_y^{co}$ normalized with $\tilde{\Omega}_y^{co}$ $(y = x, z, s)$ for one selected section. In fig. (8, Top) the fractional part of the spin tune is $\nu' = 0.00037$ illustrating that it is not sufficient to approximate the components of $\vec{\tilde{\Omega}}$ by a polynomial of second order in the initial x' and z' phase space coordinates. In the second case (fig. (8, Bottom)) ν' is near the half integer $(\nu' = 0.40851)$. The approximation by parabolas remains valid for a large fraction of the phase space. This leads to the conclusion that the ring has to be divided into sections with ν' near the half integer. If this is done the matrices $\hat{\tilde{M}}^{spin}$ used for the determination of $\vec{\tilde{\Omega}}$, which are calculated for "typical" particles at one σ_y (see section 3.5.2), provide normally a good approximation over a large fraction of the phase space.

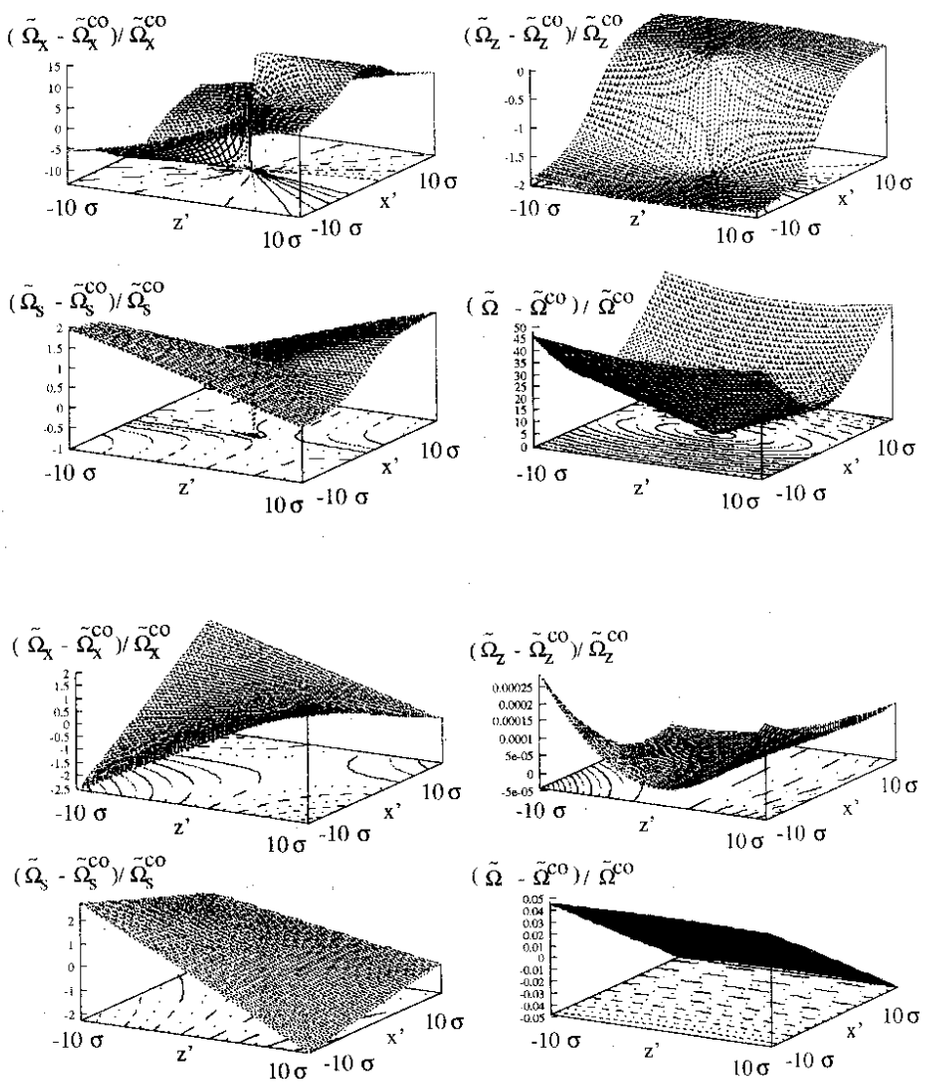

Figure 8: *Dependence of the difference between $\tilde{\Omega}_y$ and the closed orbit contribution $\tilde{\Omega}_y^{co}$ normalized with $\tilde{\Omega}_y^{co}$ ($y = x, z, s$) on the initial phase space coordinates x' and z' for one selected section,* Top*: with a fractional part of the spin tune $\nu' = 0.00037$,* Bottom*: with a fractional part of the spin tune $\nu' = 0.40851$ ($\tilde{\Omega}$ denotes the modulus of $\vec{\tilde{\Omega}}$)*

3.5.5 Excitation by quantum emission

In SITROS the stochastic photon emission is simulated by applying a single large random energy change $\Delta\delta$ to the relative energy δ of each particle at the beginning of each section (see "radiation points" in fig (5)). The energy changes $\Delta\delta$ are chosen from a centred Gaussian distribution denoted as $f(\eta)$ with unit variance, where η is a random variable. The tails of $f(\eta)$ are cut off at n in units of the variance (n denotes the "cut parameter"). The cut is introduced because the tails of the Gaussian distribution cause the emission of photons with energies far beyond the critical photon energy resulting in an unphysical excitation of the particle motion. Each energy change $\Delta\delta$ can be written in the form $K\eta$, where K is called the "excitation strength". The first nonvanishing moment $K^2 < \eta^2 >$ of the excitation distribution $Kf(\eta)$ needed to reproduce the correct beam dimensions, for example given by eq. (3.15)), can be determined in two ways:

1. Ignoring the small feedback from the x and z motion the change of the energy amplitude spread $< a^2 >$ with time is given by:

$$\frac{d}{dt} < a^2 > \simeq \frac{1}{T} N_R K^2 < \eta^2 >,$$

where N_R is the number of radiation points, K the excitation strength, $< \eta^2 >$ the second moment of the centred normalized random distribution and T the revolution time. From eq. (3.13) for the equilibrium state one has:

$$\begin{aligned} < a^2 > &= \frac{1}{2T} \tau_s N_R K^2 < \eta^2 > = 2 < \delta^2 > \\ K &= 2\sqrt{< \delta^2 >} \sqrt{\frac{T}{\tau_s} \frac{1}{< \eta^2 >}} \quad \frac{1}{\sqrt{N_R}}. \end{aligned} \tag{3.27}$$

For a Gaussian random distribution with unit variance with tails cut off at n the second moment $< \eta^2 >$ is given by (see fig. (9)):

$$< \eta^2 > = 1 - \frac{n}{\sqrt{2}} \exp\left(-n^2/2\right) / \frac{\sqrt{\pi}}{2} \Phi\left(\frac{n}{\sqrt{2}}\right), \tag{3.28}$$

where Φ is the error function[49].

2. The excitation strength K is varied during the tracking and the simulated bunch length at PM (see fig. (5)) is adjusted empirically using a "gradient method" and the step size is scaled with $|\sigma_s - \sigma_s^{lin}|$, where σ_s is the simulated (see section 3.5.6) and σ_s^{lin} is the longitudinal equilibrium beam size determined by eq. (3.15). Fig. (10, Left) gives an example for the adjustment of K in the presence of fourteen radiation points ($N_R = 14$) corresponding to sixteen sections. The tails of $f(\eta)$ are cut off at $n = 1$. All particles are started on the closed orbit. When the simulated bunch length σ_s reaches the equilibrium value corresponding to the initially chosen K value ($K = 0$ and $K = 6.9 \times 10^{-5}$) and if σ_s is not yet equal to the predicted σ_s^{lin} K is changed and the process is repeated. After a fixed time which is given by the damping time of the energy oscillations $\tau_s \sim 7$ msec (330 turns) it is assumed that the system is again in equilibrium and σ_s is again checked against σ_s^{lin}. As can be seen K converges to $K = 3.5 \times 10^{-5}$ for both starting conditions. This result is in agreement with the K value calculated using eq. (3.27) which is denoted as "$K(N_R = 14)$" in fig. (10, Left).

In fig. (10, Right) the solid line describes the excitation value K calculated for different numbers N_R of radiation points using eq. (3.27). The spots correspond to the simulated values obtained

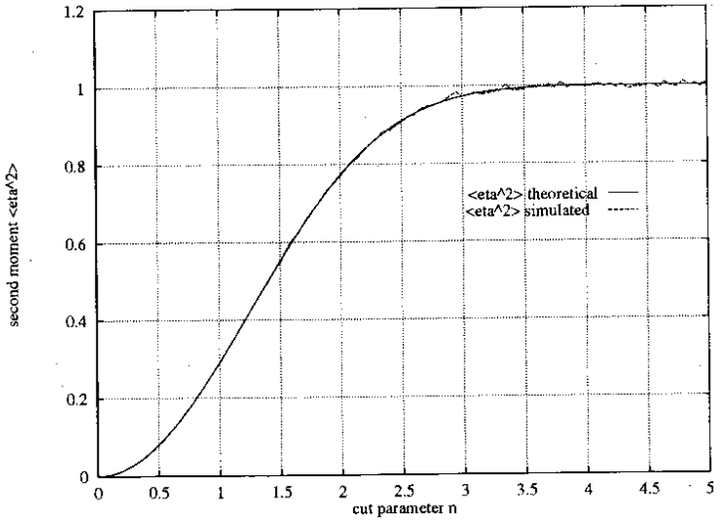

Figure 9: *Analytical (eq. (3.28)) and simulated result using the random number generator "RANNOR" [50] for the second moment of a normalized Gaussian distribution with unit variance for different cut parameters n*

using the second method. The results of the analytical and the empirical method are in good agreement showing the validity of the simple model described by eq. (3.27).
For a typical run with $N_R = 14$, $f(\eta)$ cut off at $n = 1$, $\tau_s = 7.15$ msec, $< \delta^2 >= 4.2 \times 10^{-7}$, K is equal to 3.5×10^{-5}. The second moment $K < \eta^2 >= 1.1 \times 10^{-5}$ corresponds to an rms energy change of ~300 KeV at 26.666 GeV and a maximum of ~900 KeV, which is large compared with the critical photon energy ~60 KeV. A cut off at $n = 3$ would cause maximum photon energies of ~ 2 MeV. After the adjustment of the bunch length SITROS normally reaches the linearly predicted beam sizes in the x and z direction automatically. The fact that all three beam sizes acquire their correct values simultaneously is a confirmation that the feed through of energy oscillations into the transverse motion expected from the $\delta - x$, $\delta - z$ coupling terms in the 6×6 orbit transformation is well simulated in SITROS even with the limited number of radiated photons per turn. Otherwise one has to readjust the sections in a way that the one turn integral in eq. (3.14) is represented in a correct way by the radiation points. If the lattice is periodic in the arcs this requirement is easy to fulfil. As shown in fig. (10, Right) simulations have been performed for different numbers of radiation points N_R leading to the conclusion that the emission of a limited number of "high energy" photons has no significant influence on the simulation of the orbital motion.

3.5.6 Simulation of the beam sizes

Another way to check the tracking algorithm is to observe the way the beam sizes reach equilibrium for an ensemble in which all N particles start on the closed orbit. For this one chooses a position s_0 in the lattice (s_0 =PM, see fig. (5)), where the dispersion functions D_x and D_z and the beam ellipse twist are small and one defines the beam size σ_y ($y = x, z, s$) to be the

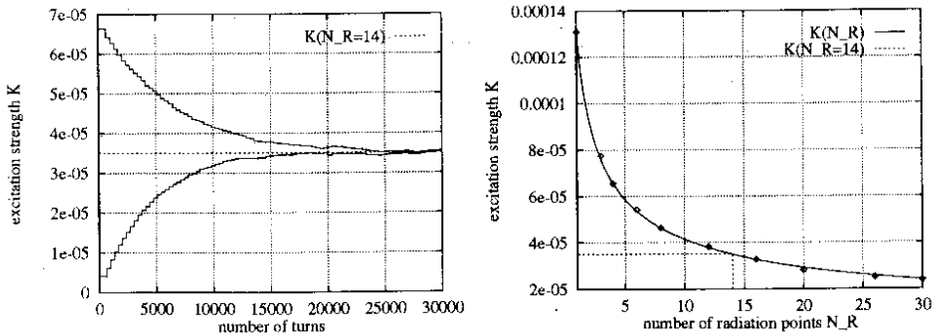

Figure 10: Left*: Adjustment of the excitation strength K in the presence of fourteen radiation points ($N_R = 14$) for two different initial K values $K = 0$ or $K = 6.9 \times 10^{-5}$ respectively. The time step for the change of K is taken to be the damping time of the energy oscillations $\tau_s = 7$ msec corresponding to 330 turns. The dashed line represents the analytical result given by eq. (3.27),* Right*: The dots describe the adjusted K for different numbers of chosen radiation points N_R and the solid line the analytical result derived from eq. (3.27)*

rms amplitude of the ensemble:

$$\sigma_y = \sqrt{\frac{1}{N}\sum_i^N a_{y_i}^2} \quad = \sqrt{< a_y^2 >} \tag{3.29}$$

where the amplitudes a_{y_i} are the quantities $a_{y_i} = \sqrt{\beta_y \epsilon_{y_i}}$ and the ϵ_{y_i} are the single particle emittances [51]:

$$\begin{aligned} \epsilon_{x_i} &= \gamma_x {x_i}^2 + 2\alpha_x x_i x_i' + \beta_x {x_i'}^2 \\ \epsilon_{z_i} &= \gamma_z {z_i}^2 + 2\alpha_x z_i z_i' + \beta_z {z_i'}^2 \\ \epsilon_{s_i} &= \gamma_s {\ell_i}^2 + 2\alpha_s \ell_i \delta_i + \beta_s {\delta_i}^2. \end{aligned} \tag{3.30}$$

α_y, β_y, γ_y are the optical functions of the linear machine at the point s_0. One then expects, assuming the validity of a simple one dimensional diffusion model with damping and noise [52], that $\sigma_y(t)$ grows asymptotically in time like:

$$\sigma_y(t) = \sigma_y^{lin} \sqrt{1 - \exp\left(-2\frac{t}{\tau_y}\right)}, \tag{3.31}$$

where τ_y is the damping time of the mode y and σ_y^{lin} is taken from linear theory. Fig. (11) illustrates the comparison between simulation and theory for an ensemble of N =1000 particles and it is again seen that SITROS produces the expected results. After a few hundred turns the equilibrium distributions are reached for all modes. In SITROS typically 5×10^3 turns are tracked to establish the beam equilibrium. To illustrate the shape of the particle distributions in the equilibrium state for a typical HERA optic with chromaticity and sextupole correction turned on the phase space with 1000 particles was projected onto the (x, x'), (z, z'), (ℓ, δ) plane after 5000 turns corresponding to 15 damping times τ_s. The distributions were histogrammed in 50 channels to show the form of the distribution functions. As can be seen in fig. (12, Right) the distributions are close to Gaussians in form. The given ellipses (1σ,2σ) in fig. (12, Left) correspond to the beam sizes σ_y which means that the variances of the fitted Gaussian distributions are smaller by a factor $\sqrt{2}$.

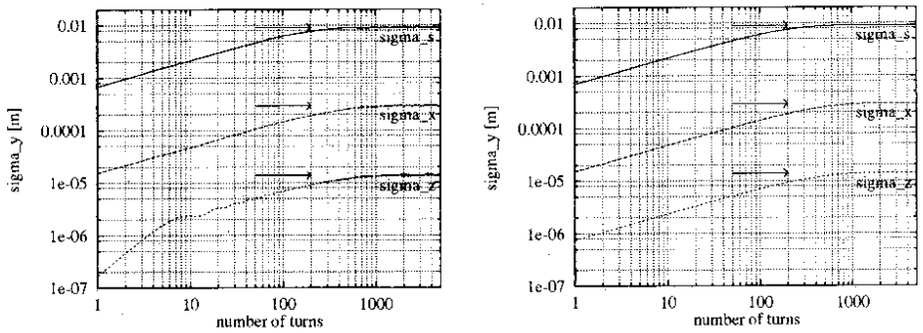

Figure 11: *Change of σ_y with time:* Left*: The simulation uses an ensemble of N =1000 particles which are started on the closed orbit. The ensemble is tracked for 5000 turns corresponding to ~ 0.1 sec in the presence of damping and noise,* Right*: The analytical result given by eq. (3.31). The arrows denote the equilibrium values σ_y^{lin})*

3.5.7 Calculation of the equilibrium polarization

Under the assumption that the depolarization process can be described by an exponential the polarization build up process $P_{\tau_{eff}}(t)$ is given by:

$$P_{\tau_{eff}}(t) = P_{eff}\left(1 - \exp\left(-\frac{\tau_p + \tau_d}{\tau_p \tau_d} t\right)\right). \tag{3.32}$$

with

$$\begin{aligned} P_{eff} &= P_\infty \frac{1}{1 + (\tau_p/\tau_d)} \\ \tau_{eff} &= \frac{\tau_p \tau_d}{\tau_p + \tau_d}, \end{aligned} \tag{3.33}$$

where P_∞ and τ_p are given by eq. (2.7,2.8). Fig. (13) illustrates the typical interplay between the spin diffusion process and polarization build up for the case where P_∞ determined by eq. (2.7) is P_∞=90% and the polarization build up time τ_p given by eq. (2.8) is τ_p=2000 sec at 28 GeV in HERA. Assuming a depolarization time of τ_d=3600 sec the equilibrium polarization P_{eff} in eq. (3.33) is calculated to be P_{eff}=57%. Since, as can be seen, it takes $\sim 1 \times 10^8$ turns to reach P_{eff}, it is not possible to simulate the system until the polarization equilibrium is reached. Instead SITROS is used to estimate the depolarization time τ_d by tracking a particle ensemble (typically N =50) over a few thousand turns (typically 10 betatron damping times) starting in the orbital equilibrium state and with all spins parallel to the $\vec{n}_0$-axis. The asymptotic polarization P_{eff} is then extracted from eq. (3.33).
The polarization $P_{\tau_d}(t_1)$ with respect to the $\vec{n}_0$-axis of an ensemble of particles at a certain time t_1 is given by the ensemble average:

$$P_{\tau_d}(t_1) = P_\infty \frac{1}{N} \sum_{i=1}^{N} \vec{S}_i(t_1) \cdot \vec{n}_0.$$

The decay of P_{τ_d} with time is represented by:

$$P_{\tau_d}(t) = P_\infty \exp\left(-\frac{t}{\tau_d}\right).$$

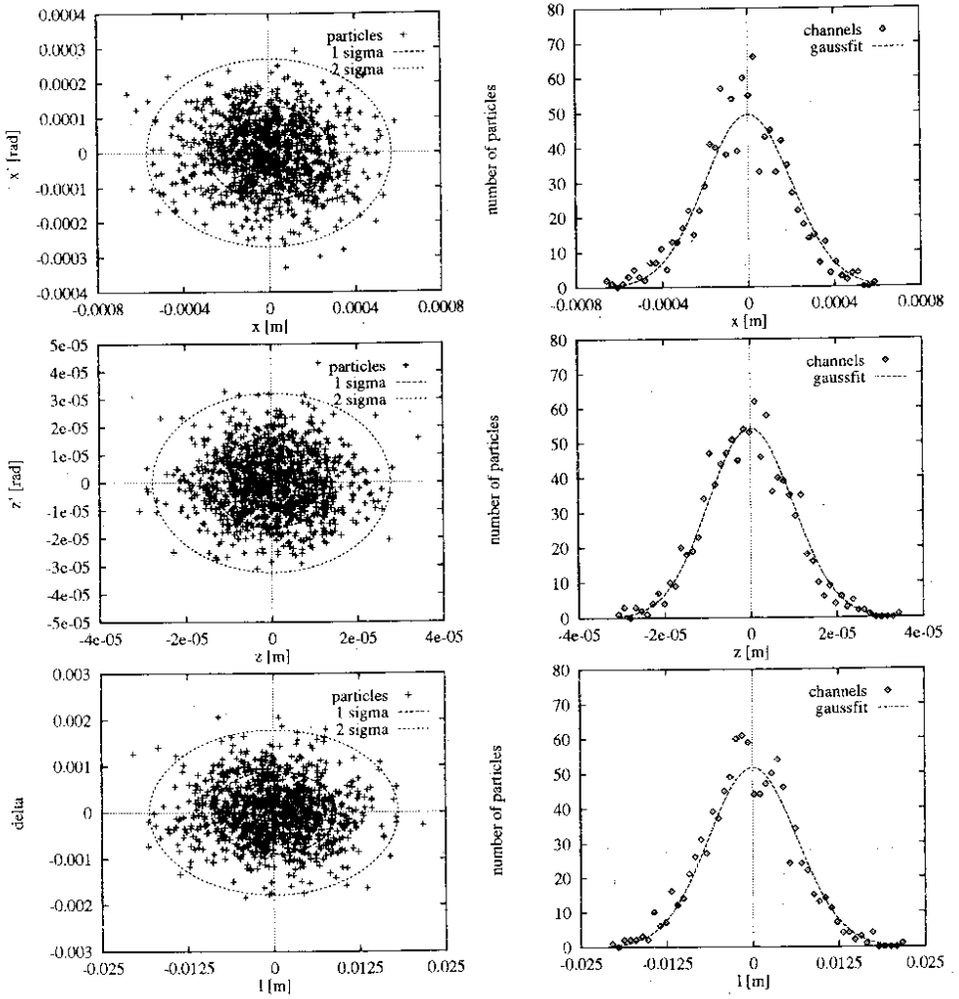

Figure 12: Left*: Phase space projections for N =1000 particles onto the (x, x'), (z, z'), (ℓ, δ) plane,* Right*: Particle distribution functions for x, z, ℓ*

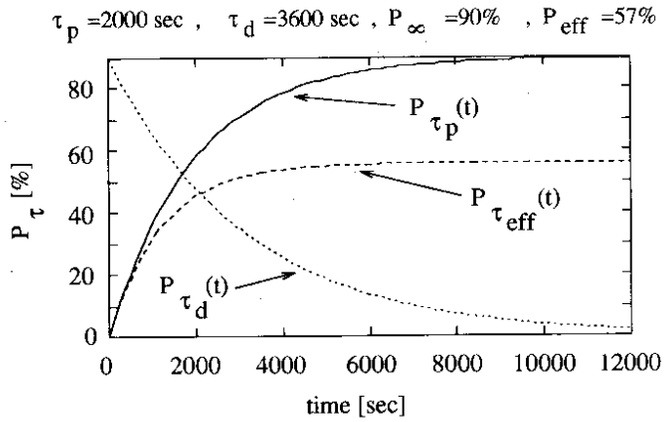

Figure 13: *Illustration of the effective polarization build up process $P_{\tau_{eff}}$ in the presence of an exponential depolarization process P_{τ_d} for a HERA optic with one rotator pair at an energy of 28 GeV*

One can determine $1/\tau_d$ using the relation:

$$-\frac{1}{\tau_d}(t_1) = \frac{\log(P_{\tau_d}(t_1)) - \log(P_{\tau_d}(t_0))}{t_1 - t_0}.$$

Fig. (14) shows the variation of the quantity $\log(P_{\tau_d}(t)/P_\infty)$ with time using time steps of $\sim 21\mu$sec starting all spins parallel to the $\vec{n}_0$-axis ($\log(P_{\tau_d}(t_0)/P_\infty = 0)$ at $t_0 = 0.11$ sec for a typical run. The overall $1/\tau_d$ is obtained from the gradient which is calculated by a one-parameter fit to the values $(1/\tau_d)(t_i)$. The fluctuations in fig. (14) are due to the fact that one is dealing with a stochastic process applied to a finite number of particles. The rms error on this estimate of $1/\tau_d$ is:

$$\Delta\left(\frac{1}{\tau_d}\right) = \sqrt{<\left(\frac{1}{\tau_d}\right)^2> - <\left(\frac{1}{\tau_d}\right)>^2},$$

where the brackets denote averaging over the number of samples (see $\pm\sigma$ in fig. (14)). The error of the extrapolated P_{eff} is calculated to be:

$$\Delta\left(P_{eff}\right) = P_\infty \frac{\tau_p}{\left(1 + (\tau_p/\tau_d)\right)^2} \quad \Delta\left(\frac{1}{\tau_d}\right). \tag{3.34}$$

By tracking a larger number of particles this error decreases approximately with $1/\sqrt{N}$. The numerical result for the example with $N = 50$ is $1/\tau_d = (2.8 \pm 0.25) \times 10^{-4}$ sec^{-1} and therefore $P_{eff} = 57 \pm 2\%$. It should be mentioned, that from the fact that the projection $(1/N)\sum_i \vec{s}_i \cdot \vec{n}_0$ decreases with time one cannot conclude that the ensemble averages over the spin components in the plane perpendicular to $\vec{n}_0$ vanish. This is a necessary condition for a "real" depolarization process which is fulfilled in the example presented and will be discussed in detail in section 5.3.

3.6 Limitations of the SITROS program

A general problem with Monte-Carlo calculations is that adequate sampling of the parameter space requires an enormous amount of computer power. This is also the case with SITROS

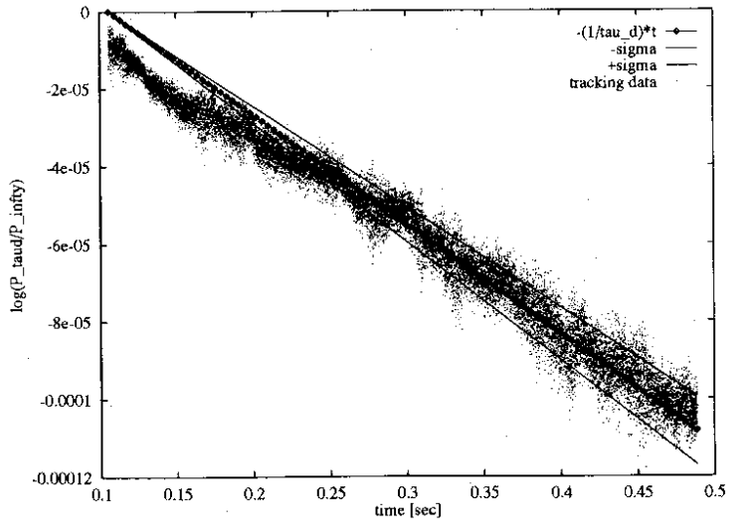

Figure 14: *Simulation of the depolarization process in a logarithmic scale $\log(P_{\tau_d}(t)/P_\infty)$ for a HERA optic with one rotator pair at an energy of 28 GeV. All spins are started parallel to the $\vec{n}_0$-axis at $t_0 = 0.11$ sec. The tracked time interval corresponds to 2×10^4 turns. The samples are taken every turn*

where it is impractical to track for more than about 2×10^4 turns corresponding to $\sim$0.4 sec real time in HERA. The aim of the following one-dimensional treatment is to get a rough idea about the time scales of the particle diffusion into the tails.
For an ensemble consisting of N particles starting on the closed orbit, the time τ_{diff_y}, ($y = x, y, s$) in which 63% of the ensemble have passed a boundary defined by y_b, is given by the Kramers formula [53][43]:

$$\begin{aligned} \tau_{diff_y} &= \tau_y \frac{\exp\left(y_b^2/\sigma_y^2\right)}{2y_b^2/\sigma_y^2} \\ N(t) &= N\left[1 - \exp\left(-\frac{t}{\tau_{diff_y}(y_b^2)}\right)\right], \end{aligned} \tag{3.35}$$

where $\sigma_y^2 = 2 < y^2 >$ is the equilibrium beam size and τ_y denotes the damping time of the y motion. For $y = x$ using $\tau_x \sim$15 msec and $\sigma_x = 3 \times 10^{-4}$ m, $\tau_{diff_x}(x_b)$ is shown as a function of the boundary x_b in fig. (15). After 1×10^4 turns 63% of the particles have passed the $3\sqrt{< x^2 >}$ boundary. To push the same percentage of particles through the $5\sqrt{< x^2 >}$ boundary 1×10^7 turns would be necessary in order to test the effect of the tails of the distribution beyond $\sim 3.5\sigma_x$ on the polarization. It is not generally practical in SITROS to track the spins for long enough so that they have been out in the tails of the approximately Gaussian phase space distribution and have experienced the stronger diffusion to be expected at large amplitudes.
How important are the particles in the tails ?
An answer can be given by a diffusion model introduced by T. Limberg [22]. In the one dimensional case the depolarization time constant τ_d can be approximated by:

$$\frac{1}{\tau_d} = \int_{n_1}^{n_2} dn \frac{\exp(-n)}{\tau_{d(n_1,n2)}} + \int_{n_2}^{n_3} dn \frac{\exp(-n)}{\tau_{d(n_2,n3)}} + \ldots \tag{3.36}$$

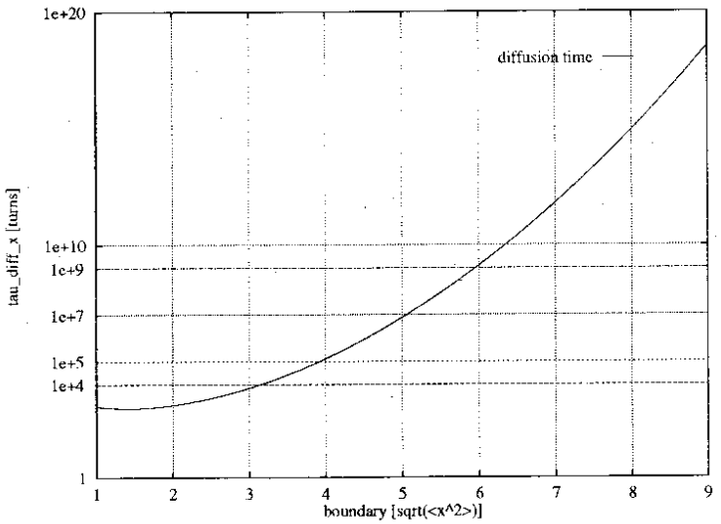

Figure 15: *Diffusion time τ_{diff_x} in number of turns given by eq. (3.35) versus the boundary in the x direction in units of $\sqrt{< x^2 >}$ for the damping time $\tau_x \sim 15$ msec corresponding to 700 turns and the equilibrium beam size $\sigma_x = 3 \times 10^{-4}$ m*

with $n = y^2/\sigma_y^2$. $\tau_{d(n_i,n_j)}$ is an average depolarization time for the interval $(y_i^2/\sigma_y^2, y_j^2/\sigma_y^2)$. This is a phase space weighted depolarization rate appearing also in [55][54]. For two intervals $(n_1, n_2) = (0, 8)$ (corresponding to $(0, 4\sqrt{< y^2 >} = 2.8\sigma_y)$) and $(n_2, n_3) = (8, \infty)$ τ_d is calculated to be:

$$\frac{1}{\tau_d} = \frac{1 - \exp(-8)}{\tau_{d(0,8)}} + \frac{\exp(-8)}{\tau_{d(8,\infty)}}.$$

For $\tau_{d(0,8)}$=3600 sec, $\tau_{d(8,\infty)}$ has to be of the order of one second to contribute to $1/\tau_d$ significantly! In practice it is not easy to determine the local depolarization rates specified in eq. (3.36). But the previous calculation indicates that it is "unlikely" that the contributions from the tails are important.
To estimate the effect of the tails simulations were made for 10 particles over 1×10^7 turns. No decrease of the polarization was observed. This shows that particles with large amplitudes are not important for the determination of the equilibrium polarization in these particular cases. However a general conclusion cannot be drawn. It is always necessary to verify whether one can neglect the contributions from the tails.

3.7 Structure of the SITROS program

SITROS is a program consisting of several modules (SITA, SITB, SITC, SITD, SITE, SITF) which are responsible for different parts of the algorithm. The following short descriptions of the modules are directly related to the topics of this section and in this form they give an overview over the entire algorithm (see fig. (16)):

Module SITA :

- Set initial parameters (central energy, number of energy points n_e, energy range, etc.)

- Read an optic file and set special distortions (harmonic bumps, decoupling bump, etc.)
- Perform calculations based on linear orbit theory (closed orbit, optical functions, equilibrium beam sizes, etc.)
- Calculate $\vec{n}_0$ at PM, P_∞ and τ_p for the chosen energy points
- Build sections consisting of strings of ring elements:
  set up the 6×28 part of the matrices for the description of the orbital motion at the central energy including chromaticity effects and sextupole corrections,
  set up the $(n_e \cdot 4) \times 28$ part of the matrices for the determination of $\vec{\Omega}$ at n_e energy points around the central energy

Module SITB :

- Repeat some linear calculations performed by SITA
- Set the start value of the excitation strength K and the time between steps for the K control procedure in SITC
- Set parameters for the particle tracking in SITC and SITD (Number of particles N, starting particle distributions, beam-beam parameters, etc.)

Module SITC :

- Perform orbital tracking for N particles at the central energy using the 6×28 part of the matrices
- Determine equilibrium beam sizes σ_y at IP_1 by tracking the ensemble for a few damping times (typically 5000 turns)
- Check the simulated σ_y against the beam sizes given by SITA

Module SITD :

- Set parameters for the depolarizer
- Perform orbital and spin tracking for N particles using the $(6 + n_e \cdot 4) \times 28$ matrices starting the spin vectors of the ensemble parallel to the $\vec{n}_0$-axis at IP_1
- Project the individual particle spin vectors onto the $\vec{n}_0$-axis at IP_1, take the ensemble average and note the result for each of typically 5000 turns

Module SITE :

- Calculate τ_d and $P_{eff} = P_\infty \tau_d/(\tau_p + \tau_d)$
- Graphical output of P_{eff} including the statistical error for n_e energy points

Module SITF :

- Set various parameters including: the central energy, the number of energy points n_e and the energy range
- Read an optic file and set special distortions (harmonic bumps, decoupling bump, etc.)
- Perform linear orbit calculations (closed orbit, optical functions, equilibrium beam sizes, etc.)
- Calculate P_∞, τ_p and $\vec{n}_0$
- Calculate τ_d using first order perturbation theory and determine $P_{eff} = P_\infty \tau_d/(\tau_p + \tau_d)$

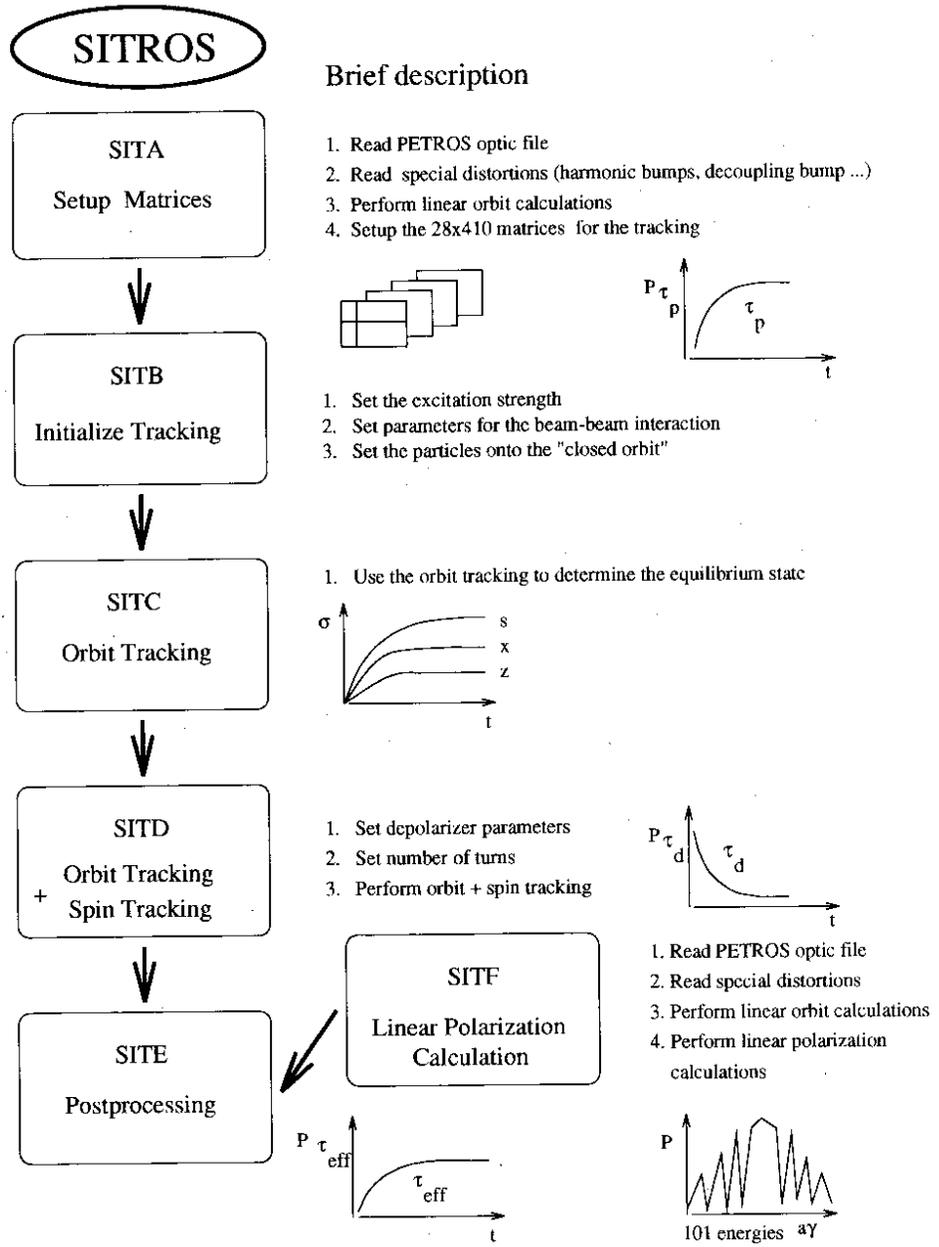

Figure 16: *Visualization of the SITROS program structure*

4 Classification of depolarizing resonances

In this section a classification of depolarizing resonances will be presented. The arguments will be heuristic and will aim to provide a basic insight into the different sources of resonances so that the polarization calculations in the following sections can be interpreted.
The starting point is a perfectly "flat" ring without any distortions. The equilibrium polarization direction $\vec{n}_0(s)$ is parallel to the direction of the main bending field $\vec{B}$ which points in the direction of $\vec{e}_z$. Due to the presence of horizontal dispersion D_x horizontal betatron oscillations and synchrotron oscillations are excited by quantum emission. No vertical betatron oscillations are induced. Because of the fact that a particle starting with a spin vector $\vec{S}$ parallel to $\vec{n}_0(s_0)$ at a position s_0 in the ring experiences only magnetic fields which are parallel to $\vec{n}_0$, $\vec{S}$ remains parallel to $\vec{n}_0$. The precession frequency $\nu(1+\delta)$ of $\vec{S}$ with $\nu = a\gamma_0$ (in the following the index 0 will be omitted) for a spin vector starting slightly tilted with respect to $n_0(s_0)$ is modulated by the energy oscillations. Since there is no depolarization mechanism the equilibrium polarization reaches the Sokolov-Ternov level of $P_\infty \sim 92.4\%$.
In real machines the magnet alignment is imperfect and the closed orbit is not exactly centered in the quadrupoles. In addition correction coils are needed. Thus a spin vector moving on the closed orbit experiences horizontal fields. As a result $\vec{n}_0$ can be tilted significantly from the vertical $\vec{e}_z$ even for a nominally flat ring. For small imperfections this tilt depends linearly on the closed orbit. This enables the use of special orbit correction schemes to reduce the $\vec{n}_0$-axis tilt (see appendix A). The tilt becomes extreme near integer spin tunes $\nu = k$. In this case the polarization build up effect becomes weaker (see eq. (2.6)) due to the decrease in the scalar product $(\vec{n}_0\vec{b})$. Furthermore spurious vertical dispersion D_z is generated resulting in the excitation of vertical betatron oscillations. As can be seen in eq. (A.14) the occurrence of a tilted $\vec{n}_0$ or vertical dispersion leads immediately to spin diffusion. The resulting depolarization is normally far more significant than the weakening of the Sokolov-Ternov effect mentioned above. In the following the most important **spin resonances** which might appear will be summarized. The depolarization effects will be divided into two main classes namely, first order effects and higher order effects.

First order effects are those discussed in appendix A. As can be seen there, the spin motion in the rotating reference frame has been linearized and the precession vector $\vec{\omega} = \vec{\Omega} - \vec{\Omega}^{co}$, where $\vec{\Omega}^{co}$ describes the closed orbit part of $\vec{\Omega}$ (see appendix A), is linearized so that it is a first order function of the orbit vector $\vec{X}$. In this approximation the integrands in the integrals appearing in the components of the diffusion vector $\vec{d}$ are of first order in the orbital coordinates and proportional to the quadrupole strength. Each term contains a factor $(a\gamma + 1)$ and an "excitation factor" accounting for the strength of the excitation of that orbital mode due to emission of photons. There are also denominators which vanish when $\nu = k \pm Q_y$ and these lead to a first order resonance behaviour of $1/\tau_d$ which is illustrated in fig. (17, Top). The presence of the $(a\gamma + 1)$ factor ensures that the diffusion effects increase with energy. These resonances affect the equilibrium polarization over a large fraction of the interesting energy range. They normally define the upper limit of the achievable polarization. These resonances can be further classified as follows:

Vertical betatron resonances (condition: $\nu = k \pm Q_z$)
These resonances are induced by vertical betatron oscillations excited by photon emission at positions where there is vertical dispersion. The integral eq. (A.14) receives contributions at quadrupoles where $\vec{n}_0(s)$ is not pointing exactly in the horizontal $\vec{e}_x$ direction. This happens, for example, when $\vec{n}_0(s)$ (i.e. the average spin direction) is almost vertical as in a typical storage ring. The integrand then

describes the backward/forward tilting of the spins around the radial quadrupole fields illustrated in fig. (1).

In a ring with a superperiodicity, first order vertical betatron resonances only appear for values of k (eq. (2.9)) which are an integer multiple of the superperiodicity. This can be easily be seen by analyzing the harmonic content, with respect to the azimuthal position s, of the integrands contributing to these resonances. However, in practice there are gradient errors in the quadrupoles and the superperiodicity in the β functions is lost and vertical betatron resonances can occur for all integer values of k.

Horizontal betatron resonances (condition: $\nu = k \pm Q_x$)
These resonances are induced by the excitation of horizontal betatron oscillations at positions where there is horizontal dispersion and at quadrupoles where $\vec{n}_0(s)$ is not pointing exactly in the $\vec{e}_z$ direction. This is typically the case for a "flat" ring with imperfections. Then $\vec{n}_0(s)$ is slightly tilted and there can be stochastic precessions around the vertical quadrupole fields. Horizontal motion at positions where there is a skew quadrupole component can also lead to these resonances whenever $\vec{n}_0$ is not pointing exactly in the $\vec{e}_x$ direction.

Synchroton resonances (condition: $\nu = k \pm Q_s$)
These precession mechanisms are analogous to those acting in the case of the betatron motion except that in this case the spin diffusion is driven by motion on vertical or horizontal dispersion orbits instead of vertical or horizontal betatron orbits. These resonances are strong for imperfect rings at high energy and can limit the polarization to a few percent (~20% at HERA). Because the synchrotron tune Q_s is usually small (~ 0.07 in HERA at 26.666 Gev) the polarization near the integer values of the spin tune $\nu = k$, which are 440.625 MeV apart in energy, is normally destroyed by the strong surrounding Q_s resonances.

Higher order effects occur primarily due to the nonlinear nature of the three dimensional spin motion (see section 3.5.2) and they appear even if the orbital motion is determined by fields which are completely linear in the orbital coordinates and even if $\vec{\omega}$ is a linear function of the orbit vector $\vec{X}$. The strength of the higher order resonances can be estimated by extending the treatment in appendix A to include the square root term in eq. (A.5)(A.7), i.e. by not linearizing the spin motion and keeping the $\vec{\omega}\vec{n}_0$ term. It is then found that the diffusion vector $\vec{d}$ has a much more complicated resonance structure. The first order resonance terms in $\vec{d}$ discussed so far contain a single $(a\gamma + 1)$ factor and a one turn integral over first order orbit variables. A term with an nth order resonance denominator contains a factor $(a\gamma + 1)^n$ and nth order multiple integrals over nth order products of the orbit variables. There is also an emittance excitation factor and an $(n-1)$th order product of orbital amplitudes. In calculating $< |\vec{d}|^2 >$ to obtain $1/\tau_d$ (see appendix A) the orbit amplitudes are converted into emittance factors. The higher order resonances originate in photon emission at non-zero orbit amplitude and higher order resonances become stronger as the emittances increase. This was already indicated in section 3.6, where the possible influence of the tails of the beam was discussed.

Two important subclasses of the higher order resonances will be now discussed:

synchrotron sidebands (condition: $\nu = k + m_x Q_x + m_z Q_z + m_s Q_s, \quad |m_x| + |m_z| \leq n, |m_s| \leq m$)
This is the strongest and most important subclass of higher order spin resonances in high energy storage rings. Synchrotron oscillations with large amplitudes cause a

large frequency modulation of ν. Similarly to the mechanism of frequency modulation in RF waves, synchrotron sidebands appear in the spectrum of the spin motion. This leads to sidebands up to the order m to each of the previously discussed depolarizing resonances with $|m_x| + |m_z| \leq n$. On the basis of a formalism introduced by Buon [56], S. Mane [57][58] and K. Yokoya [59] the strength of the sidebands can be quantified. The relevant parameter is the tune modulation index λ^2:

$$\lambda^2 = \left(\frac{a\gamma\sigma_\delta}{Q_s} \right)^2 ,$$

which is basically a product of a spin tune factor $a\gamma$ and the energy spread σ_δ which depends on the longitudinal emittance. After averaging over the phase space and making some reasonable approximations the sideband strengths only depend on the strength of the parent resonances and on powers of λ^2. The tune modulation index increases quadratically with the energy and the energy spread. For rings like HERA with an energy spread $\sigma_\delta \sim 1 \times 10^{-3}$ at 26.666 GeV the sideband resonances to $\pm Q_y$ are strong up to high order ($m \geq 4$). The notation $\pm Q_y$ describes resonances satisfying the conditions $\nu = k + Q_y$ and $\nu = k + 1 - Q_y$. For the resonance notation used in the pictures see fig. (17, Bottom).

The intuitive approach to calculating $\vec{d}$, explained in appendix A, allows the estimation of resonance strengths due to betatron motion in nonlinear fields which are called

nonlinear betatron resonances (condition: $\nu = k + m_x Q_x + m_z Q_z, \quad |m_x| + |m_z| \leq n$)
These higher order spin resonances are driven by magnetic multipole fields of n-th order ($n > 1$). For example for a sextupole field (n=2)

$$B_z^{sex} = \frac{1}{2} g' \left(x^2 - z^2 \right), \quad B_x^{sex} = g' xz$$

will mainly drive nonlinear spin resonances with $|m_x| + |m_z| = 2$.
One can see this by noting that $\vec{\omega}$ is a second order function of the orbit motion. By integrating the spin motion, second order resonance denominators appear. However, in contrast to the second order resonances generated in quadrupoles, the $\vec{d}$ vector for these "sextupole" resonances contains only a single $(a\gamma + 1)$ factor. Thus at HERA energies ($\nu = 60.5$) these resonances should be much weaker than those generated by quadrupoles [58]. This is confirmed in section 5.2.

The fact that the first order spin resonances occur near integer spin tunes for the preferred orbital tunes at HERA implies that the best working point for polarization measurements is half way between two integer values of the spin tune. For HERA the energy 26.666 GeV was chosen corresponding to a spin tune of $a\gamma = 60.5$. Although the strength of the resonances is energy dependent the resonance pattern repeats more or less after every integer value of $a\gamma$. The equilibrium polarization P_{eff} can be significantly reduced by these resonances. For an average $\vec{n}_0$-axis tilt of 20 mrad with respect to the vertical at $a\gamma = 60.5$ generated by imperfections in the "flat" HERA ring, the polarization is reduced to about 20% by very strong synchrotron resonances at $\nu = 60 + Q_s$ and $\nu = 61 - Q_s$ (see fig. (26)) that are driven by the motion on horizontal dispersion orbits. Since in a machine like HERA there are limits to how well the machine can be aligned in the vertical plane and since horizontal dispersion and horizontal emittance excitation can never be brought to zero the only remedy is to decrease the average $\vec{n}_0$-axis tilt. It is clear that this should help because already for first order effects the

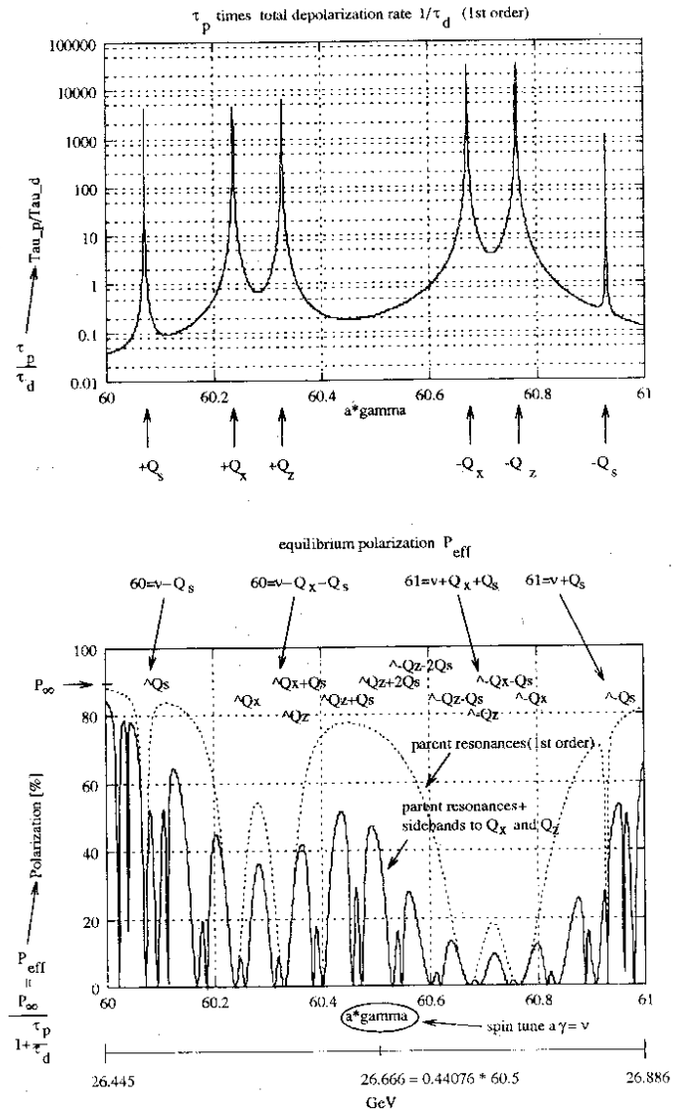

Figure 17: *Notation used in pictures:* Top: *Logarithmic graph illustrating the energy dependence of the total depolarization rate* $1/\tau_d = \sum_y 1/\tau_{dy}$ $(y = x, z, s)$ *multiplied with* τ_p *which is given by eq. (2.8) including the first order resonances* $\pm Q_s$, $\pm Q_x$ *and* $\pm Q_z$. *The depolarization rate is large at values of the spin tune where the resonance condition* $60 = \nu - Q_y$ *or* $61 = \nu + Q_y$ *is fulfilled,* Bottom: *Corresponding equilibrium polarization* $P_{eff} = P_\infty/(1 + \tau_p/\tau_d)$. P_∞ *is determined by eq. (2.7). At the top of the graph the resonance notation used in the following is explained. The pictures are taken from section 6, where a comparison between SITROS and analytical approaches in the case of weak depolarization will be performed.*

$|\vec{d}|^2$ depends quadratically on the $\vec{n}_0$-axis tilt. Besides conventional orbit corrections, in HERA a special harmonic bump scheme (see appendix A) is used to reduce the tilt [60]. Even after the optimization with these special orbit corrections leading to a reduction of the tilt down to 10 mrad strong synchrotron resonances, betatron resonances and synchrotron sidebands occur limiting P_{eff} to $\sim 80\%$.

Another reason for requiring good vertical alignment of the machine is to avoid the generation of spurious vertical dispersion. As we have seen this leads to the excitation of vertical betatron resonances and the excitation of a contribution to the synchrotron resonances.

5 Analysis of depolarizing effects in HERA

In this section the Monte-Carlo program SITROS is used to study the depolarizing effects in HERA. The influences of various orbit correction schemes on the polarization are analyzed and compared with the existing experimental results. Calculations for a HERA optic with one rotator pair for the HERMES experiment are presented. Furthermore the influence of a time dependent radial dipole field is studied.

5.1 First polarization measurements

The aim of the following subsection is to get a qualitative understanding of the behaviour of HERA concerning polarization during the run period in 1991. No protons were filled and the experiments ZEUS and H1 were switched off during the measurements. Thus no influence of the beam-beam interaction or badly compensated solenoids is taken into account in the simulations. At the beginning of the run period, a twist of the equilibrium beam ellipse (see eq. (3.16)) of about $\sim$ 120 mrad was observed at the location of the polarimeter and at the interaction point of the H1 experiment. Together with the fact that a localized skew quadrupole component could not be detected by difference orbit measurements this led to the conclusion that the twist was generated by a systematic evenly distributed skew quadrupole component in the ring, believed to be an effect of the iron of the proton magnets on the stray fields of the electron dipole magnets. This coupling could be compensated by a special "decoupling bump" [61].

5.1.1 The decoupling bump

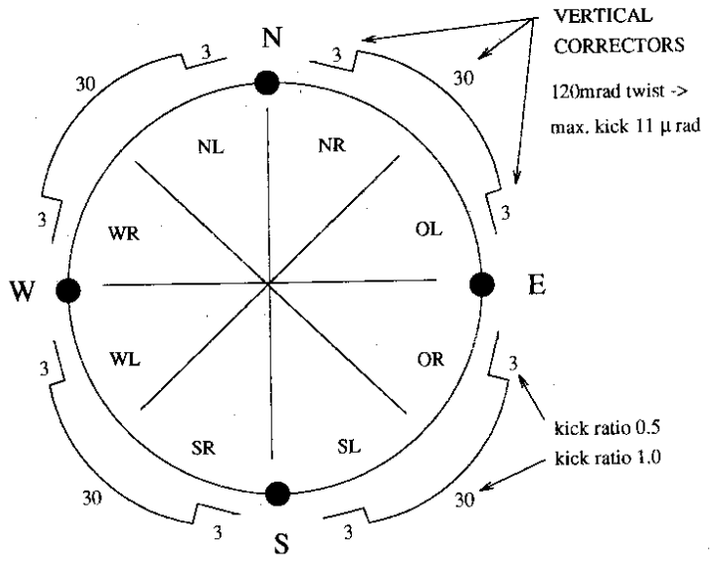

Figure 18: *Schematic drawing of the decoupling bump distributed over the four arcs of HERA. The whole orbit is shifted vertically by the bump to generate an evenly distributed skew quadrupole component in the sextupoles in order to minimize the equilibrium beam ellipse twist*

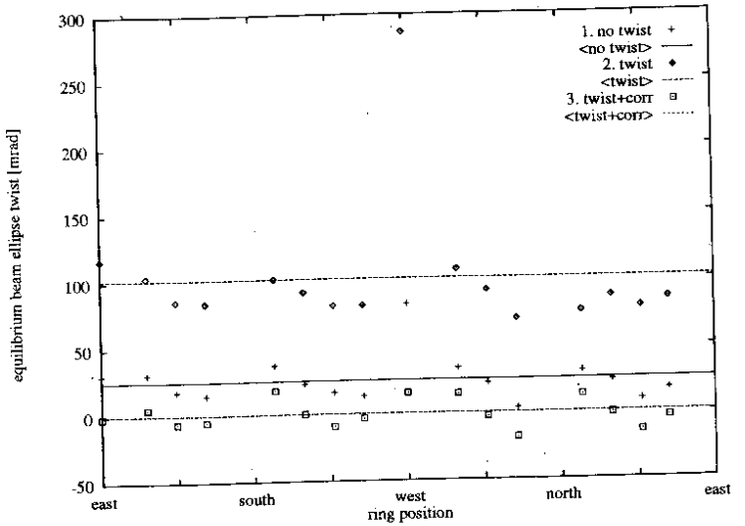

Figure 19: *Beam ellipse twist versus ring position for three cases: 1. without an additional angle error of the main quadrupoles, 2. with an additional systematic angle error of 4.3 mrad of the main quadrupoles, 3. with compensation of the resulting equilibrium beam ellipse twist by the decoupling bump (see fig. (18))*

The idea of the decoupling bump is to shift the whole orbit vertically to generate an evenly distributed skew quadrupole component in the sextupoles (see section 3.3) to minimize the equilibrium beam ellipse twist. This is done by the correction scheme illustrated in fig. (18) consisting of 144 vertical correction coils in the arcs of HERA. The effect of this bump spanning the whole ring on the polarization will be studied in detail.
The optic which is used as a starting point for the following simulations is that for the standard HERA lattice (no rotators) with randomly Gaussian distributed distortions ($\Delta x_{rms} = \Delta z_{rms} = 0.3$ mm for positional errors, $\Delta strength_{rms} = 0.5 \times 10^{-3}$ for relative strength errors and $\Delta angle_{rms} = 0.35$ mrad for angle errors) of quadrupoles and sextupoles plus orbit correction with the MICADO [62] correction scheme. This algorithm is used as the standard orbit correction tool for HERA. MICADO analyzes the monitor data and tries to find the most effective corrector or combinations of correctors for the minimization of the rms orbit. This distorted and corrected optic has a systematic twist of the equilibrium beam ellipse of $\sim$ 25 mrad due to the given distortion distribution ("no twist" in fig. (19)). To reproduce the measured twist of $\sim$ 120 mrad an additional systematic angle error of 4.3 mrad of the main quadrupoles with respect to the magnet axis is introduced in the simulation ("twist" in fig. (19)). To compensate the resulting twist the average vertical kick applied by a single corrector in the decoupling bump has to be $\sim$ 10 μrad ("twist+corr" in fig. (19)). The rms values about the mean values of the closed orbit are not affected by the application of the bump.
What is the effect on the polarization ?
Due to the betatron coupling the first order $Q_x = 0.11$, $Q_z = 0.19$ spin-orbit resonances are stronger than in the uncoupled case. This can be seen by looking at the contributions of Q_x and Q_z to the depolarization time τ_d. The ratios τ_p/τ_{d_y} are plotted in fig. (20). The results are taken from the program SITF which calculates the equilibrium polarization using the first order SLIM formalism (see appendix A). The application of the decoupling bump reduces the

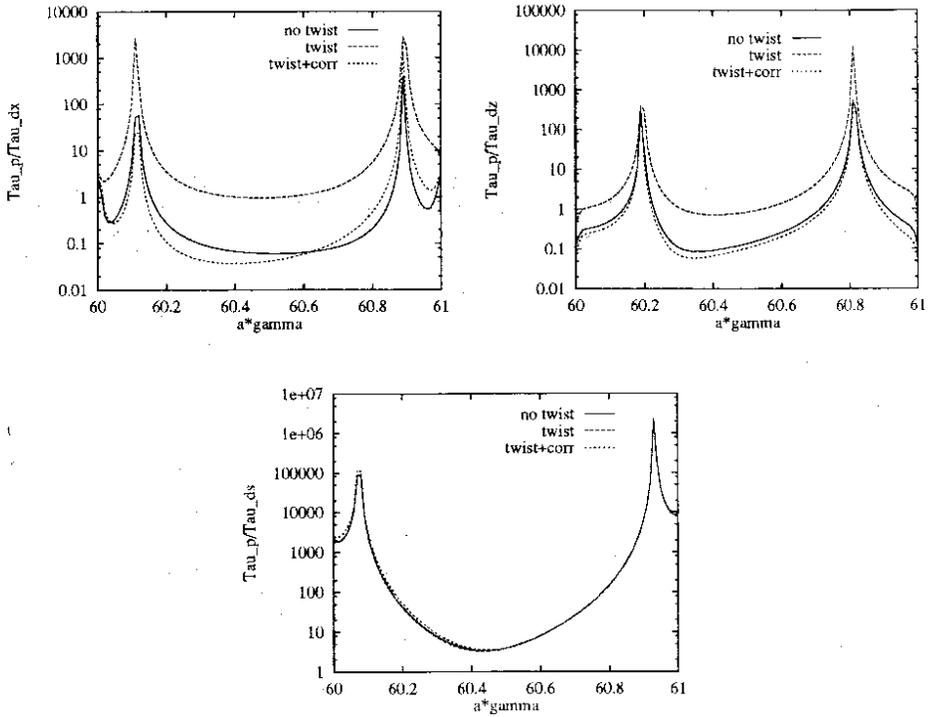

Figure 20: *Contributions of the depolarization rates $1/\tau_{d_y}$ $(y = x, z, s)$, multiplied with the polarization build up time $\tau_p \sim 2500$ sec given by eq. (2.8), to the total depolarization rate $1/\tau_d$:* Top,Left*: contribution of the $\pm Q_x$ resonances ($\nu = 60 + Q_x$, $\nu = 61 - Q_x$ with $Q_x = 0.11$),* Top,Right*: contribution of the $\pm Q_z$ resonances ($\nu = 60 + Q_z$, $\nu = 61 - Q_z$ with $Q_z = 0.19$).* Bottom*: contribution of the $\pm Q_s$ resonances ($\nu = 60 + Q_s$, $\nu = 61 - Q_s$ with $Q_s = 0.07$)*

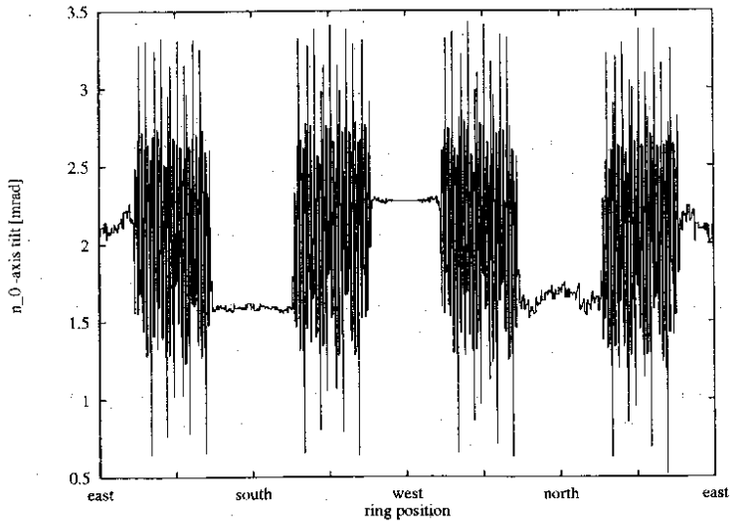

Figure 21: *Tilt of the equilibrium polarization axis $\vec{n}_0$ by the presence of the decoupling bump for a HERA optic without distortions. The average tilt of the $\vec{n}_0$-axis is calculated to be $\sim$2 mrad*

strength of the Q_x,Q_z resonances to their original values. For the Q_s resonances ($Q_s = 0.07$) the behaviour is different. Due to the additional vertical distortion generated by the bump the average tilt of the $\vec{n}_0$-axis is increased. To illustrate the effect on the $\vec{n}_0$-axis the decoupling bump was applied to a HERA optic without distortions (see fig. (21)). The additional average tilt of the $\vec{n}_0$-axis is calculated to be only $\sim$2 mrad compared to an rms tilt of $\sim$20 mrad generated by other errors in the machine with imperfections. The small increase of the average $\vec{n}_0$-axis tilt and of the vertical dispersion results in slightly stronger Q_s resonances after the compensation. This leads to the following situation:
The strong first order Q_s resonances limit the polarization to a maximum of $\sim$ 22% (see fig. (22)). Due to slightly stronger Q_s resonances after the compensation of the coupling the maximum decreases by 2% on the first order level. But at higher order the situation is totally different. The sidebands to Q_x,Q_z ($\pm Q_{x/z} + m_s Q_s$) are driven by the parent resonances which are weakened by the decoupling bump. These sidebands are dangerous in the region around the half integer ν=60.5 because they are of low order ($|m_s| < 4$), resulting in an increase of polarization on the higher order level (see fig. (22)). This explains why the decoupling bump is a helpful tool to increase the polarization under the condition that the vertical dispersion and the average $\vec{n}_0$-axis tilt is not significantly increased (for a more theoretical treatment see also [60]).
The first polarization measurements were made with a decoupling bump only applied in one arc (OR/SL) (see fig. (18)) of HERA. The resulting $\vec{n}_0$-axis tilt was bigger by a factor of four and thus resulted in a significant decrease of polarization on the first order level. But the orbital tunes Q_x,Q_z were shifted by $\sim$0.1 towards the half integer compared with the example just discussed. This makes the explained discrepancy between first and the higher order calculations even stronger [36]. It was found in the measurements that the polarization increases from 0.45% to 3.02% at 26.62 GeV and from 4.46% to 8.12% at 26.64 GeV [63]. The stated energies correspond to real machine energies with an uncertainty of $\pm$2 MeV. Using

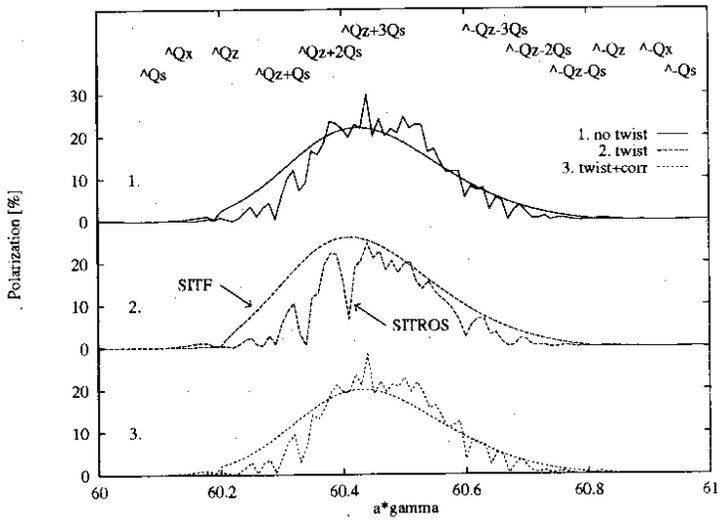

Figure 22: *Polarization versus energy for three cases: 1. without an additional angle error of the main quadrupoles, 2. with an additional systematic angle error of 4.3 mrad of the main quadrupoles, 3. with compensation of the resulting equilibrium beam ellipse twist by the decoupling bump (see fig. (18)). Some of the most important resonances (especially sidebands to the $\pm Q_z$ resonances appearing in the SITROS result) are shown at the top of the graph (for the notation see fig. (17)). The SITROS calculation shows that several sidebands of Q_z are weakened and the first order SITF result reflects the increase of vertical dispersion and the average $\vec{n}_0$-axis tilt due to the application of the decoupling bump*

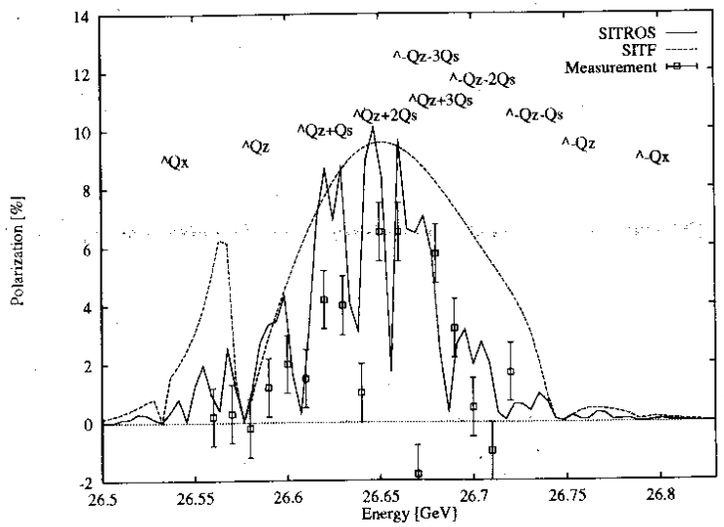

Figure 23: *Comparison of simulation and measurement for an energy scan made during a polarization run in november 1991. Some of the most important resonances are shown at the top of the graph. The solid/dashed line corresponds to the SITROS/SITF result and the points with errorbars are the experimental data taken from [63]. The energy range corresponds to a spin tune range from ν=60.12 to ν=60.88*

the method of energy calibration by resonant spin depolarization the beam energy was found to be 33-36 MeV below the nominal energy given by the integrated field of the main dipoles (see section 5.1.1). Fig. (23) shows the results of a single SITROS run and the corresponding measurement. The simulation takes into account the following machine conditions:

1. The used optic reproduces the measured null orbit of HERA (hypothetical orbit after subtracting the corrector kicks) to within about 90% [64]. The strongest vertical closed orbit kicks recalculated from the measured null orbit are taken into account by equivalent vertical quadrupole displacements. In addition randomly Gaussian distributed distortions are superposed.

2. After the correction with MICADO the rms values of the closed orbit are comparable to the measured values ($z_{rms} \sim 1.1$ mm).

3. The measured tunes $Q_x = 0.19, Q_z = 0.28, Q_s = 0.069$ are reproduced.

4. The coupling of $\sim$ 120 mrad is simulated by an additional systematic angle error of the main quadrupoles.

5. The decoupling bump in the arc (OR/SL) is applied for the compensation of the coupling.

The agreement between the realistic simulation and the measurement is encouraging. The Q_z resonance (26.57 GeV) and four measured synchrotron sidebands to Q_z spaced by 30 MeV can be identified. The maximum measured polarization during the run period was 9.2% at 26.64 GeV compared to the simulation result of 10 %.
Thus the behaviour of HERA concerning polarization during the 1991 run can be understood quantitively on the basis of the Monte-Carlo studies.

5.2 Polarization optimization

The polarization optimization process in 1992 will be described in detail and compared to the corresponding simulation studies.
The reconstruction of the measured null orbit in 1991 showed already that several quadrupoles must have had vertical misalignments around 1 mm. These quadrupoles and the strong decoupling bump in the arc (OR/SL) led to the low polarization level in 1991 (fig. (23)).
The following actions were taken to increase the polarization in 1992:

1. During the shutdown 91/92 the alignment of the quadrupoles was checked and selected magnets realigned.

2. The tilt of the beam ellipse was corrected by a decoupling bump which this time was distributed evenly around the ring (fig. (18)).

3. The orbital tunes were shifted towards the integer values (60,61) to increase the region between the Q_z and $-Q_z$ spin resonances.

4. A spin-orbit correction scheme ("harmonic bump scheme") [60][65] was applied to minimize the coupling between the orbital and the spin motion.

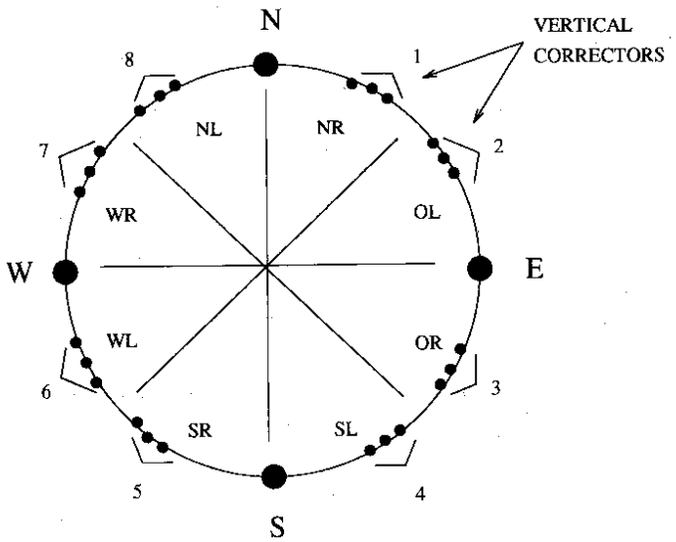

Figure 24: *Schematic drawing of the harmonic bump scheme consisting of eight bumps each of which consists of three successive vertical correction coils in the arcs of HERA. The scheme is used to minimize the average $\vec{n}_0$-axis tilt in the arcs leading to an significant increase of the equilibrium polarization in first order approximation [60]*

For all these steps Monte-Carlo studies were done before the application in the control room:

1. To represent the realignment of the quadrupole magnets the assumption is made that the vertical displacements of the magnets have now a Gaussian distribution with an rms value of 0.3 mm. The orbit was corrected with MICADO to $z_{rms} = 0.7$ mm. In the following,

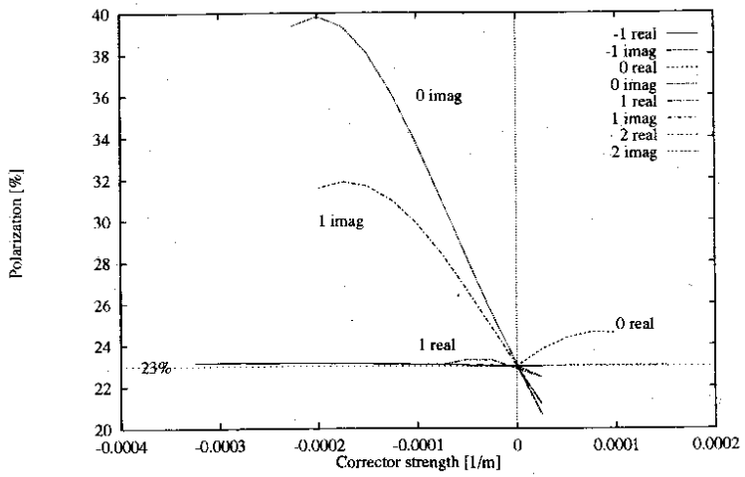

Figure 25: *Empirical optimization of the polarization using the harmonic bump scheme consisting of eight bumps controlling the most important complex Fourier harmonics f_k with k=60+(-1,0,1,2) of the spin-orbit coupling function (eq. (A.16)). The corrector strength has to be multiplied with the length of the corrector magnet of 300 mm to get the maximum kick inside the individual bump*

results for a certain error distribution will be presented which is realistic but not identical with the distribution in HERA. This means that the strengths of individual resonances can be different.

2. The tilt correction with a distributed decoupling bump was already studied in the last subsection.

3. The shift of the orbital tunes is based on the experience (both from simulation and measurement) that the Q_z resonances and the corresponding sidebands $\pm Q_z + m_s Q_s$ are important for the maximum achievable polarization level in HERA. By shifting the fractional part of Q_z towards the integer just the sidebands of higher order ($|m_s| > 3$) are in the region around the half integer. In addition the condition $Q_z - Q_x \approx Q_s$ was imposed in order to put the synchrotron sidebands of the parent resonances on top of each other. This minimizes interference effects between various resonances. The orbital tunes in the simulation are Q_x=0.108, Q_z=0.197 and Q_s=0.072. One has to avoid the situation that the condition $Q_z - Q_x = Q_s$ is exactly fulfilled because the orbital $Q_z - Q_x$ coupling resonance is driven at this working point leading to an enhancement of the vertical emittance.

4. The optimization with the harmonic bump scheme (see fig. (24)) was implemented in the SITROS program to simulate the optimization process.

Before the correction given in item 4 was applied SITROS predicted a maximum polarization of $\sim 20\%$ (see fig. (22),(26)) which is already a 12% improvement in comparison to the calculations made for the 1991 measurements. The fact that the polarization was nevertheless still low can

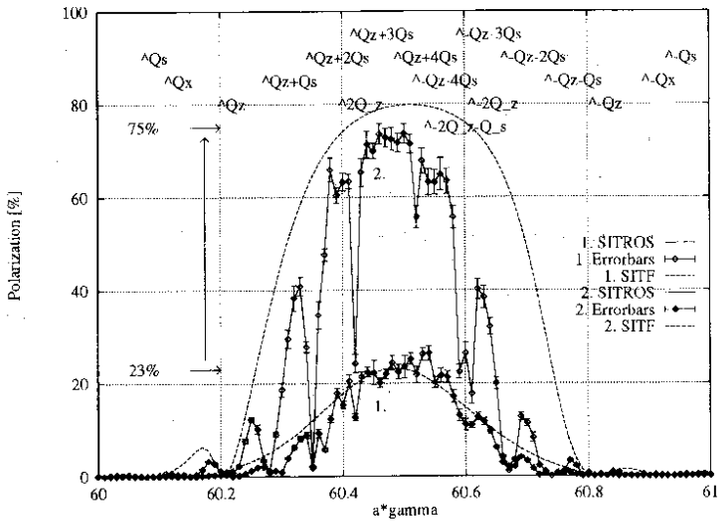

Figure 26: *Increase of the polarization from 23% to 75% after the superposition of four (0 real/imag, 1 real/imag) of the individually optimized bumps (see fig. (25)) (Q_s=0.07216). The dashed curves correspond to the first order and the points with errorbars to the SITROS simulation results. For the calculation of the errorbars see eq. (3.34)*

be explained by the relatively large average $\vec{n}_0$-axis tilt of $\sim$ 22 mrad at the half integer spin tune $\nu = 60.5$ corresponding to 26.666 GeV, shown in fig. (27) which is induced by a strong spin-orbit coupling (see section 4). The average is taken over the tilts of the $\vec{n}_0$-axis at the main quadrupole magnets in the arcs of HERA. To increase the polarization it is thus necessary to reduce the coupling between the orbital and the spin motion. This is done by the correction of the so called spin-orbit coupling function derived in appendix A (see eq. (A.16)) resulting in a reduction of the average $\vec{n}_0$-axis tilt.
The harmonic bump scheme reduces special harmonics of this spin-orbit coupling function. Four harmonics f_k with k=60+(-1,0,1,2) near to the integer spin tune ν=60 can be corrected. Each has a real and an imaginary part. A family of eight closed vertical bumps each consisting of three coils is used, to reduce the strength of a particular harmonic [60]. For each harmonic the eight bumps have certain kick ratios, implying that the harmonic can be described by a single parameter namely the kick strength of the strongest coil in the bump scheme (fig. (25)). It is not possible to calculate the parameter value for which the harmonic in the real machine is minimized because the strength depends on the actual magnet misaligments in the ring which are normally not known exactly. Consequently the bumps have to be optimized by measuring the polarization. The same method is used in SITROS to simulate the control room optimization procedure. Due to the orthogonality and linearity of the parameters the optimum is found in SITROS by optimizing them separately and superposing them afterwards. A simulation result is shown in fig. (25). The program simply increases/decreases the parameter "corrector strength" until a maximum of polarization is found. Although the scheme has been designed to minimize the vertical dispersion generated by the individual bumps, vertical dispersion is nevertheless generated and the presence of sextupoles inside the bumps can cause closure problems of the bumps that enhance depolarization. Thus one drops the ineffective bumps (in this case (-1 real/imag) and (2 real/imag) corresponding to the complex Fourier

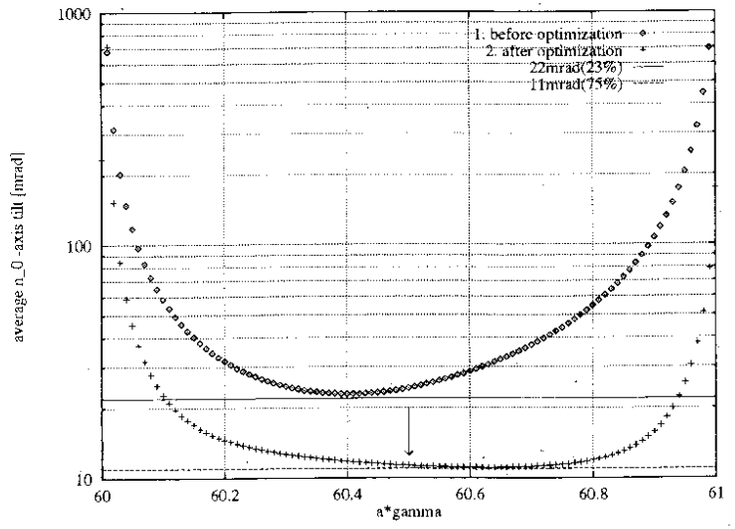

Figure 27: *Decrease of the average $\vec{n}_0$-axis tilt $< \delta\vec{n}_0 >$ due to the harmonic bump optimization. The depolarization rate $1/\tau_d$ and thus the polarization depends in first order quadratically on the tilt variation $< \delta\vec{n}_0 >$*

harmonics f_k with $k = 59$ and $k = 62$) and add the remaining bumps to the optic. The result of the numerical optimization procedure is shown in fig. (26). The average $\vec{n}_0$-axis tilt $< \delta\vec{n}_0 >$ went down from 22 to 11 mrad at 26.666 GeV and the polarization increased from 23% to 80% (fig. 27). This remarkable increase is consistent with the fact that the first order depolarization rate $1/\tau_d$ due to horizontal synchrotron and betatron oscillations is proportional to $|\vec{d}|^2$ in eq. (2.12) and thus has approximately a quadratic dependence on $< \delta\vec{n}_0 >$. Due to the fact that the strength of the first order resonances is reduced significantly by the average $\vec{n}_0$-axis tilt correction, also the synchrotron sidebands to these parent resonances are weakened (see section 4). This explains why the simulation shows also a significant increase in polarization. Nevertheless the sidebands especially of the $\pm Q_z$ resonances remain strong after the optimization. The polarization plateau around the half integer is limited by the Q_z+3Q_s and $-Q_z-3Q_s$ resonance defining a width of 80 MeV for the plateau.
A few comparisons with measurements made in 1992 will now be presented. Fig. (29) contains various measurements and the simulation results just discussed. Since the main aim of the 1992 run was to optimize the polarization with the harmonic bump scheme (fig. (28)) only partial energy scans were performed. The solid curve (3a.) corresponds to a scan performed before the reduction of the harmonics and should be compared with the simulation result represented by curve (1.). The measurement conditions were slightly different from those in the simulation: Q_x=0.14, Q_z=0.20, Q_s=0.082. Two resonances can be easily identified as Q_z+3Q_s (ν=60.446) and Q_x+4Q_s (ν=60.468). The maximum measured polarization was $\sim$ 25% corresponding to 23% in the simulation. The second scan (3b.) was made near the end of the run period, after the successful completion of the correction studies which are to be compared with (2.). Again the conditions were different: Q_x=0.15, Q_z=0.21, Q_s=0.071 (Q_x=0.12, Q_z=0.20, Q_s=0.076 for the last three points). The measured strong resonances correspond to $-Q_z-4Q_s$ (ν=60.506) and $-Q_z-3Q_s$ (ν=60.577) respectively. The latter resonance might be identified as $-Q_z-2Q_s$ (or $-Q_x-3Q_s$). The maximum polarization measured was $\sim$ 44%. This value is much lower

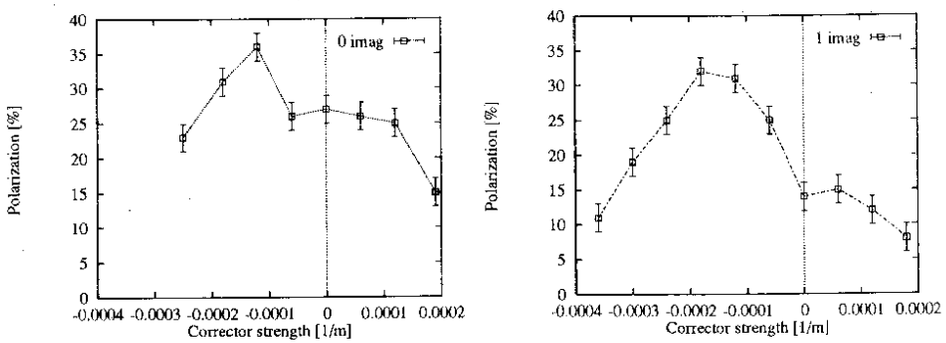

Figure 28: *Experimental polarization studies for two of the most important harmonics performed in summer 1992 [8]. Some of the points are believed to be too low with respect to neighbouring points because of build up time effects, see fig. (25) for comparison with the simulated optimization process*

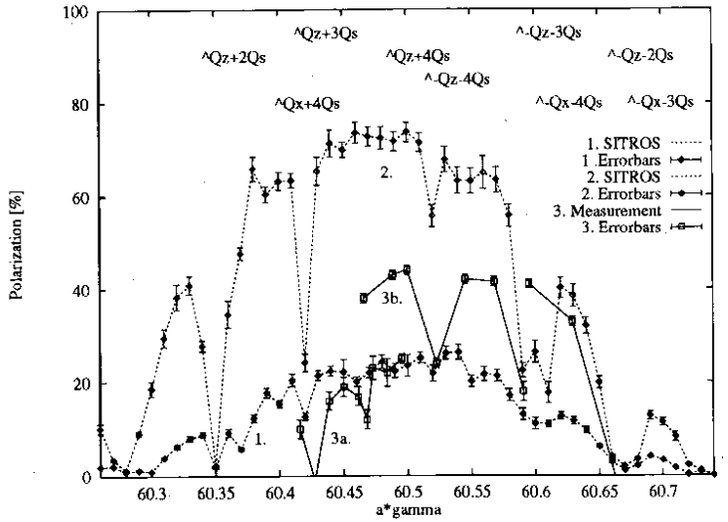

Figure 29: *Comparison of simulation and measurement for various energy scans made in summer 1992 [8]. The simulation results are those given in fig. (26). The experimental data (3a.) have been taken before the reduction of the harmonics and the data (3b.) after the successful completion of the correction studies*

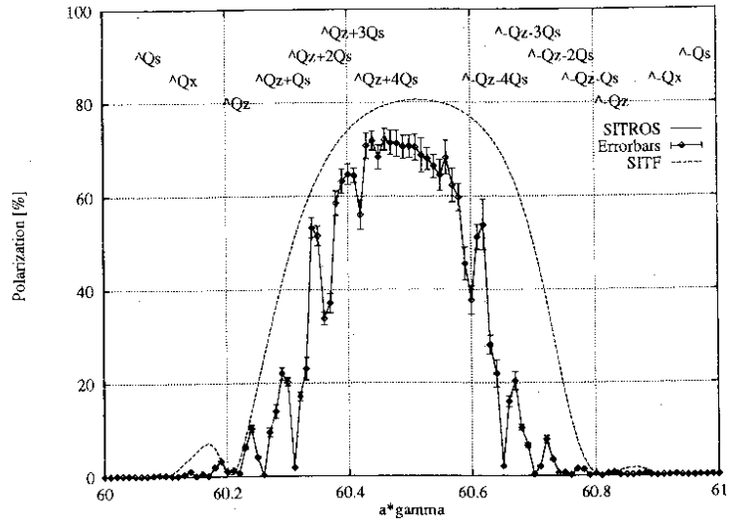

Figure 30: *Energy scan for a small synchrotron tune $Q_s = 0.05380$ which compared with the scan for a large $Q_s = 0.07216$ given by curve (2.) in fig. (26) illustrates that large Q_s values are not always helpful to increase the polarization*

than the simulation result of $\sim 75\%$ but might be explained by the following observations:

1. The data were recorded after waiting only 25 minutes after changing a bump and may be consistent with a maximum measured polarization of $\sim 56\%$ considering the effective build up time of $\tau_{eff} = 21$ min.

2. It was not possible to make sure that the optimum for all bumps was really found. Because of the large build up time a more systematic study is very time consuming.

It was already mentioned at the beginning of this section that the simulation for a single error distribution is very useful for predicting the tendencies for relative strengths of resonances. However, since the actual polarization depends on the precise magnet error distribution, a prediction for the expected polarization can be obtained only from an average of results from several misaligned machines. Such a study was performed with SITROS on four different error distributions; the average maximum polarization before the optimization with the harmonic bump scheme was found to be $26.0 \pm 6.0\%$, and the maximum was increased to $70.7 \pm 6.7\%$ by the harmonic correction.
In this context it is interesting to study the possible effect of running with a smaller synchrotron tune Q_s. On the basis of a formalism introduced by J. Buon [56], S. Mane [57] and K. Yokoya [59] and others the strength of the sidebands can be quantified. The relevant parameter is the tune modulation index λ^2:

$$\lambda^2 = \left(\frac{a\gamma\sigma_\delta}{Q_s}\right)^2 .$$

The sideband strengths depend on powers of λ^2, e.g. an nth order sideband is about a factor λ^{2n} less in strength in the case where $\lambda < 1$. The formula describing the sidebands to parent betatron resonances can be found in section 6.2. For the above comparison between measurement and simulation λ^2 is calculated to be ~ 0.7. By changing the synchrotron tune

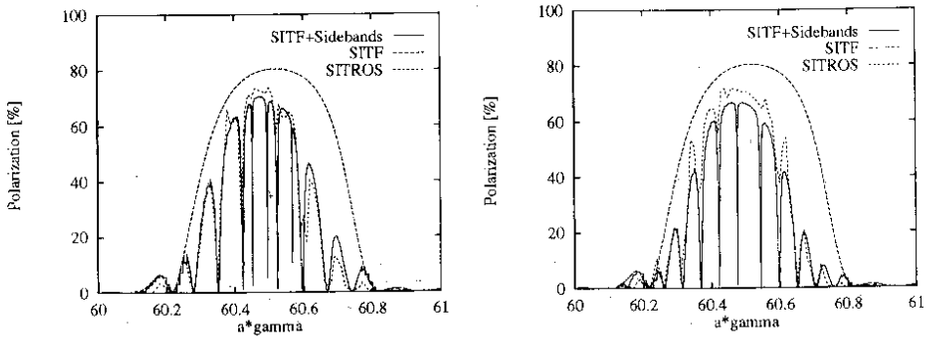

Figure 31: *Comparison between SITROS and SITF with superposed sidebands to Q_z ($\nu = k \pm Q_z + m_s Q_s$ with $|m_s| \leq 5$) for:* Left: $Q_s = 0.07216$, Right: $Q_s = 0.05380$

to Q_s=0.0538, λ^2 increases by a factor of 1.8. Thus one expects a significant increase of the sideband strengths and a decrease of the equilibrium polarization. Fig. (30) shows the simulation result for $Q_s = 0.0538$ which should be compared to curve (2.) in fig. (26). In fig. (31) a comparison between SITROS and the predictions by the sideband model (see also section 4) is performed for two different Q_s values. Sidebands to $\pm Q_z$ satisfying the resonance condition $\nu = k \pm Q_z + m_s Q_s$ with $|m_s| \leq 5$ are taken into account. The SITF result and these sidebands are superposed by fitting the sideband strength for $|m_s| = 1$ to the corresponding one given by SITROS at $Q_s = 0.07216$. The comparison for $Q_s = 0.05380$ uses the same Q_s independent fit parameter with an increased λ^2. The result given by the sideband model is consistent with the simulation result. This is a confirmation of the good modelling, i.e. sufficient sampling of the tails, of the energy spread in the Monte-Carlo calculation. The SITROS resonance structure is quite well approximated by taking only sidebands of Q_z into account. This indicates the dominating influence of these resonances. The effect of stronger sidebands on the polarization around the spin tune $\nu = 60.5$ is not so strong as expected. Much more important is the fact that the strong sidebands of low order $\pm Q_z + m_s Q_s$ ($|m_s| < 5$) are shifted towards the $\pm Q_z$ resonances. The spacing between the sidebands is $\sim$ 23 MeV instead of $\sim$ 32 MeV in the simulation with high Q_s. In particular the strong $Q_z + 3Q_s$ and $-Q_z - 4Q_s$ resonances are shifted by -27 MeV and $+36$ MeV respectively broadening the polarization plateau around $\nu = 60.5$ where no strong sidebands appear by 63 MeV. Although the "naive" application of the sideband model to SLIM results indicates that large Q_s could be beneficial [66][56], this example shows that it is not possible to draw the general conclusion that a higher Q_s is always helpful for realistic parameter values.

What is the influence of the nonlinear orbit motion introduced by chromatic effects and their compensation with sextupole fields on the polarization ?

To answer this question the chromatic terms in eq. (3.17) are neglected and the sextupoles are switched off in the simulation. The result is shown in fig. (32). Several spin resonances driven by the sextupoles ($|m_x| + |m_z| = 2$) are missing compared with fig. (26), namely $\pm 2Q_z$ and the corresponding sidebands $2Q_z + Q_s$ and $-2Q_z - Q_s$. The maximum polarization level is not significantly reduced by the nonlinear orbit effects.
Taking into account the uncertainties in the measurement mainly introduced by build up time effects and in the simulation mainly introduced by the missing knowledge of the exact magnet error distribution, measurement and simulation are in good agreement. The identification of the main limiting resonances is possible. The Monte-Carlo results suggest that the maximum

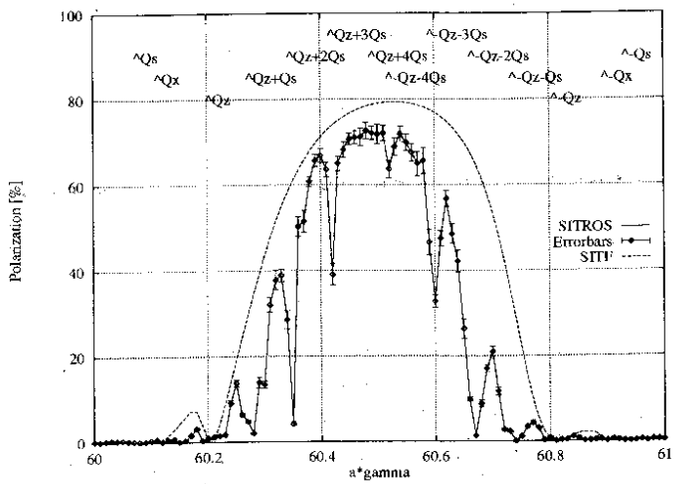

Figure 32: *Energy scan neglecting chromatic effects and sextupole corrections for a synchrotron tune $Q_s = 0.07216$ which compared with fig. (26) shows that several spin resonances driven by sextupoles ($|m_x| + |m_z| = 2$) are missing, namely $\pm 2Q_z$ and the corresponding sidebands $2Q_z + Q_s$ and $-2Q_z - Q_s$*

achievable polarization has not yet been reached. In fact in 1993 nearly 70% polarization were observed. A measured build up curve corresponding to this asymptotic polarization value is shown in fig. (33).

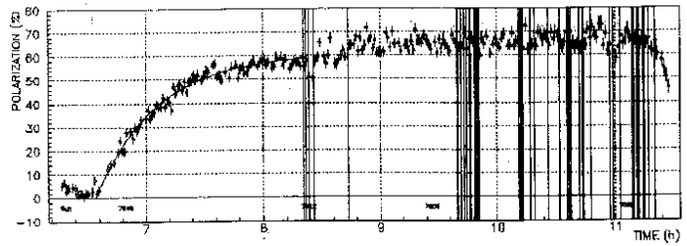

Figure 33: *Measured polarization build up curve. The fitted effective rise time τ_{eff} corresponds to an equilibrium polarization of $P_{eff} \sim 65\%$. After changing the tunes at 8:26h the polarization increased to maximum values close to 70% [67] (see also section 3.5.7). The polarization values just given are preliminary, because the systematic error on the measurement has to be analyzed in detail*

5.3 HERA with one pair of spin rotators

In this subsection calculations for a HERA machine with one rotator pair in the east straight section will be presented.
As mentioned earlier, the polarization builds up antiparallel to the main bending field. Thus the equilibrium polarization axis $\vec{n}_0$ has to be vertical in the arcs of HERA. To provide longitudinal polarization at the interaction point of the HERMES experiment in the east straight section the $\vec{n}_0$-axis has to be rotated from the vertical to the longitudinal direction before the interaction point and back again to the vertical before the arc. This rotation could be performed by a combination of very strong solenoidal fields and dipole fields [68].
But it can also be achieved using moderate dipole fields as in the "Mini-Rotator" scheme of Buon and Steffen [20] which is the scheme chosen for HERA. These rotators are placed at the ends of the arcs and involve combinations of vertical and horizontal bending fields arranged so that the horizontal bending fields replace one cell of the arc and so that the total vertical deflection and translation of the orbit is zero. This is no problem since the required orbital deflections are typically only tens of milliradians and therefore almost commute. However, the corresponding spin precessions angles are $a\gamma$ times larger than the orbit deflections and therfore do not commute. The noncommutative spin rotations add up to an effective rotation into the longitudinal direction which is illustrated in fig. (34). In this figure the angles are multiples of 45 degrees and are chosen so as to explain the basic principle in a clear way. In reality the angles are close to those shown only at 29.788 GeV. To obtain the required spin transformation at other energies the magnetic fields must be changed appropriately and so therefore must the transverse positions of the rotator magnets. To reverse the helicity at the interaction point the polarity of the vertical bend magnets must be reversed. This requires mechanically inverting the bend geometry in the vertical plane and can be achieved automatically with the help of jacks driven under remote control. The horizontal bend fields are left-right symmetric around the interaction point. The vertical bend fields are antisymmetric.

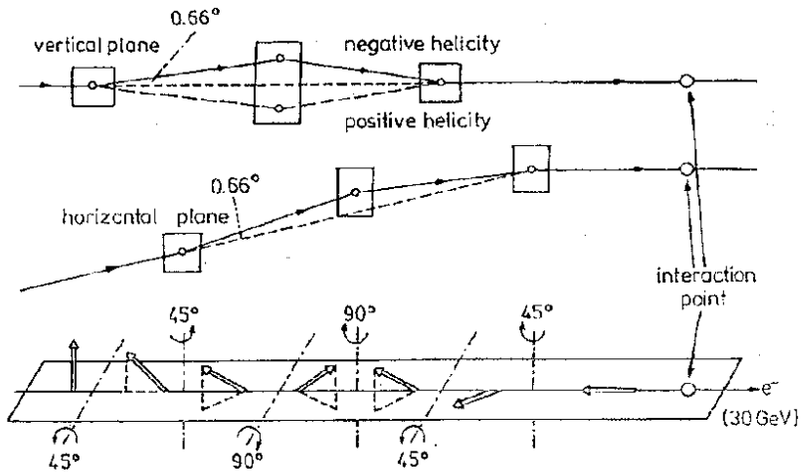

Figure 34: *Schematic drawing of the "Mini-Rotator" scheme used in HERA [20]. To change the helicity of the electrons at the interaction point the rotators have to be moved vertically, illustrated by the dashed lines*

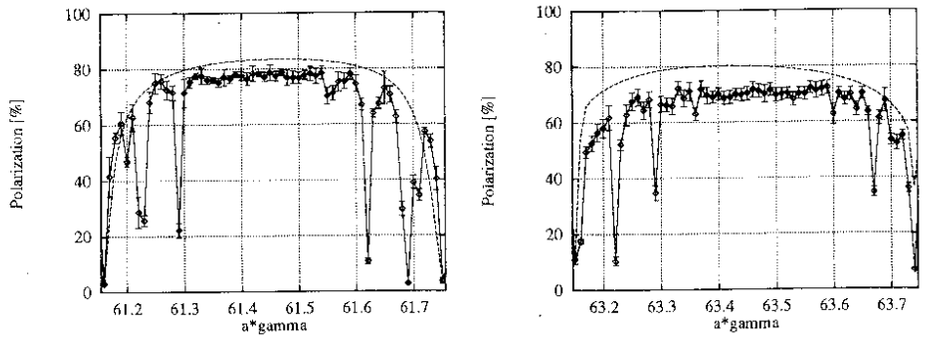

Figure 35: *Equilibrium polarization between the $\pm Q_z$ resonances with $Q_z = 0.2$ for an undistorted spin matched HERA optic with one pair of rotators in the east straight section for a central spin tune of $\nu = 61.5$, corresponding to an energy of 27.08 GeV* (Left) *and $\nu = 63.5$ corresponding to 27.96 GeV* (Right)*. The specified spin tune scale $a\gamma$ has to be shifted by ~ -0.05 to get the "real" spin tune ν. This shift is induced by the presence of the rotator magnets. The points with errorbars are the SITROS results and the dashed line describes the first order SITF result.*

Even in a perfect ring spin rotators introduce "spin diffusion". As explained in section 4 a tilted $\vec{n}_0$-axis in quadrupoles results in spin diffusion driven by horizontal oscillations excited in the arcs. The relevant terms are given by eq. (A.14) in appendix A. $\vec{n}_0$-axis tilts are usually nonsystematic and are caused by misalignments. However, the rotators in effect cause a systematic tilt of 90 degrees over a large section of the ring, namely between the rotators, and this can obviously be a source of massive spin diffusion and thus depolarization (see also fig. (1)). Moreover the vertical bending fields inside the rotator generate vertical dispersion leading to the excitation of vertical betatron oscillations and thus in the case of a longitudinal $\vec{n}_0$-axis to further spin diffusion. The same mechanisms cause spin diffusion in the case of energy oscillations of the particle (see eq. (A.14)).
To overcome these problems one tries to restore the "spin transparency" which is automatically available in the case of a perfectly flat ring. The spin diffusion is described by the diffusion vector $\vec{d}$ derived in appendix A in first order approximation. Thus the optic with rotators has to be designed so that the condition $|\vec{d}| = 0$ is fulfilled at all longitudinal positions where $1/|\rho^3|$ is large. This "spin matching" procedure has been applied to the present optic with one pair of rotators in the east straight section [69][70]. It is worth noting that the vertical spin match depends on energy.
SITROS is applied to a lattice which has been spin matched at a spin tune of $\nu = 61.5$ corresponding to an energy of 27.08 GeV and at $\nu = 63.5$ corresponding to 27.96 GeV. The results for the undistorted optic are shown in fig. (35). The spin tune range of the energy scans corresponds to the distance between the $\pm Q_z$ resonances with Q_z=0.2. Due to the fact that the rotators modify the spin precession geometry of the ring the "real" spin tune ν is shifted by ~ -0.05 with respect to the "nominal" spin tune $a\gamma$. In both cases the maximum equilibrium polarization is calculated to be ~80 % because the straight section layout means in practice that it is not possible to get a perfect spin match [71]. In a range of about 200 MeV around the half integer no strong higher order resonanes occur. The plateau is limited by sidebands to the $\pm Q_z$ resonances ($\pm Q_z + m_s Q_s$ with $m_s < 3$ and Q_s=0.07). Resonances to $\pm Q_x$ with Q_x=0.1 are not visible, indicating a very good horizontal spin match.
This lattice is then distorted randomly as in subsection 5.2. The MICADO orbit correction

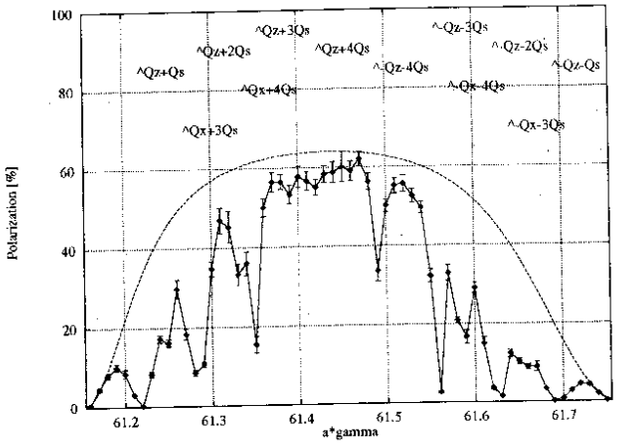

Figure 36: *Equilibrium polarization between the $\pm Q_z$ resonances with $Q_z = 0.2$ for a spin matched HERA optic with imperfections, corrections with MICADO and the harmonic bump scheme, for a central spin tune of $\nu = 61.5$ corresponding to an energy of 27.08 GeV. The points with errorbars are the SITROS results and the dashed line describes the first order SITF result.*

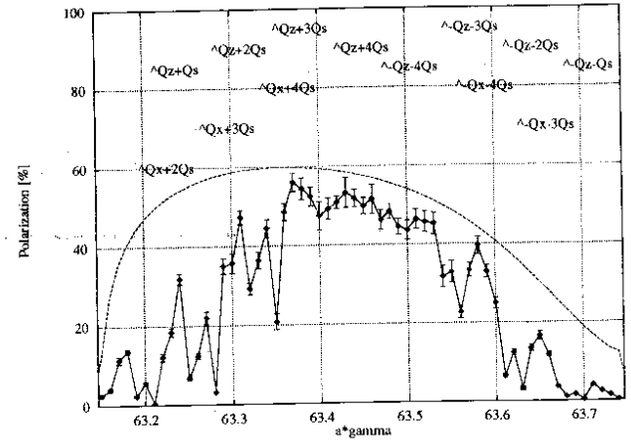

Figure 37: *Equilibrium polarization between the $\pm Q_z$ resonances with $Q_z = 0.2$ for a spin matched HERA optic with imperfections and corrections with MICADO and the harmonic bump scheme, for a central spin tune of $\nu = 63.5$ corresponding to an energy of 27.96 GeV* (Left) *and $\nu = 63.5$, corresponding to 27.96 GeV* (Right)*. The points with errorbars are the SITROS results and the dashed line describes the first order SITF result.*

scheme is applied to correct the rms values of the orbit down to x_{rms}=1 mm and z_{rms}=0.9 mm, respectively. In the next step the harmonic bump scheme appropriate for a ring including the rotators, is applied to minimize the spin-orbit coupling. The results for both energy regions are shown in fig. (36) and fig. (37). The maximum achievable equilibrium polarization is calculated to be ~60 %. Strong sidebands to the first order spin resonances $\pm Q_z$ and $\pm Q_x$ appear.

A comparison with the result for an optimized machine without rotators presented in fig. (26, curve 2) shows that the achievable equilibrium polarization is reduced by 20 % due to the presence of the rotators. Sidebands to the $\pm Q_x$ spin resonances are much stronger for a machine with rotators than without. Nevertheless, longitudinal polarization values above 50 % are possible.

5.4 Depolarization with a time dependent radial magnetic field

Assuming that the equilibrium polarization axis $\vec{n}_0$ is parallel to the vertical direction $\vec{e}_z$ an ensemble of particles can be depolarized by rotating the spin vectors permanently into the horizontal plane. This is done by widening the precession cone of the individual particles with respect to $\vec{n}_0$ as demonstrated in fig. (38). The widening can be performed by time dependent radial magnetic fields. The frequency of the depolarizing field is given by:

$$\Omega_{Dp} = \mid \pm a\gamma \pm k \mid \omega_c, \quad k = \text{integer}, \tag{5.1}$$

where ω_c is the relativistic cyclotron frequency in eq. (2.5). Eq. (5.1) illustrates the direct relation between the depolarizer frequency and the energy E_0 of the beam. Thus the measurement of Ω_{Dp} allows the beam energy to be calibrated with a precision mostly determined by the error of the frequency measurement and the width of the induced resonance ($\sim$ 1 MeV for an integrated field of $Bl = 1$ Gm) which is much smaller than the energy spread of the beam ($\sigma_S \sim 30$ MeV at 26.666 GeV). The latter can be explained by the fact that the characteristic time for the depolarization process is much longer ($\tau_{Dp} \sim 14$ sec for $Bl = 1$ Gm) than the period of the synchrotron frequency (~ 300 μsec) and the damping time of the energy oscillations (~ 7 msec) of the particles. The method allows an energy calibration down to the 1 MeV level. In contrast to this precision the knowledge of the integral field of the main dipoles at 26.66 GeV in HERA leads to an uncertainty in energy of ± 50 MeV. This depolarizing mechanism has been demonstrated for example at DORIS[11], PETRA[74], LEP[12] and recently also at HERA [67].

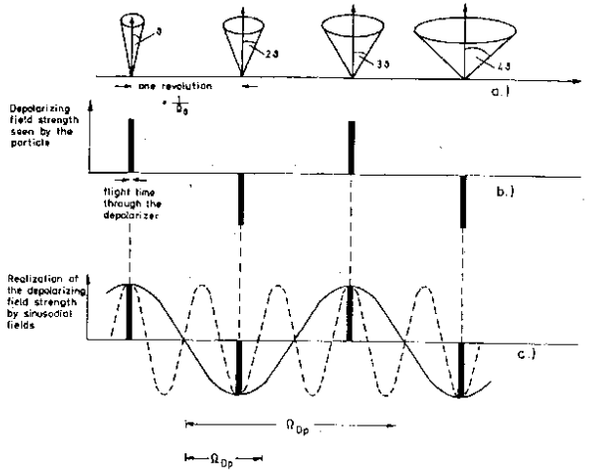

Figure 38: *Depolarizer in the case $a\gamma = n \pm 0.5$. The depolarizing field must change its sign from revolution to revolution [74]*

Already in 1982 J. Kewisch [72] used SITROS to simulate the influence of time dependent dipole fields on the polarization, one of the main advantages of this tracking code compared with other methods of determining the equilibrium polarization. In this section simulation results for HERA will be presented [73].
The rotation of a spin vector for a given field strength is almost independent of the energy for magnetic fields perpendicular to the velocity vector (see eq. (2.4)) of the particle. The rotation

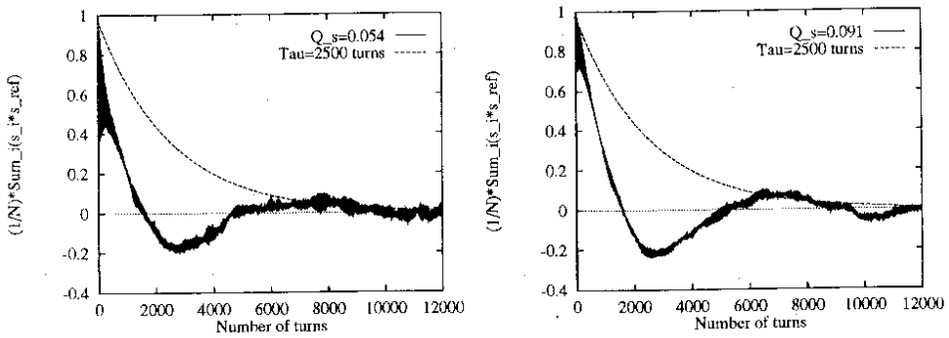

Figure 39: *Coherence decay of the instantaneous horizontal polarization component for two different synchrotron tunes $Q_s = 0.054$ (Left) and $Q_s = 0.091$ (Right) for a HERA optic at $a\gamma = 60.4$. The decoherence time $\tau_{dec} = 2.5 \times 10^3$ turns is calculated from the dashed exponential curve*

angle for a single passing of a localized radial field B is given by:

$$\vartheta = \frac{e}{m_e c}\left(a + \frac{1}{\gamma}\right) Bl, \quad l = \text{depolarizer length}, \tag{5.2}$$

with $ea/m_e c = 0.068$ mrad/Gm. Assuming an exact accumulation of the spin tilt from turn to turn one would expect a time of $\sim$ 23000 turns (= 0.5 sec in HERA) to rotate the spin of a single particle by $\pi/2$ using $Bl = 1$ Gm.
What conditions are required to depolarize an ensemble of particles?
Quantum fluctuations lead to a spin diffusion process in the horizontal plane. One can simulate the decoherence time τ_{dec} of the decay of the instantaneous horizontal polarization component by starting all particles with spin vectors in the horizontal plane and looking at the average over the projections of the individual spins onto a reference spin vector $\vec{S}_{ref}$ belonging to the closed orbit particle which by definition suffers no quantum fluctuations:

$$\frac{1}{N}\sum_i^N \vec{S}_i \cdot \vec{S}_{ref}.$$

This quantity is shown in fig. (39) over 1.2×10^4 HERA turns and yields a $\tau_{dec} = 2.5 \times 10^3$ turns. The decoherence time does not depend on Q_s. But the fluctuations become smaller due to synchrotron oscillations with higher frequency.
To depolarize an ensemble of particles starting with all spin vectors parallel to the $\vec{n}_0$-axis it is necessary that the time τ_{Dp} which is needed to bring all spins from the direction $\vec{n}_0$ to the horizontal plane is large compared to τ_{dec}, otherwise there is nearly no decay of the instantaneous horizontal polarization component. If the coherence were not lost, it would be possible to flip the average spin vector into a direction which is antiparallel to the $\vec{n}_0$-axis ("polarization-flip")[12].
To calculate a resonance curve of the artificial resonance induced by a depolarizer with an integrated field of $Bl = 1$ Gm one varies the frequency around the chosen working point of $a\gamma = 60.4$ ($\Omega_{Dp} = 0.4$ in units of ω_c). Under the condition that the instantaneous horizontal polarization component vanishes the average spin vector $(1/N)\sum_i \vec{S}_i$ is parallel to the $\vec{n}_0$-axis. The depolarization process of the vertical polarization component can be described by an increase of the tilt of a fictitious unit spin vector $\vec{S}_f$ with respect to the $\vec{n}_0$-axis ($\vec{S}_f \cdot \vec{n}_0 =$

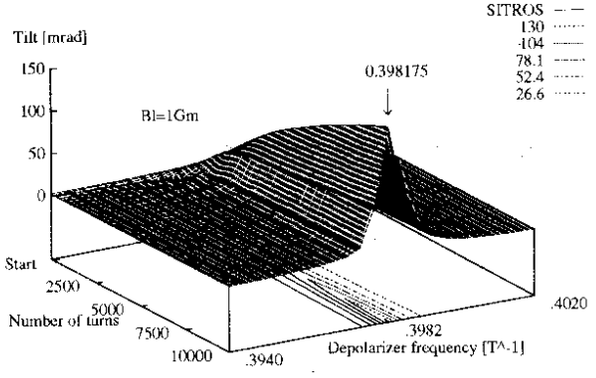

Figure 40: *Tilt of the fictitious unit spin vector $\vec{S}_f$ ($\vec{S}_f \cdot \vec{n}_0 = |(1/N)\sum_i \vec{S}_i|$) with respect to the $\vec{n}_0$-axis for $Bl = 1$ Gm. The depolarizer frequency Ω_{Dp} is varied from 0.3940 to 0.4020 in units of the revolution frequency T^{-1}. $1{\times}10^4$ turns (0.21 sec) are shown after the time varying field was switched on at "Start". The arrow designates the centre of the resonance corresponding to a fractional spin tune of 0.398175. The numbers given in the key correspond to constant tilt contours which are shown at the bottom of the graph. The coherence decay shows up in the damped oscillations of the surface*

$|(1/N)\sum_i \vec{S}_i|$). Fig. (40) shows the evolution of this tilt over 1×10^4 turns (0.21 sec) for a frequency range $\Delta\Omega_{Dp}$ of $0.394 \leq \Omega_{Dp} \leq 0.402$ in units of ω_c corresponding to a frequency range of [18.656, 19.035] KHz or an energy range of [26.6193, 26.6228] GeV. No orbital excitations due to the presence of the additional radial field are included. The simulations are performed for a HERA lattice without imperfections (x_{rms} =0.3 mm, z_{rms} =0 mm) with an equilibrium polarization of $\sim$ 92%. All spin vectors of the ensemble are started parallel to $\vec{n}_0$. At the central energy E_0 of the particle motion at $\Omega_{Dp} = 0.398175$, indicated by the arrow the time varying depolarizer field is in resonance with the central spin precession frequency $a\gamma$. The difference of Ω_{Dp} to the fractional spin tune $a\gamma = 0.4$ can be explained by the fact that the total bending angle of the HERA optic used has an absolute error of $6\pi \times 10^{-5}$ leading to an absolute spin tune shift of 1.82×10^{-3} at $a\gamma = 60.4$. This integrated error is generated by the finite precision of the definition of the bending fields in the optic file. The shift due to the presence of sextupoles and the additional bending fields caused by the closed orbit in the quadrupoles is more than one order of magnitude smaller. Assuming an exponential decay of the polarization (which is sensible under the condition that the ensemble becomes decoherent on a time scale which is much smaller than the time scale of the depolarization time) the calculated τ_{Dp} for N =500 particles at the central frequency is 6.8×10^5 turns ($\sim$ 14 sec in HERA) which is indeed large compared with the decoherence time τ_{dec}. Fig. (41, Bottom) describes the dependence of τ_{Dp} on the strength of the integrated depolarizer field Bl between 1 and 100 Gm and the corresponding tilt evolution in Fig. (41, Top) for the central frequency $\Omega_{Dp} = 0.398175$. Starting from eq. (5.2) one would expect a $1/Bl$ behaviour for τ_{Dp}. The fit in fig. (41, Bottom) shows that the SITROS results for τ_{Dp} are in agreement with a $1/(Bl)^2$ dependence.

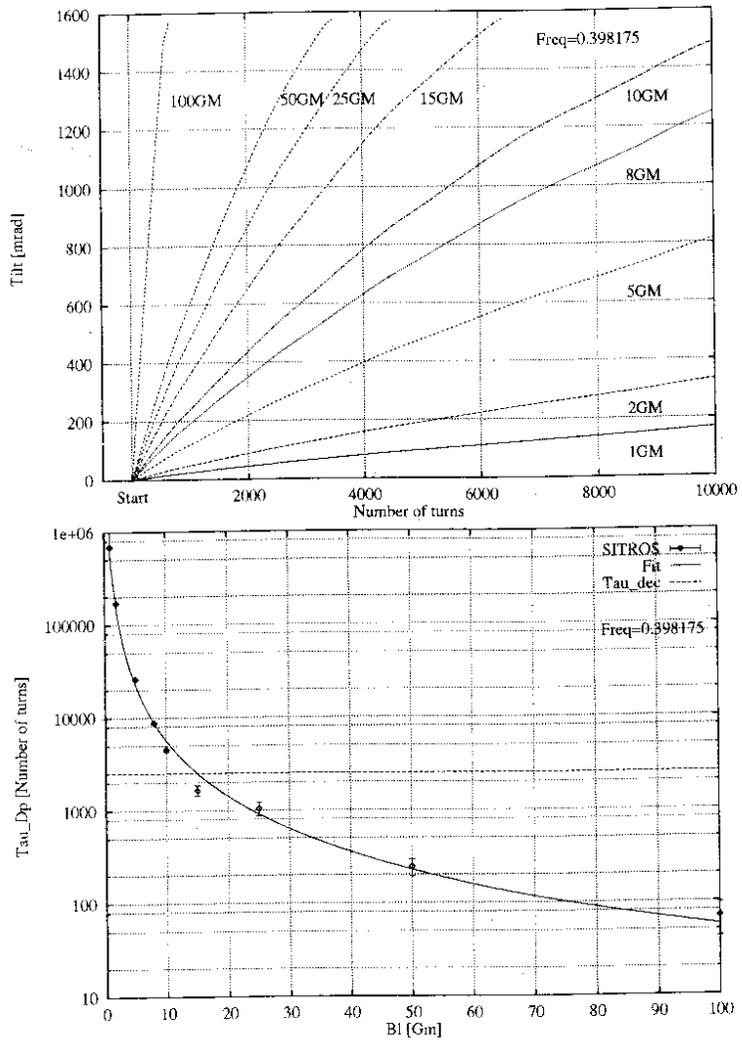

Figure 41: Top: *Tilt of the fictitious unit spin vector $\vec{S}_f$ with respect to the $\vec{n}_0$-axis for different integrated field strengths Bl over $1{\times}10^4$ turns*, Bottom: *Corresponding depolarization times τ_{Dp} (points) versus Bl and a fit showing that τ_{Dp} has approximately a $1/(Bl)^2$ behaviour. The dashed straight line corresponds to the previously calculated decoherence time τ_{dec}. The calculation of τ_{Dp} is based on the assumption of an exponential depolarization process which is only valid if τ_{Dp} is large compared with τ_{dec}*

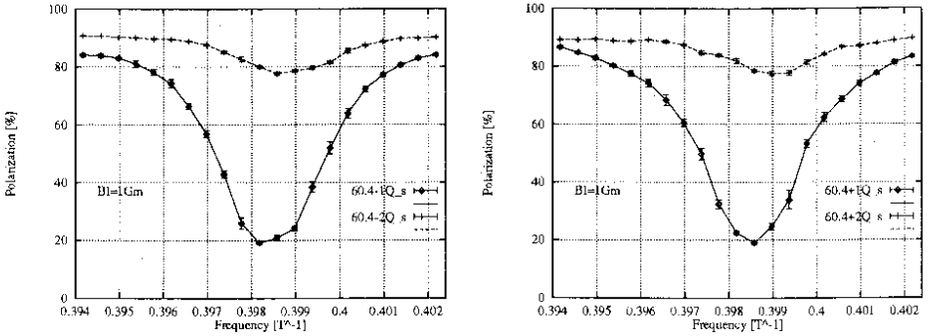

Figure 42: *Sidebands to the central depolarizer resonance near* $a\gamma = 60.4$ *for energies* $a\gamma = 60.4 - Q_s$, $a\gamma = 60.4 - 2Q_s$ *(*Left*) and* $a\gamma = 60.4 + Q_s$, $a\gamma = 60.4 + 2Q_s$ *(*Right*) with* $Q_s = 0.072$ *for a depolarizer with an integrated field of* $Bl = 1$ *Gm and a frequency range from 0.394175 to 0.402175*

As already mentioned the error of the energy calibration is mostly determined by the width of the resonance induced by the depolarizer. In fig. (43, Top) resonance curves for various integral field values between 0.5 and 2.5 Gm are shown. The results presented include the depolarization process and the competing build up process due to the Sokolov-Ternov effect (see fig. (43, Top)). The width depends essentially linearly on the strength of the applied integral field (see fig. (43, Bottom)). For $Bl = 1$ Gm the width is about 1 MeV corresponding to a frequency range of $\Delta\Omega_{Dp} \sim 100$ Hz.

Owing to the fact that the particles are undergoing synchrotron oscillations the individual precession frequencies are modulated with the synchrotron tune leading to sidebands to the main depolarizer resonance at 60.398175 separated by Q_s. For $Q_s = 0.072$ sidebands appear at $60.398175 + m_s \cdot 0.072$ with $m_s \neq 0$. The sidebands with $|m_s| \leq 2$ are shown in fig. (42). The simulations are performed for energies with a spacing of ~32 MeV corresponding to Q_s calculated at $a\gamma = 60.4$ at either side of the main resonance. Thus the change of the synchrotron tune with energy leads to a small shift of the sidebands in the depolarizer frequency domain. The results indicate that the first order sidebands are strong. Therefore if one wants to perform an energy calibration it is necessary to find out whether the depolarization takes place on a sideband or the main resonance. This can be easily done by the variation of Q_s shifting the sidebands in the frequency domain.

The results presented are not completely realistic in the sense that the radial field of the depolarizer produces a nonnegligible orbital excitation depending on the vertical β function at the position of the magnet which can lead to a broadening of the depolarizer induced resonance [74]. The frequency scans were performed for fixed frequencies Ω^i_{Dp} ($i \leq n$, $n=$ number of frequencies). In reality the depolarizer sweeps around Ω^i_{Dp} with a certain frequency range $\Delta\Omega^i_{Dp}$ and a certain speed $d\Omega^i_{Dp}/dt$. Depending on $\Delta\Omega^i_{Dp}$, $d\Omega^i_{Dp}/dt$ and the width of the resonance the effective depolarization time τ_{Dp} is changed. The calculations describe the limiting case $\Delta\Omega^i_{Dp} \to 0$ and $d\Omega^i_{Dp}/dt \to 0$. Nevertheless it is interesting to compare these results with the first measurements performed in autumn 1993 [67].

At HERA the beam was depolarized with an integrated field of <2 Gm in less than 1 minute which is consistent with τ_{Dp} ~14 sec for $Bl = 1$ Gm given by SITROS (see fig. (41, Bottom)). As predicted by the presented simulations ($\tau_{dec} \sim 50$ msec $<< \tau_{Dp}$ ~14 sec), no "polarization-flip" was observed. The width of the resonance was measured to be smaller than Ω_{Dp} <200 Hz (2 MeV) which fits to the results shown in fig. (43, Bottom). The beam energy was found

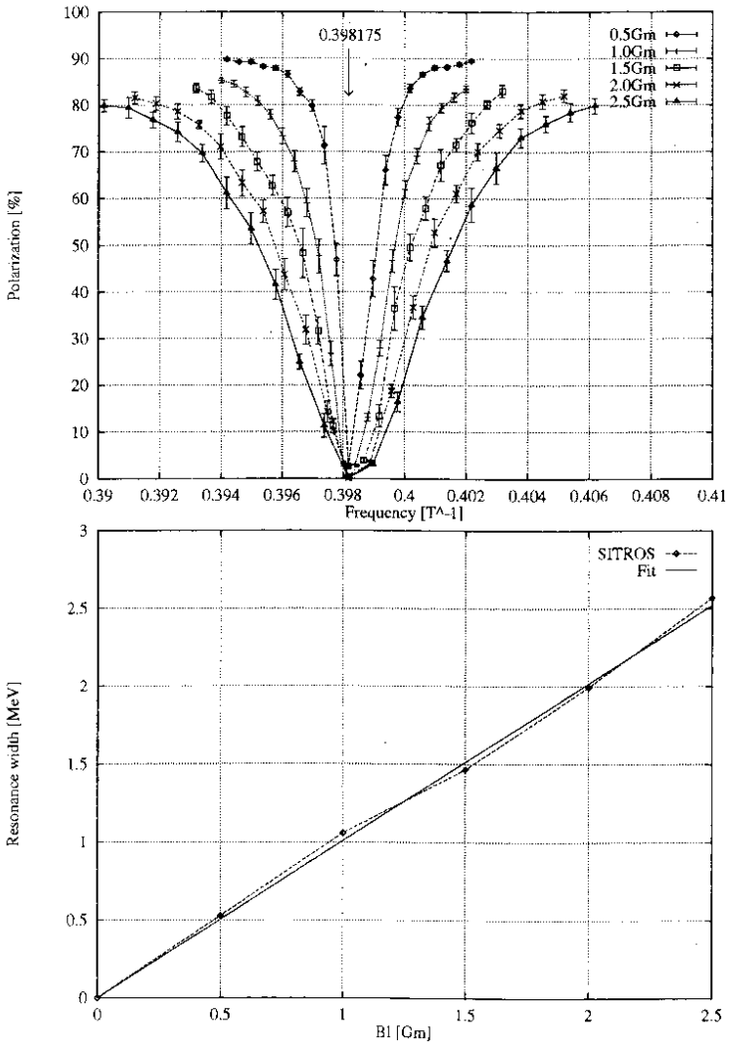

Figure 43: Top*: Resonance curves for different integrated field strengths Bl,* Bottom*: Corresponding resonance widths (points) versus Bl and a fit showing that the calculated resonance width depends linearly on the depolarizer strength*

to be about 33-36 MeV below the nominal energy given by the integrated field of the main dipoles. It was checked by a Q_s shift that the main resonance had been found. These results are preliminary and not published yet. The simulations presented are consistent with the first depolarizer measurements at HERA.

6 Comparison of SITROS with analytical approaches

In this section comparisons between SITROS and other methods to calculate the equilibrium polarization level in the presence of depolarizing effects will be performed. The main aim of this section is to show that SITROS results are in good agreement with results derived by the program SODOM [34] using a completely different treatment. Furthermore a comparison with a sideband model for the betatron resonances [57] will be presented showing qualitative agreement, where the differences, as will be demonstrated, can be explained by the restrictions of the sideband model.

6.1 Comparison with SODOM

SODOM ((S)pin-(O)rbit (D)ynamics using (O)ne-turn (M)ap) is a tracking code for the calculation of equilibrium electron polarization P_{eff} using one-turn spin maps written by K. Yokoya [34]. SODOM evaluates $\vec{n}$ and $\gamma\partial\vec{n}/\partial\gamma$ from the information of numerical tracking of the spin-orbit motion without radiation. P_{eff} is then calculated using the Derbenev-Kondratenko formula (eq. (2.14)).
SODOM tracks particles with certain starting conditions in phase space to determine the derivative of $\vec{n}$ with respect to γ and to perform the integration of $\gamma\partial\vec{n}/\partial\gamma$ and $|\gamma\partial\vec{n}/\partial\gamma|^2$ over the orbital phase space. A special problem is the sampling of the longitudinal phase space because $\vec{d}$ depends strongly on the particle amplitudes in the longitudinal direction. One has to decide what the maximum amplitude is which has to be included in the evaluation of the integrals. This decision is related to the question of how important the particles in the tails of the distribution are for the determination of the equilibrium polarization (see section 3.6).

```
CELL(B)     = QFH D B D QDH QDH D B D QFH
HRING(BV)   = CELL(BV) 32*CELL(B) CAV 32*CELL(B) CELL(BV)
RING        = HRING(BUP) HRING(BDOWN)
QFH         quad.  length 0.5m.  k=+0.09121608/m
QDH         quad.  length 0.5m.  k=-0.08381805/m
D           drift space.  length 0.5m.
B           bend.  length 6m.  angle 1.40625deg.
BUP         vertical bend.  6m.  +0.1deg.
BDOWN       vertical bend.  6m.  -0.1deg.
CAV         rf cavity.  length 0m.  peak voltage 75MV.
```

Table 1: *Structure of the model ring from [75]*

Because SODOM is not able to handle nonlinear orbit motion up to now and the possibility to introduce magnet distortions has just been included recently [76], the comparison with SITROS is performed for a model ring consisting of 128 identical FODO cells plus four vertical S-bend cells (see tab. (1)). The betatron tunes are Q_x=33.264 and Q_z=28.379. The synchrotron tune Q_s, σ_s and σ_δ are 0.06243, 6.503×10^{-3}m and 1.137×10^{-3} at E_0 =20.74 GeV. The closed orbit was determined neglecting radiation effects ($x_{rms} = 1.5 \times 10^{-5}$m, $z_{rms} = 0$m). In this model the $\vec{n}_0$-axis is parallel to the vertical direction $\vec{e}_z$ except in the S-bend cells where it is tilted longitudinally by $\sim$ 80 mrad at $E_0 \sim$ 20 GeV. The average vertical dispersion D_z generated is calculated to be ~20 mm. As a result a first order synchrotron resonance $(47+Q_s)$ is excited. Owing to the spin tune modulation due to synchrotron oscillations higher order sideband resonances are induced $(47 + Q_s + m_s Q_s, m_s > 0)$ in the energy region $47 \leq \gamma a \leq 47.3$. This region was chosen because the effect of the betatron resonances Q_x, Q_z is very small in this interval due to the superperiodicity conditions of the lattice. Fig. (44) shows

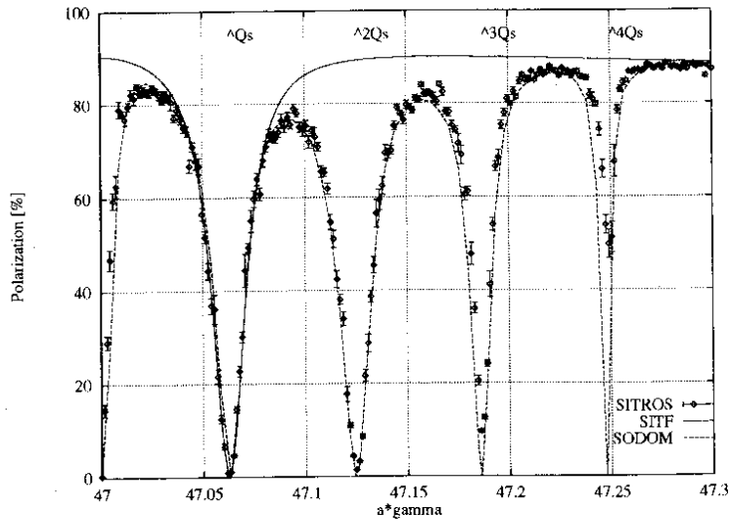

Figure 44: *Equilibrium polarization for a model ring (tab. (1)) calculated by SODOM (dashed line) and SITROS (points with errorbars). The solid curve shows the first order result from SITF*

the SODOM result (dashed curve), the first order calculation with SITF (solid curve) and the SITROS result (points with errorbars). The maximum longitudinal particle amplitude used in SODOM to perform the integration over the longitudinal phase space is $3\sigma_s$. Contributions from particles with larger amplitudes have a neglegible effect on P_{eff}. The SITROS calculation takes into account particles up to $2.3\sigma_s$ (see fig. (12)). Small differences due to the different tail sampling have been corrected by an increase of σ_s by a factor of 1.2 in SITROS adjusting the excitation strength K properly. The agreement between SODOM and SITROS is perfect. The linear optical parameters are almost identical and the differences for the calculated equilibrium polarization between 47 and 47.3 are neglegible.
At least for this artificial example these totally different treatments lead to to the same result. Furthermore both programs demonstrate that the effect of depolarization far out in the tails of the energy distribution can be neglected in this example, where the depolarization is weak.

6.2 Comparison with a sideband model for betatron resonances

In the following subsection a comparison between SITROS and a sideband model for betatron resonances introduced by S. Mane [57] will be performed.
The sideband model predicts the strengths of sidebands to a given isolated betatron resonance due to tune modulation characterized by the tune modulation index λ^2:

$$\frac{\frac{11}{18}\langle \oint \frac{ds}{|\rho(s)|^3} \left|\gamma \frac{\partial \vec{n}}{\partial \gamma}\right|^2 \rangle}{\oint \frac{ds}{|\rho(s)|^3}} = A_{x/z}^{+/-} \sum_{m_s=-\infty}^{\infty} \left\{ \frac{\exp(-\lambda^2)}{(\nu - k \mp Q_{x/z} + m_s Q_s)^2} \left[J_{x/z} I_{m_s}(\lambda^2) + J_s \frac{\lambda^2}{2} \left(I_{m_s-1}(\lambda^2) + I_{m_s+1}(\lambda^2) \right) \right] + \frac{\exp(-\lambda^2)}{\nu - k \mp Q_{x/z} + m_s Q_s} \frac{m_s J_s}{Q_s} I_{m_s}(\lambda^2) \right\}, \qquad (6.1)$$

where $A_{x/z}^{+/-}$ characterizes the strength of the betatron resonance at $\nu = k \pm Q_{x/z}$, $J_{x/z}$ and J_s are the damping partition numbers, I_{m_s} is a modified Bessel function, m_s denotes the order of the sidebands $\nu = k \pm Q_{x/z} + m_s Q_s$. This equation describes the main contribution to depolarization in the Derbenev-Kondratenko formula (eq. (2.14)) under the condition that the depolarization due to a tilt of $\vec{n}_0$-axis is small. In this case the left part of eq. (6.1) can be identified with the ratio of the polarization buildup time τ_p and the depolarization time τ_d:

$$\frac{\tau_p}{\tau_d} = \frac{\frac{11}{18}\langle \oint \frac{ds}{|\rho(s)|^3} \left|\gamma \frac{\partial \vec{n}}{\partial \gamma}\right|^2 \rangle}{\oint \frac{ds}{|\rho(s)|^3}}.$$

The equilibrium polarization is determined by eq. (2.11).
The calculations are performed for a HERA lattice without imperfections but with an additional systematic quadrupole twist of 0.1 mrad in the energy range $60 \leq a\gamma \leq 61$ at a working point $Q_x = 0.238$, $Q_z = 0.328$, $Q_s = 0.072$. This sytematic distortion leads to a beam ellipse twist of ~ 35 mrad and a small $\vec{n}_0$-axis tilt of ~ 0.03 mrad around $a\gamma = 60.5$ and ~ 5 mrad at integer spin tune. The generated vertical dispersion is $D_z \sim 1$ mm. The rms values for the closed orbit are x_{rms}=0.54 mm and z_{rms}=0.004 mm. The finiteness of the vertical closed orbit originates in the fact that the energy loss and gain leads to a small horizontal closed orbit distortion and thus in the presence of skew quadrupole components to a small vertical closed orbit distortion. The Q_y resonances are induced by betatron coupling and the vertical dispersion. The tune modulation index is calculated to be $\lambda^2 \sim 0.6$.
The $A_y^{+/-}$ are determined by fitting the ratios τ_p/τ_{dy} evaluated from the first order spin integrals (in fact SITF uses a different approach, see appendix A) for the individual oscillation modes neglecting interference effects in the calculation of $\vec{d}$ (see appendix A). The fit function for isolated first order resonances of mode y is given by:

$$\frac{\tau_p}{\tau_{dy}}(\nu) = \frac{A_y^+ J_y}{(\nu - 60 - Q_y)^2} + \frac{A_y^- J_y}{(\nu - 61 + Q_y)^2} \qquad (6.2)$$

with $J_x = J_z = 1$, $J_s = 2$. Fig. (45) shows the SITF result for the first order spin integrals and the fit for τ_p/τ_{dy} using eq. (6.2). Large τ_p/τ_{dy} correspond to small equilibrium polarization values. The last picture compares $\tau_p(\sum_y 1/\tau_{dy})$ with the SITF result, which **includes** interference effects. The significant difference between SITF and the fit can be explained by the neglect of interference terms when adding up the squares of spin integrals for the individual modes. The sidebands of the betatron resonances are given by eq. (6.1) using the fitted $A_{x/z}^{+/-}$. Considering sidebands which satisfy the resonance conditons $\nu = k \pm Q_{x/z} + m_s Q_s$ with $|m_s| \leq 5$ and the synchrotron resonances at $\nu = k \pm Q_s$ one can try to compare the result for the equilibrium polarization (fig. (46), Bottom) with the corresponding SITROS result (fig. (46), Top). The resonance structure looks similar although the maximum predicted polarization around the half integer is different.
The sideband model is very helpful to identify sideband resonances and to get an overview over the resonance structure which is dominated by the first order betatron resonances and their sidebands. But it is not able to predict the absolute polarization level. The main drawback of the method is the assumption of isolated resonances and non-interference which is clearly not fulfilled in the case of HERA.

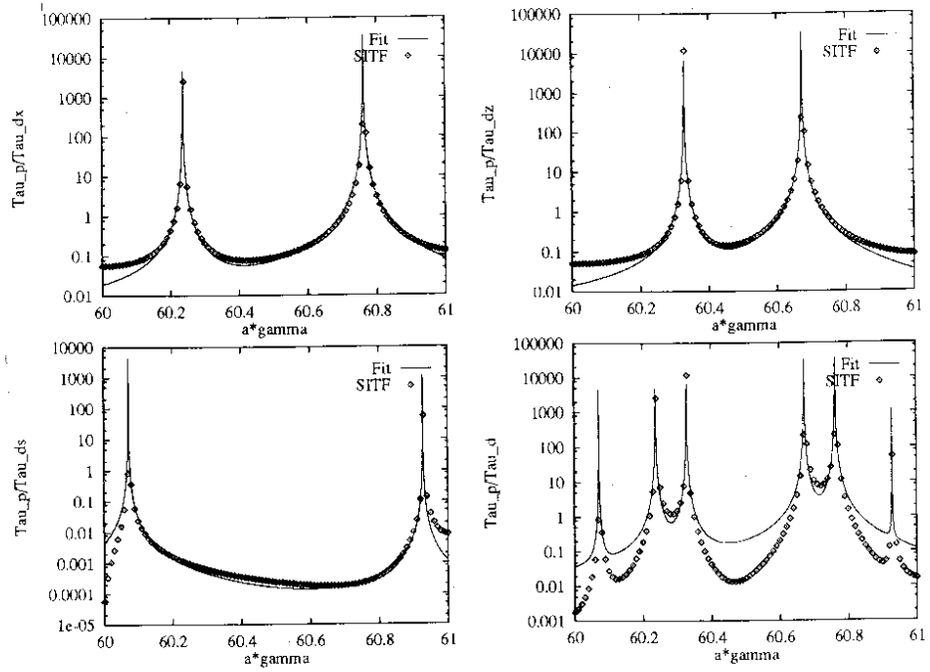

Figure 45: *SITF results and resonance fits of τ_p/τ_{d_y} for the $\pm Q_y$ resonances to determine the resonance strength factors for a HERA optic without imperfections but with an additional systematic quadrupole twist of 0.01 mrad (Top: τ_p/τ_{d_x} and τ_p/τ_{d_z}, Bottom: τ_p/τ_{d_s} and $\tau_p(\sum_y 1/\tau_{d_y})$)*

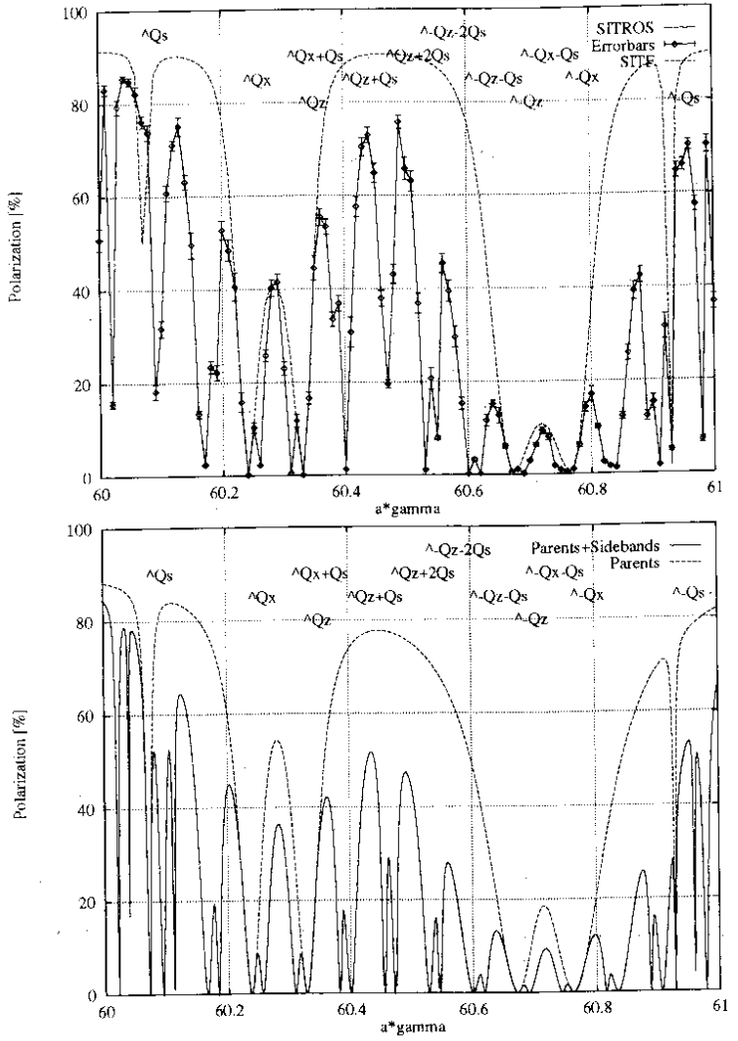

Figure 46: *Comparison between SITROS and a sideband model for Q_x and Q_z resonances introduced by S. Mane [57] for a HERA optic without imperfections but with an additional systematic quadrupole twist of 0.01 mrad. Sidebands satisfying the condition $\nu = k \pm Q_{x/z} + m_s Q_s$ with $|m_s| \leq 5$ are taken into account in the model*

7 Summary

In this work the algorithm of the Monte-Carlo program SITROS originally written by J. Kewisch has been analyzed in detail. Several checks have been performed to make sure that the approximations which are needed to overcome computing time limitations are physically sensible and that these have no undesirable influence on the simulation results. The systematic and statistical errors of the Monte-Carlo treatment have been studied in detail. The potential problems introduced by the bad sampling of the tails of the tracked particle distributions have been discussed.
On the basis of this analysis the program has been applied to a HERA machine without rotators and comparisons have been made with several polarization measurements. The simulations contain a realistic description of the machine conditions pertaining during the measurements. The influence on the equilibrium polarization of the beam ellipse twist introduced by an evenly distributed skew quadrupole component in the ring observed in 1991 and the correction with a decoupling bump have been studied in detail. The simulation results are in good agreement with the performed measurements. The behaviour of HERA concerning polarization in 1991 can be understood on the basis of the Monte-Carlo studies.
A special spin-orbit correction scheme has been tested in SITROS before the application in the control room in summer 1992. The simulations show an significant increase in polarization due to the application of the scheme although the correction method is based on first order perturbation theory. Nevertheless, the synchrotron sidebands to the horizontal and vertical betatron spin resonances are predicted to remain strong. The sidebands to vertical betatron spin resonances are especially strong up to high order. Again comparisons between measurements and simulations with realistic machine conditions have been performed. The agreement is encouraging.
On the basis of the experience with SITROS for HERA without rotators the program has been used to predict the equilibrium polarization level for a machine with one spin rotator pair in the east straight section of the ring. This rotator pair will be installed in 1994 to provide longitudinal polarization for the HERMES experiment. The simulations indicate that it is possible to get a high degree of polarization by a proper spin matching of the optic and a correction of special harmonics of the spin-orbit coupling function with the above mentioned correction scheme.
The effect of an oscillating radial magnetic dipole field on the polarization has been studied. The dependence of the widths of the induced resonances on the strength of the integrated dipole field have been calculated. The possibility of polarization flip has been studied. The first measurements made in 1993 are consistent with the simulation results.
SITROS has been compared with the program SODOM written by K. Yokoya in which he uses a different approach to calculate the equilibrium polarization. For a model ring which is similar to TRISTAN, operated at KEK, the results of both programs are in excellent agreement. In addition SITROS has been applied to a weakly distorted HERA optic to compare it with a sideband model introduced by S. Mane which is based on the assumption of isolated betatron spin resonances in the case of an only slightly tilted $\vec{n}_0$-axis. It has been found that the assumption of isolated resonances cannot be made, leading to quantitatively different results. Nevertheless the sideband model represents a good method to get a quick overview over the sideband structure.

It has been demonstrated that SITROS is able to model HERA in a realistic way. Thus all changes to the machine conditions can be simulated in SITROS to estimate the possible influence on the equilibrium polarization. In the future the influence of the beam-beam interaction has to be studied in detail to answer the question whether a high degree of longitudinal polarization is possible under luminosity conditions.

8 Acknowledgements

First I would like to thank Dr. D.P. Barber for continuous support and guidance and many valuable ideas and illuminating discussions.
Special thanks to Dr. R. Brinkmann and Dr. E. Gianfelice-Wendt for many valuable ideas and suggestions.
I would like to thank Prof. Dr. B. Wiik for making the thesis possible and for his continuous interest in the polarization studies at HERA.
I am grateful to Prof. Dr. P. Schmüser for careful reading of the manuscript and many helpful and valuable suggestions.
Thanks to Prof. Dr. A. Wagner for the continuous support of the thesis and his patience during the last months.
Especially I want to thank my colleagues in the polarimeter group and several members of the HERMES experiment for the good collaboration and many stimulating discussions.
I would like to thank all my colleagues in the machine group for providing excellent working conditions and a nice atmosphere. Among these are the Dipl.Phys., resp. Dres., Oliver Brüning, Winfried Decking, Klaus Flöttmann and Anuschka Pauluhn. In many stimulating discussions I got innumerable good and valuable suggestions and hints.
I would like to thank Dr. H. Grote for fruitful discussions and for his hospitality during my visit at CERN.
Furthermore helpful discussions with the Dres. J.P. Koutchouk, T. Limberg and R. Schmidt are warmly acknowledged.
Finally, I want to thank the DESY directorate for giving me the possibility to write a thesis in the field of accelerator physics and for continuous support.

A Polarization calculation in first order approximation

This appendix is written with the intention to give a short introduction to the first order polarization theory and thus to introduce the quantities which are necessary for the interpretation of the tracking results. In fact many results given by the spin tracking can be interpreted on the basis of first order polarization theory. Furthermore the first order polarization calculations performed by SITF are an important independent check of the tracking calculations. The appendix follows the argumentation of K. Yokoya [77]. Following section 3.4 the spin motion is governed by the Thomas-BMT equation:

$$\vec{S}\,' = \vec{\Omega} \times \vec{S}, \tag{A.1}$$

where $\vec{\Omega}$ describes the precession with respect to the design coordinate frame and is given for example at $\delta = 0$ by:

$$\begin{aligned}
\Omega_x &= (a\gamma+1)\left(h_z + j_z + \epsilon_z + \left(k - h_z^2 - j_z h_z - \epsilon_z h_z\right) z\right. \\
&\quad \left. + \left(-k - h_z h_x - j_z h_x - \epsilon_z h_z\right) x - \epsilon_{s0} z'\right) - a\gamma h_s x' - h_z \\
\Omega_z &= (a\gamma+1)\left(h_x + j_x + \epsilon_x + \left(-k + h_x^2 + j_x h_x + \epsilon_x h_x\right) x\right. \\
&\quad \left. + \left(k - h_x h_z - j_x h_z - \epsilon_x h_x\right) z - \epsilon_{s0} x'\right) - a\gamma h_s z' - h_x \\
\Omega_s &= (1+a)\left(h_s - h_s h_x x - h_s h_z z\right) - (a\gamma+1)\left(\epsilon_z x' - \epsilon_x z'\right)
\end{aligned}$$

$\vec{\Omega}$ can be written as a sum of two parts (see eq. (3.23)):

$$\vec{\Omega} = \vec{\Omega}^{co} + \vec{\omega}, \tag{A.2}$$

where $\vec{\Omega}^{co}$ denotes the angular frequency vector on the closed orbit which is a periodic quantity $\vec{\Omega}^{co}(s) = \vec{\Omega}^{co}(s+L)$ and $\vec{\omega}$ describes the aperiodic contributions of the orbital motion to $\vec{\Omega}$. The solution of the corresponding differential equation for the periodic part $\vec{\Omega}^{co}$:

$$\vec{S}\,' = \vec{\Omega}^{co} \times \vec{S} \tag{A.3}$$

can be expressed as a linear combination of three orthonormal solutions $\vec{n}_0(s)$, $\vec{m}(s)$ and $\vec{l}(s)$, where $\vec{n}_0(s)$ is the periodic solution defined in eq. (3.21). The vectors $\vec{m}(s)$ and $\vec{l}(s)$ satisfy the condition:

$$\begin{pmatrix} \vec{m}(s+L) \\ \vec{l}(s+L) \end{pmatrix} = \begin{pmatrix} \cos(2\pi\nu) & -\sin(2\pi\nu) \\ \sin(2\pi\nu) & \cos(2\pi\nu) \end{pmatrix} \begin{pmatrix} \vec{m}(s) \\ \vec{l}(s) \end{pmatrix}, \tag{A.4}$$

where ν is the spin tune. The formal solution $\vec{S}$ of eq. (A.1) can be written in terms of this orthonormal spin basis:

$$\vec{S} = \sqrt{1-\alpha^2-\beta^2}\quad \vec{n}_0 + \alpha\vec{m} + \beta\vec{l}, \tag{A.5}$$

where α and β are solutions of the following nonlinear system of differential equations:

$$\alpha' = \sqrt{1-\alpha^2-\beta^2}\quad \vec{\omega}\vec{l} - \beta\vec{\omega}\vec{n}_0 \tag{A.6}$$

$$\beta' = -\sqrt{1-\alpha^2-\beta^2}\quad \vec{\omega}\vec{m} + \alpha\vec{\omega}\vec{n}_0. \tag{A.7}$$

These equations contain two different sources of nonlinearity of the spin motion:

1. The aperiodic function $\vec{\omega}$ is in general a nonlinear function of the phase space coordinates, which is the case even for completely linear motion.

2. The fact that the solutions of the Thomas-BMT equation are three dimensional rotations leads to the $\sqrt{1-\alpha^2-\beta^2}$ terms and the terms including $\vec{n}_0$ in eq. (A.7). Even if $\vec{\omega}$ is linear in the phase space coordinates the solutions α and β have a nonlinear dependence on these coordinates due to the nonlinearity of eq. (A.7) in α and β.

Eq. (A.7) is linearized by considering only linear orbit motion, linearizing $\vec{\omega}$ in the orbital coordinates and by assuming that the spin vector $\vec{S}$ remains close to $\vec{n}_0$ which leads to the situation that α and β are always small quantities. Thus the system of differential equations reduces to:

$$\begin{aligned}
\alpha' &= \vec{\omega}\vec{l} \\
\beta' &= -\vec{\omega}\vec{m}
\end{aligned} \tag{A.8}$$

and $\vec{S}$ is given by:

$$\vec{S} = \vec{n}_0 + \alpha\vec{m} + \beta\vec{l}.$$

Neglecting the contributions from the bending magnets which are mainly absorbed by the periodic solution $\vec{n}_0$ and assuming that no skew quadrupole fields are present $\vec{\omega}$ becomes in linear approximation:

$$\vec{\omega} = (a\gamma+1)k\left(z\vec{e}_x - x\vec{e}_z\right), \tag{A.9}$$

where k denotes the quadrupole strength. Now consider a particle undergoing no synchro-betatron oscillations. At $s = s_0$ a photon of the energy $\Delta\delta = -\Delta E/E_0$ is emitted. After the emission of the photon the motion is given by:

$$\begin{aligned}
x_\beta(s) &= \frac{1}{2}\Delta\delta\left[a_x(s_0)\sqrt{\beta_x(s)}\exp\left(i\phi_x(s)\right) + a_{-x}(s_0)\sqrt{\beta_x(s)}\exp\left(-i\phi_x(s)\right)\right]\exp\left(-\frac{1}{\tau_x}\frac{s-s_0}{c}\right) \\
z_\beta(s) &= \frac{1}{2}\Delta\delta\left[a_z(s_0)\sqrt{\beta_z(s)}\exp\left(i\phi_z(s)\right) + a_{-z}(s_0)\sqrt{\beta_z(s)}\exp\left(-i\phi_z(s)\right)\right]\exp\left(-\frac{1}{\tau_z}\frac{s-s_0}{c}\right) \\
\delta(s) &= \frac{1}{2}\Delta\delta\left[a_s(s_0)\exp\left(i\phi_s(s)\right) + a_{-s}(s_0)\exp\left(-i\phi_s(s)\right)\right]\exp\left(-\frac{1}{\tau_s}\frac{s-s_0}{c}\right),
\end{aligned} \tag{A.10}$$

where

$$\begin{aligned}
a_{\pm x}(s_0) &= \frac{-D_x \pm i\left(D_x'\beta_x + D_x\alpha_x\right)}{\sqrt{\beta_x}}\exp\left(\mp i\phi_x(s_0)\right) \\
a_{\pm z}(s_0) &= \frac{-D_z \pm i\left(D_z'\beta_z + D_z\alpha_z\right)}{\sqrt{\beta_z}}\exp\left(\mp i\phi_z(s_0)\right) \\
a_{\pm s}(s_0) &= \exp\left(\mp i\phi_s(s_0)\right)
\end{aligned}$$

and β_y, α_y, ϕ_y, D_y, D_y' $(y = x, z, s)$ denote the usual machine functions. The τ_y are the damping times derived in section 3.1. Substituting $x = x_\beta + \delta\cdot D_x$ and $z = z_\beta + \delta\cdot D_z$ in eq. (A.9) $\vec{\omega}$ becomes:

$$\vec{\omega}(s) = \frac{1}{2}\Delta\delta\sum_j a_j(s_0)\vec{\omega}_j(s)\exp\left(-\frac{1}{\tau_j}\frac{s-s_0}{c}\right), \quad j = \pm x, \pm z, \pm s \tag{A.11}$$

with

$$\begin{aligned}
\vec{\omega}_{\pm x} &= -(a\gamma+1)k\sqrt{\beta_x}\exp\left(\pm i\phi_x(s)\right)\vec{e}_z \\
\vec{\omega}_{\pm z} &= (a\gamma+1)k\sqrt{\beta_z}\exp\left(\pm i\phi_z(s)\right)\vec{e}_x \\
\vec{\omega}_{\pm s} &= (a\gamma+1)k\left(D_z\vec{e}_x - D_x\vec{e}_z\right)\exp\left(\pm i\phi_s(s)\right).
\end{aligned}$$

The $\vec{\omega}_j$ take over the quasi-periodicity of the synchro-betatron oscillations:

$$\vec{\omega}_{\pm y}(s+L) = \exp\left(\pm i2\pi Q_y\right)\vec{\omega}_{\pm y}(s), \quad y = x, z, s, \tag{A.12}$$

where Q_y are the orbital tunes. The spin motion after the emission of a photon $\Delta\delta$ at s_0 can be obtained by solving eq. (A.8) with $\vec{\omega}$ given by eq. (A.11) in the form:

$$\vec{S} = \vec{n}_0 + \Delta\delta\vec{d}(s, s_0),$$

with

$$\vec{d}(s, s_0) = \frac{1}{\Delta\delta}\left(\alpha(s, s_0)\vec{m} + \beta(s, s_0)\vec{l}\right).$$

For $s \to \infty$ the quantities $\alpha(s, s_0)$ and $\beta(s, s_0)$ converge to constants $\alpha(\infty, s_0)$ and $\beta(\infty, s_0)$. $\vec{d}(s_0)$ is then given by [77]:

$$\vec{d}(s_0) = \frac{1}{2} Im\left[\vec{K}^*(s_0)\left(C_x + C_{-x} + C_z + C_{-z} + C_s + C_{-s}\right)\right] \tag{A.13}$$

with

$$\vec{K}(s) = \vec{m}(s) + i\vec{l}(s) = K_x\vec{e}_x + K_z\vec{e}_z + K_s\vec{e}_s$$

and

$$\begin{aligned}
C_{\pm x}(s_0) &= \frac{a\gamma + 1}{\exp\left(i2\pi(\nu - Q_x)\right) - 1} a_{\pm x}(s_0) \int_{s_0}^{s_0+L} ds' \left[K_z \cdot k\sqrt{\beta_x}\exp\left(\pm i\phi_x\right)\right]_{s'} \\
C_{\pm z}(s_0) &= -\frac{a\gamma + 1}{\exp\left(i2\pi(\nu - Q_z)\right) - 1} a_{\pm z}(s_0) \int_{s_0}^{s_0+L} ds' \left[K_x \cdot k\sqrt{\beta_z}\exp\left(\pm i\phi_z\right)\right]_{s'} \\
C_{\pm s}(s_0) &= \frac{a\gamma + 1}{\exp\left(i2\pi(\nu - Q_s)\right) - 1} a_{\pm s}(s_0) \int_{s_0}^{s_0+L} ds' \left[(D_z K_x - D_x K_z) \cdot k\exp\left(\pm i\phi_s\right)\right]_{s'}.
\end{aligned} \tag{A.14}$$

This solution for $\Delta\delta\vec{d}$ describes the contributions a particle spin vector gets in the $\vec{m}$ and $\vec{l}$ direction by the emission of a photon with energy $\Delta\delta$ at an arbitrary position s_0 in the ring. Thus $\vec{d}$ can be identified with the more general object $\gamma\partial\vec{n}/\partial\gamma$ given in the Derbenev-Kondratenko formula eq. (2.14 under the condition that the spin vector remains close to the $\vec{n}_0$-axis. This allows to calculate the depolarization rate $1/\tau_d$ using eq. (2.12) in first order approximation.
Eq. (A.14) contains resonance denominators which lead to large $\vec{d}$ und thus large d arization rates $1/\tau_d$ whenever the spin tune ν is near to one of the orbital tunes Q_y:

$$\nu = k + m_x Q_x + m_z Q_z + m_s Q_s, \quad \text{with} \quad |m_x| + |m_z| + |m_s| = 1, \tag{A.15}$$

where k,$m_{x,z,s}$ are integers. The $a_{\pm y}$ lead to "excitation factors" in $|\vec{d}|^2 = \alpha^2(\infty, s_0) + \beta^2(\infty, s_0)$ of the form:

$$a_{\pm y}a_{\pm y}^* = \frac{D_y^2 + \left(D_y'\beta_y + D_y\alpha_y\right)^2}{\beta_y}$$

with $y = x, z$, which shows for example that D_z generated by imperfections in a "flat" ring can be dangerous and enhance depolarization. Thus the vertical dispersion should be minimized.

Although the estimates for the linearized motion just given is based on intuitive arguments, the same result can be obtained by a more formal method. At the linear level (eq. (A.8)) the differential equation for the spin coordinates α and β can be combined with the 6×6 equations of the orbit motion to obtain an 8×8 system of linear stochastic differential equations for combined spin-orbit motion [31][32]. These can be solved to obtain the rate of increase of $< \alpha^2 + \beta^2 >$ and then the depolarization rate $1/\tau_d$. This method has been implemented in the programs SLIM [31] and SITF. All first order polarization calulations presented in the text are performed with the program SITF. The SLIM formalism has been reformulated to describe

the orbital motion in terms of β functions and dispersion [78]. An 8×8 system of stochastic equations is again obtained. But now $1/\tau_d$ is written in terms of one turn integrals involving β functions and dispersion. The results obtained are numerically almost identical to those given by the original SLIM formalism. The expressions are identical to those (eq. (A.14)) derived from the heuristic approach introduced at the beginning of this appendix.

Eq. (A.8) can also be applied to the periodic orbit motion on the closed orbit. One defines a $\vec{n}_0$ on the design orbit and calculates $\delta\vec{n}_0$, which is induced by imperfections in the ring, to obtain $\vec{n}_0 + \delta\vec{n}_0$ on the closed orbit by solving eq. (A.8), where $\delta\vec{n}_0 = \alpha^{co}\vec{m} + \beta^{co}\vec{l} = Rc\left[(\alpha^{co} - i\beta^{co})\vec{K}\right]$ and contains one turn integrals and resonance denominators (see eq. (A.14). The solutions can be Fourier analyzed in the orbital coordinates:

$$(\alpha^{co} - i\beta^{co})(s) = -i\sum_k \frac{f_k}{k - \nu}\exp\left(i2\pi k\frac{s}{L}\right). \tag{A.16}$$

It is clear that the Fourier harmonics f_k which are near to the integer part of the spin tune are the most dangerous. The values of the f_k depend linearly on the distortions of the ring elements. In the case of HERA it was found that four of these harmonics need to be controlled. This is done by the application of a special harmonic bump scheme [60] consisting of eight bumps in the arcs of HERA which is controlled by eight independent parameters for the correction of the harmonics. The harmonics can be minimized separately and the result is given by linear superposition.

B Changes to the SITROS code

The main problem in using SITROS was due to limitations in computing time:

1. The small number of tracked turns (≤ 3000)
2. The bad sampling of the tails of the tracked particle distribution
3. The small number of particles to represent the beam (≤ 50)
4. The small number of sections and radiators to represent the elements in the ring and the dynamical behaviour of the particles due to quantum excitation (≤ 8)

What was done to overcome these problems ?
The program was transferred from a relatively slow IBM 3090/6 with strong computing time limitations to a UNIX based Hewlett Packard workstation of the type HP 9000/730 with an advanced processor architecture. Central tracking routines, implemented in the Assembler language on the IBM, were rewritten to fit to this architecture (mainly effecting the matrix operations). SITROS got a new X Windows[1] based user interface which allows it to make efficient use of the program features. Due to the gain in available computing time on several workstations (including DEC Station(s) 3100 and a SUN Sparcstation 10) it was possible to push the limits to a regime where they do no harm (ensembles with 1000 particles, 32 sections corresponding to 30 radiation points, tracking for 1×10^7 turns). Special runs can be made where one tracks more particles for a longer time. Several important checks on the remaining limitations were performed which can be found in section 3. Further improvements to the program include :

1. Some linear orbit calculations were implemented to get more information about the linear behaviour of the program including the calculation of equilibrium beam sizes and beam twists, which was important for the analysis of the HERA performance (see section 3).
2. The knowledge of these quantities allowes a much better and automatized control of the main tracking conditions (beam sizes) and was used to implement an excitation control algorithm.
3. The program was rewritten to simulate polarization optimizations with a special harmonic bump scheme [60] to predict the maximum attainable polarization. This scheme was later successfully used to increase the polarization in HERA (section 5).
4. SITROS is now able to handle various bump schemes including bumps reducing the coupling between vertical and horizontal motion and dispersion bumps to increase the polarization.
5. A time varying dipole field was introduced to simulate the effect on the polarization (see depolarizer calculations in section 5.3) stepping over a certain frequency range to get resonance curves which can be compared with corresponding measurements.
6. Various post processing routines exist to examine the output of the Monte-Carlo program. Interfaces to several standard graphic programs are available.

In tab. (1) the computing time needed for the different parts of the SITROS program is summarized for three types of workstations. The chosen input parameters given in the column "Comments" are "typical" parameters for a SITROS run.

[1]The X Window System is a trademark of the Massachusetts Institute of Technology.

Program	f77 options	HP 9000/730	SUN Sparc 10	DEC 3100	Comments
SITA	-O2 -K	2m55		6m29	linear calculations
	-O3		6m19		(c.o., $\vec{n}_0$, τ_p, P_∞)
	-fast -O3		5m00		16 sections
	-O4		6m26		101 energies
SITB	-O2 -K	0m08		0m20	tracking parameters
	-O3		0m11		and initialization
	-fast -O3		0m11		of files
	-O4		0m11		
SITC	-O2 -K	2m52		5m20	orbital tracking
	-O3		4m20		at central energy
	-fast -O3		3m48		(6×6-matrices)
	-O4		4m42		50 particles, 5000 turns
SITD	-O2 -K	1h42m14		7h11m50	orbital+spin tracking
	-O3		5h37m36		for 101 energies
	-fast -O3		4h48m45		(410×28-matrices)
	-O4		5h38m05		50 particles, 5000 turns
SITE	-O2 -K	1m04		2m25	postprocessing
	-O3		1m33		
	-fast -O3		1m33		
	-O4		1m33		
SITF	-O2 -K	1m52		4m42	linear polarization
	-O3		3m27		calculations
	-fast -O3		2m56		(perturbation theory
	-O4		3m37		1st order)

Table 1: *Computing time needed by the modules of the SITROS program for three types of workstations*

References

[1] Schott,G.A., Electromagnetic Radiation, Cambridge University, Cambridge (1912).

[2] Ternov,I.M., Loskutov,Yu.M. and Korovina,L.I., Sov.Phys. JETP 14 (1962) 921.

[3] Belbeoch,R. et al., Proc. USSR National Conf.Part.Accel. (1968) 129.
Baier,V.N., Sov.Phys.Uspekhi 14 (1972) 695.

[4] MacKay,W.W., Phys.Rev. D29 11 (1984).
Learned,J.G, Resvanis,L.K. and Spencer,C.M., Phys.Rev.Lett. 35 (1975) 1688.
Serednyakov,S.I. et al., Sov.Phys. JETP 44 (1976) 1063.
Artamonov,A.S. et al., Phys.Lett. 137B (1984).

[5] Bremer,H.D., DESY 82-026 (1982).
Barber,D.P., Phys.Lett. 135B (1984) 498.

[6] Assmann,R. et al., To be published in Part.Accel.

[7] Nakajima,K., Proc. 10th Int.Symp. on High Energy Spin Physics, Nagoya (1992) 919.

[8] Barber,D.P. et al., DESY 93-038 (1993).
Barber,D.P. et al., Nucl.Instr.Meth. A338 (1994) 166.

[9] Derbenev, Ya.S. et al., Part.Accel. 10 (1980) 177.

[10] Bukin,A.D. et al., Sov.J.Nucl.Phys. 27 (1978) 516.
Barkov,L.M. et al., Nucl. Phys. B148 (1979) 53.
Serednyakov,S.I., Phys.Lett. 66B (1977) 102.

[11] Barber,D.P. et al., DESY 83-067 (1983).

[12] Placidi,M., in: Poole,J. (ed.), CERN SL/93-19 (DI) (1993) 281.

[13] Wu,C.S. et al., Phys.Rev. 105 (1957) 1413.

[14] Prescott,C.Y. et al., Phys.Lett. 84B (1979) 524.

[15] Ashman,J. et al., EMC Collab., Phys.Lett. B206 (1988) 364.
Ashman,J. et al., EMC Collab., Nucl.Phys. B328 (1989) 1.

[16] Hughes,V.W. et al., Phys.Lett. B212 (1988) 511.
Baum,G. et al., Phys.Rev.Lett. 51 (1983) 1135.

[17] HERMES Collab., Technical Design Report, DESY-PRC 93/06 (1993).

[18] Wolf,G., DESY 86-089 (1986).

[19] Brinkmann,R., DESY HERA 88-03 (1988).

[20] Buon,J. and Steffen,K., Nucl.Inst.Meth. A245 (1986) 248.

[21] Kewisch,J. et al., Phys.Rev.Lett. 62 (1989) 419.

[22] Limberg,T., Ph.D. thesis, DESY HERA 88-14 (1988).

[23] Mane,S.R., Phys.Rev. A36 (1987) 105.

[24] Sokolov,A.A. and Ternov,I.M., Sov.Phys.Dokl. 8 (1964) 1203.

[25] Thomas,L., Philos.Mag. 3 (1927) 1.

[26] Bargmann,V., Michel,L. and Telegdi,V.L., Phys.Rev.Lett. 2 (1959) 435.

[27] Baier,V.N.,Katkov,V.M. and Strakhovenko,V.M., Sov.Phys. JETP 31 (1970) 908.

[28] Montague,B.W., Polarized Beams in High Energy Storage Rings, Phys.Rep. 113, Vol.1 (1984).

[29] Froissart,M. and Stora,R., Nucl.Instr.Meth. 7 (1960) 297.

[30] Baier,V.N. and Orlov,Yu.F., Sov.Phys.Dokl. 10 (1966) 1145.

[31] Chao,A.W., Nucl.Instr.Meth. 180 (1981) 29.

[32] Mais,H. and Ripken,G., DESY 83-62 (1983).

[33] Derbenev,Ya.S. and Kondratenko,A.M., Sov.Phys. JETP 37 (1973) 968.

[34] Yokoya,K., KEK 92-6 (1992).

[35] Eidelman,Yu. and Yakimenko,V., Proc. IEEE Part.Acc.Conf., San Francisco (1991) 269.

[36] Barber,D.P., Böge,M. and Gianfelice,E., Proc. High Energy Acc. Conf., Hamburg (1992) 1088.

[37] Jackson,J.D., Classical Electrodynamics, 2nd edition, John Wiley (1970).

[38] Jowett,J.M., SLAC-PUB-4033 (1986).

[39] Barber,D.P.,Heinemann,K.,Mais,H.,Ripken,G., DESY 91-146 (1991).

[40] Schmüser,P., Basic Course on Accelerator Optics, DESY HERA 87-02 (1982).

[41] Kewisch,J., Ph.D. thesis, DESY 85-109 (1985).

[42] Mais,H.,Ripken,G., DESY M-82-05 (1982).

[43] Sands,M., The Physics of Electron Storage Rings: An Introduction, SLAC-121 (1970).

[44] Chao,A.W., J.Appl.Phys. 50.(1979).

[45] Piwinski,A., CERN Accelerator School, General Accelerator Physics, Gif-sur-Yvette,Paris (1984) 432.

[46] Ripken,G. and Willeke,F., DESY 88-114 (1988).

[47] Zotter,B., CERN Accelerator School, General Accelerator Physics, Gif-sur-Yvette,Paris (1984) 415.

[48] Ripken,R., DESY 85-084 (1984).

[49] Gradshteyn, Ryshik, Tables of Integrals, Series and Products, Academic Press, New York, London (1965).

[50] CERN Program Library "CERNLIB", Short Writeups (1993).

[51] Barber,D.P. et al., DESY 86-147 (1986).

[52] Honerkamp,J., Stochastische dynamische Systeme, VCH, Weinheim (1990).

[53] Kohaupt,R.D., DESY H2-77/05 (1977).

[54] Barber,D.P., Heinemann,K. and Ripken,G., DESY M-92-04 (1992).

[55] Derbenev, Ya.S. and Kondratenko, A.M., Sov.Phys. JETP 25 (1972) 230.

[56] Buon,J., Proc. 8th Int.Symp. on High Energy Spin Physics, Minneapolis (1988) 963.

[57] Mane,S.R., Nucl.Instr.Meth. A292 (1990) 52.

[58] Mane,S.R., Nucl.Instr.Meth. A321 (1992) 21.

[59] Yokoya,K., Part.Accel. 13 (1983) 85.

[60] Gianfelice,E., in: Willeke,F. (ed.), DESY HERA 92-07 (1992) 202.
Barber,D.P. et al., DESY 85-044 (1985).

[61] Brinkmann,R., Private communication.

[62] Autin,B. and Marti,Y., CERN ISR-MA/73-17 (1973).

[63] Barber,D.P. et al., DESY 92-136 (1992).
Barber,D.P. et al., Nucl.Instr.Meth. A329 (1993) 79.

[64] Brinkmann,R., Private communication.

[65] Rossmanith,R. and Schmidt,R., Nucl.Instr.Meth. A236 (1985) 231.

[66] Barber,D.P., Private communication.

[67] Düren,M., Preliminary Results of the 1993 HERA Polarization Studies, Hamburg (1993).

[68] Barber,D.P. et al., Part.Accel. 17 (1985) 243.

[69] Barber,D.P., Private communication.

[70] Gianfelice,E. and Böge,M., Proc. 10th Int.Symp. on High Energy Spin Physics, Nagoya (1992) 915.

[71] Barber,D.P. et al., Paper in preparation

[72] Kewisch,J., DESY 83-032 (1983).

[73] Böge,M., Proc. 10th Int.Symp. on High Energy Spin Physics, Nagoya (1992) 419.

[74] Neumann,R. and Rossmanith,R., Nucl.Instr.Meth. 204 (1982) 29.

[75] Yokoya,K., Proc. High Energy Acc. Conf., Hamburg (1992) 1103.

[76] Grote,H., Proc. 10th Int.Symp. on High Energy Spin Physics, Nagoya (1992) 409.

[77] Yokoya,K., KEK TRISTAN 81-19 (1982).

[78] Mais,H. and Ripken,G., DESY 86-29 (1986).